uOttawa

L'Université canadienne
Canada's university

FACULTÉ DES ÉTUDES SUPÉRIEURES ET POSTOCTORALES

uOttawa

L'Université canadienne
Canada's university

FACULTY OF GRADUATE AND POSDOCTORAL STUDIES

Qinrong Yu

AUTEUR DE LA THÈSE / AUTHOR OF THESIS

Ph.D. (Physics)

GRADE / DEGREE

Department of Physics

FACULTÉ, ÉCOLE, DÉPARTEMENT / FACULTY, SCHOOL, DEPARTMENT

Distributed Brillouin Sensing Using Polarization-maintaining Fibers with High Measurement Accuracy

TITRE DE LA THÈSE / TITLE OF THESIS

Xiaoyi Bao (absent)

DIRECTEUR (DIRECTRICE) DE LA THÈSE / THESIS SUPERVISOR

Liang Chen

CO-DIRECTEUR (CO-DIRECTRICE) DE LA THÈSE / THESIS CO-SUPERVISOR

EXAMINATEURS (EXAMINATRICES) DE LA THÈSE / THESIS EXAMINERS

Alain Bellerive

Robin Williams

Wojtek Bock

Peter Piercy

Gary W. Slater

Le Doyen de la Faculté des études supérieures et postdoctorales / Dean of the Faculty of Graduate and Postdoctoral Studies

Distributed Brillouin Sensing Using Polarization-Maintaining Fibers with High Measurement Accuracy

by

Qinrong Yu

Thesis submitted to
The Faculty of Graduate and Postdoctoral Studies
In partial fulfillment of the requirements for the Degree of

Doctor of Philosophy

Ottawa-Carleton Institute for Physics
University of Ottawa

Your file Votre référence
ISBN: 978-0-494-25895-8
Our file Notre référence
ISBN: 978-0-494-25895-8

ABSTRACT

This thesis is a collection of studies on a distributed sensor based on Brillouin scattering using polarization maintaining (PM) fibers as well as single mode fibers.

With a specially designed optical fiber circuit consisting of two polarizing beam splitters and polarization controllers, PM fibers were successfully used as sensing media for the Brillouin distributed sensor developed at the University of Ottawa. The use of a single axis of a PM fiber minimizes polarization effects and therefore improves the signal to noise ratio of the Brillouin spectrum and hence, the measurement resolution. The strain and temperature dependence of Brillouin frequency, intensity and bandwidth of three types of commercial PM fibers: PANDA, Bow-tie and Tiger were investigated. The main findings from these investigations are as follows: 1) in a PM fiber, the temperature dependence of the Brillouin frequency in the slow axis is the same as that in the fast axes, and so is the strain dependence, 2) the Brillouin spectrum bandwidth is strain and temperature dependent, and 3) PANDA PM fiber shows the greatest promise for use in sensing applications and Tiger fiber is not suitable for Brillouin sensing. The feasibility of simultaneously measuring strain and temperature using PM fibers was examined.

The 2^{nd} order partial derivative of the Stokes intensity with respect to frequency and position shows a maximum or minimum at the boundary between two different strained sections. This idea was used to locate the boundary between different strain regions. This provides a spatial location accuracy between 5 cm to10 cm, which is better than the 20 cm pulse length used in the experiment.

The influences of transient phonon (defined as when pulse width is shorter than the phonon relaxation time) relaxation on the Brillouin loss spectrum have been observed and investigated. The transient phonon field lasts longer than the nature phonon lifetime (~10 ns). This transient phonon relaxation time is pump power and probe ER dependent, and it affects the strain, temperature, and location measurement accuracy.

STATEMENT OF ORIGINALITY

My research work presented in this thesis was carried out under the supervision of Dr. Xiaoyi Bao and Dr. Liang Chen in the Department of Physics, University of Ottawa.

The Brillouin sensor system used in the research was designed and constructed by the team headed by Dr. Bao at the University of New Brunswick. The system was damaged during shipping to the University of Ottawa and was rebuilt by the author, Xiaodong Zeng and Graham Ferrier in the summer of 2001 (both Zeng and Ferrier were Master's degree students at the time). Over time, some components were introduced into the system such as the free space tunable attenuator. The damaged laser and circulator were repaired or replaced. Most of the ST (Straight Tip) connectors on the components, which have a poor repeatability, were replaced with FC/PC (Face Contact/Physical Contact) connectors.

All experiments, data processing and analysis mentioned in the text were designed and conducted by the author, under the supervision of Dr. Bao and Dr. Chen. To the best of my knowledge, this thesis contains no material previously published or written by another person, except where appropriate references were made in the text. Therefore, I can claim that the results presented herein are my own, with credits attributed to my coworkers and colleagues in the fiber optic group:

- Xiaodong Zeng and Graham Ferrier helped me to get familiar with the software to operate the system and to process the experimental data.
- Fabien Ravet, a Ph.D. candidate in our fiber optic group, contributed the simulation plots (Fig.7-1) in the paper "Simple method to identify the spatial location better than the pulse length with high strain accuracy," *Optics Letters*, 30, 2215-2217(2005).
- V. P. Kalosha, a post-doctoral fellow in our fiber optic group, contributed the simulation result (Fig.8-5) in the paper "The influence of transient phonon relaxation on the Brillouin loss spectrum for nanosecond pulses," *Optics Letters*, 31, 888-890(2006).

The original results have been published in five papers by the refereed journal OPTICS LETTERS. They are summarized as follows:

1. I designed an optical circuit to use polarization-maintaining fiber as a sensing medium. The optical circuit guarantees that the input light wave is highly polarized, aligned and launched into one of the two principal axes.

2. I experimentally studied the temperature and strain dependence of Brillouin frequency, intensity and bandwidth of PANDA, Bow-tie and Tiger PM fibers using a single polarization axis. Simultaneous measurement of temperature and strain was conducted.

3. I proposed a 2^{nd} derivative approach for identifying strain boundaries. With this approach, the start and end positions of a uniform strain can be determined with a location accuracy better than the pulse width.

4. I observed and investigated influences of transient phonon relaxation on the Brillouin loss spectrum. The transient phonon relaxation time is pump power and probe ER depend, and it affects the measurement accuracy.

ACKNOWLEDGEMENTS

I would like to thank Dr. Xiaoyi Bao and Dr. Liang Chen who have been my co-supervisors at the University of Ottawa for a number of years and who have provided me with guidance throughout the course of this study. They are excellent supervisors with academic foresight in the research field and have always held the highest standards of professionalism in their work. I have benefited greatly from working with Dr. Bao and Dr. Chen.

I wish to thank ISIS (Intelligent Sensing and Innovative Structures) Canada, NSERC (Natural Science and Engineering Research Council of Canada), CFI (Canada Foundation of Innovation), The Canada Research Chair program and University of Ottawa for their financial support of this work.

The work in this thesis would not have been possible without the help of my colleagues Xiaodong Zeng, Graham Ferrier, Dr. Shahraam Afshaar V., Dr. Lufan Zou, Fabien Ravet and Dr. Vladimir Kalosha with whom I have shared the lab for some time and had many thoughtful discussions since I joined the fiber optic group in the Department of Physics, University of Ottawa.

Finally, I would like to thank my wife Li and daughter Lan for their patience and unconditional support.

TABLE OF CONTENTS

LIST OF FIGURES

LIST OF TABLES

LIST OF ACRONYMS

AEEO	Lehrstuhl für Allgemeine Elektrotechnik und Elektrooptik (Ruhr-University)
AOM	Acousto-Optic Modulator
BOFDA	Brillouin Optical Frequency Domain Analysis
BOTDA	Brillouin Optical Time-Domain Analysis
BOTDR	Brillouin Optical Time-Domain Reflectometry
CW	Continuous-Wave
DBS	Distributed Brillouin Sensing
EDFA	Erbium-Doped Fiber Amplifier
EOM	Electro-Optic Modulator
EPFL	Swiss Federal Institute of Technology (Lausanne)
ER	Extinction Ratio
FBG	Fiber Bragg Grating
FC	Face Contact
FM	Frequency Modulation
FWHM	Full Width at Half Maximum
HFWHM	Half Full Width at Half Maximum
Nd: YAG	Neodymium-doped Yttrium-Aluminum Garnet
OTDA	Optical Time Domain Analysis
OTDR	Optical Time-Domain Reflectometry
ORC	Optoelectronics Research Center (University of Southampton)
PC	Physical Contact
PM	Polarization-Maintaining
PMD	Polarization Mode Dispersion
SBS	Stimulated Brillouin Scattering
SNR	Signal-to-Noise Ratio
SOP	State of Polarization
ST	Straight Tip

Introduction

1. Optical fiber sensors

Optical fibers were developed for transmitting information in telecommunications due to their large bandwidth and low attenuation. Their unique properties also make them applicable as sensing media. Currently, a variety of sensors based on optical fibers have been used for monitoring strain, temperature, vibration, displacement, rotation, pressure, sound, flow, viscosity, and light intensity, as well as chemical, biomedical, and electrical variables [Udd, 1995; Kersey, 1996; Krohn, 2000]. The continued advances in research and technology have improved the performance of fiber sensors considerably. Meanwhile, low attenuation, high performance fibers and optoelectronics devices are becoming affordable, making optical fiber sensors more popular in scientific research, biomedical, civil engineering and other industries.

An optical fiber sensor is a device in which light transits into and out of the fiber to reach a sensing region where an environmental effect is converted into a light signal within the fiber. The basic configuration of an optical sensor consists of a light source, an optical fiber serving as a sensing element, and a receiver. According to the spatial distribution of the parameters to be measured, fiber optical sensors can be classified in two groups: point sensors and distributed sensors.

A point sensor takes the measurements at a single location (point) in space, although many point sensors can be arranged in series or in matrices to enable 'quasi' distributed sensing. There are a variety of point sensors. The most common point sensors are interferometric types such as Fabry-Perrot sensors [Udd, 1991] and Bragg grating sensors [Othonos and Kalli, 1999].

A distributed sensor measures the parameters of interest with a certain spatial resolution at any position along a single optical fiber. The fiber itself serves as a sensing medium. Examples include systems based on Rayleigh, Raman and Brillouin scattering. Distributed sensors are particularly demanded in applications where monitoring of parameters is required at a large number of points or on a continuum.

2. Rayleigh scattering and optical time domain reflectometry (OTDR)

Rayleigh scattering arises as a result of random microscopic variations in the refractive index and dopant concentration fluctuations of the optical fiber core [Lines, 1984].

Rayleigh scattering was first used for distributed sensing with the invention of optical time domain reflectometry (OTDR) [Barnowski *et al.* 1976, Barnowski *et al.* 1977] in which its concept became the foundation for all distributed sensors. In an OTDR, a laser pulse is launched into a fiber. A fraction of the light is backscattered and detected. The basic principle is shown in Fig.1-1. By monitoring the variation in the backscattered intensity, spatial variations in the fiber scattering coefficient or cross section, or attenuation can be determined. The spatial information is obtained by measuring the 'flight' time of the pulse in the fiber. For this reason, the spatial resolution of distributed sensors is commonly determined by the duration of the optical pulse. OTDR is widely used for characterizing optical fibers for intrinsic attenuation, splice losses, and fault location in fiber communications applications. For a known attenuation, it can measure the length of optical cable over 100-200km.

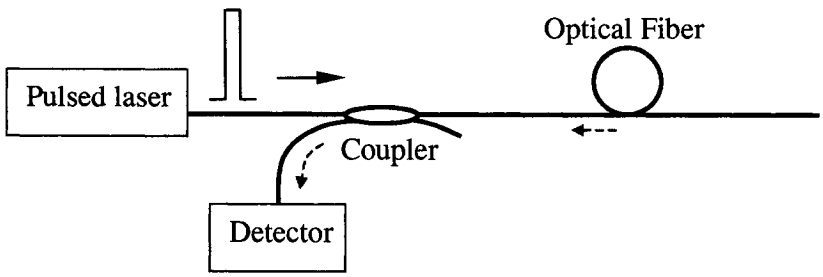

Fig. 1-1 Basic principle of an OTDR

Rayleigh scattering sensors have also been used for temperature sensing. Using the temperature dependence of the Rayleigh scattering intensity in a liquid-core fiber, Hartog achieved a ±1°C temperature resolution and a spatial resolution of a few meters [Hartog, 1983].

A Rayleigh scattering sensor is simple and inexpensive. However, its temperature dependence of the Rayleigh scattering in a glass fiber is too weak to permit sufficient temperature sensing. The temperature coefficient of the Rayleigh scattering intensity was measured as 0.015%/°C, only 1/17 that of Brillouin scattering intensity (0.26%/°C) in a glass optical fiber [Li, *et al.* 2003a].

3. Raman scattering sensor

Raman scattering is an inelastic scattering process in which incident light is scattered by molecular vibration in the optical fiber. The frequency of the scattered light suffers an down-shift (Stokes) and up-shift (anti-Stokes) from that of the incident light. The intensity of the anti-Stokes shift is dependent upon the population of optical phonons and therefore is temperature dependent. By measuring the ratio of anti-Stokes to Stokes intensity in the scattered light the temperature can be deduced. Because the Raman frequency shift (THz) is large compared to that for Brillouin scattering (GHz) the two components can be easily separated from each other (and from the Rayleigh scattering peak) by use of optical filters.

Farries *et al.* demonstrated the first successful distributed Raman sensors [Farries *et al.* 1984]. Kersey demonstrated that 1°C of temperature and 1 meter of spatial resolutions were achievable along a 10 km sensing length [Kersey, 1996].

Recently Raman and Brillouin sensors were combined for temperature compensation. A temperature resolution of 6 °C and a strain resolution of 150 $\mu\varepsilon$ with a spatial resolution of 10 m for a range of more than 23 km were demonstrated with this technique [Alahbabi *et al.* 2005].

Raman scattering is only sensitive to the temperature change, not strain change. Another drawback to the Raman sensor is the low scattering coefficient, which results in Raman scattered powers some 30 dB less than Rayleigh and 10 dB less than Brillouin scattering [Dakin *et al.* 1985, Horiguchi, *et al.* 1995]. For this reason, high power lasers and long acquisition times are needed.

4. Brillouin scattering sensor

A Brillouin sensor is based on Brillouin scattering. The incident light is backscattered by acoustic phonons in the fiber. The backscattered light experiences a Doppler frequency shift related to the speed of the acoustic waves in the fiber. Since the frequency shift depends linearly on changes in physical conditions, such as strain and temperature, these conditions can be measured by analyzing the Brillouin loss or gain spectrum of the fiber. The principle of Brillouin sensing will be discussed in detail in Chapter 1 of this thesis. A variety of Brillouin sensing techniques developed over the past years are briefly reviewed in Chapter 2.

The Brillouin scattering sensor is one of the most promising distributed sensors due to 1) low input power (a few mW) requirement, 2) high sensitivity to both strain and temperature, and 3) large measurement range from –270°C to 800°C for temperature [Fellay, *et al.* 2001, Li, *et al.* 2003b], and a few $\mu\varepsilon$ to 20,000 $\mu\varepsilon$ for strain [DeMerchant, 2000].

5. Thesis objectives

This thesis reports my research work on the distributed sensing system developed at the University of Ottawa, which is based on Brillouin loss using polarization-maintaining (PM) fibers. To the best of my knowledge, this was the first time PM fibers were studied for Brillouin sensing with a single axis in the fibers.

The objectives of this thesis are:

(1) To investigate the temperature and strain dependence of Brillouin frequency, intensity and bandwidth in PM fibers. In order to achieve this objective, an optical circuit was designed and added to the Brillouin sensor system allowing the use of PM fiber. Use of this modification made it possible to obtain the Brillouin spectra from the slow and fast axes respectively. The temperature and strain response of the Brillouin spectrum for the PM fibers was investigated. Simultaneous measurement of temperature and strain was conducted.

(2) To explore a practical method to accurately measure spatial location of boundaries of stained sections.

A 2nd derivative method was developed to identify the boundary of two strained sections, particularly when the strain difference between the two sections is small. The spatial location accuracy can be better than the probe pulse width.

(3) To study the influence of transient phonon relaxation on the Brillouin loss spectrum and the physics underlying the phenomena.

In order to observe prolonged phonon relaxation time, the two-(or three-) strain/temperature-section method was used. The phonon relaxation times at the different CW (continuous wave) power and pulse extinction ratios were experimentally estimated. This result helps us to understand the physics of Brillouin loss signal cross-talk phenomena between two adjacent sections of sensing fiber.

6. Thesis outline

Chapter 1 discusses the basic principles of Brillouin distributed sensing. Chapter 2 reviews the state of the art distributed sensing technologies based on Brillouin scattering. Next, Chapter 3 introduces PM fibers and the design of the optical circuit for the Brillouin sensing system using PM fiber.

Chapters 4 and 5 detail the temperature dependence and strain dependence of Brillouin frequency, bandwidth and intensity in three commercial PM fibers: PANDA, Bow-tie and Tiger. Chapter 6 presents simultaneous strain and temperature measurements with PM fibers and their error analysis.

Chapter 7 introduces a 2nd derivative method to identify the strain spatial location, which leads to a location accuracy better than the pulse width, and high strain accuracy.

Chapter 8 presents the observations and investigations of transient phonon relaxation, and its influence on the Brillouin loss spectra.

Finally, Chapter 9 gives the conclusions and proposed future work.

Note that Chapters 4, 5, 6, 7 and 8 were directly adapted from the papers published in OPTICS LETTERS with minor changes.

Chapter 1

Principles of distributed sensors based on Brillouin scattering

1.1 Nonlinear Optical phenomena

As derived from Maxwell's equations, the equation for electromagnetic wave propagation in a medium can be written as [Agrawal 1995]:

$$\nabla^2 \boldsymbol{E} - \frac{1}{c^2}\frac{\partial^2 \boldsymbol{E}}{\partial t^2} = \mu_0 \frac{\partial^2 \boldsymbol{P}}{\partial t^2}, \tag{1-1}$$

where $\boldsymbol{E}$ is the electric field, c is the speed of light in vacuum, and μ_0 is the magnetic permeability in vacuum, respectively. $\boldsymbol{P}$ is the field-induced polarization of electric dipoles in a dielectric medium.

The polarization is expressed generally as a power series of the electric field given by

$$\boldsymbol{P} = \varepsilon_0 [\chi^{(1)} \cdot \boldsymbol{E} + \chi^{(2)} : \boldsymbol{EE} + \chi^{(3)} \vdots \boldsymbol{EEE} + \cdots], \tag{1-2}$$

where ε_0 is the vacuum permittivity and $\chi^{(j)}$ (j =1, 2, ···) is j^{th} order susceptibility and a tensor of rank j+1. The linear susceptibility $\chi^{(1)}$ accounts for "linear optics" phenomena such as refraction and birefringence. The second-order susceptibility $\chi^{(2)}$ is responsible for second-harmonic and sum-frequency generation. However, it is nonzero only for media that lack an inversion symmetry at the molecular level. $\chi^{(2)}$ vanishes for silica optical fibers due to that SiO_2 is a symmetric molecule. The third-order susceptibility $\chi^{(3)}$ is related to third harmonic generation and phenomena such as the Kerr effect, Raman scattering and Brillouin scattering [Agrawal 1995].

Raman scattering has been used for distributed temperature sensing, whereas Brillouin scattering has been used for both temperature and strain sensing. In the following sections, discussion is mainly focused on Brillouin scattering. Since Raman scattering sensing was combined with Brillouin sensing in some of the cases, however, a brief discussion on Raman scattering is presented.

1.2 Spontaneous light scattering from a medium

Spontaneous light scattering occurs as a consequence of fluctuations in the optical properties of a material medium. There are four types of spontaneous light scattering: Rayleigh, Rayleigh-wing, Raman and Brillouin scattering.

Rayleigh scattering arises when photons encounter static inhomogeneous refractive index (and hence density) fluctuations. Rayleigh scattering is an elastic process, i.e., the frequencies of the incident and scattered light are equal. Rayleigh-wing scattering [Boyd, 2003] is scattering from fluctuations in the orientation of anisotropic molecules. Since the molecular reorientation process is rapid, this component is spectrally very broad.

Raman scattering results from the interaction of light with optical phonons that are the vibrational modes of the molecules constituting the scattering medium. Raman scattering is highly inelastic; the scattered frequency is three orders of magnitude higher than that of Brillouin scattering.

Brillouin light scattering is named after Léon Brillouin who predicted light scattering from thermally excited acoustic waves [Brillouin 1922].

Acoustic waves are propagating pressure waves, which create periodic density waves, hence refractive index waves in a medium. Brillouin scattering can also be equivalently considered to be the scattering of light from acoustic phonons. The photon-phonon inelastic interaction in silica optical fiber leads to a frequency shift (e.g. ~13 GHz and ~11 GHz for input light 1310 nm and 1550 nm respectively) of the scattered light that depends on the velocity of the sound wave, which is a function of strain and temperature. This frequency shift can also be considered as the Doppler shift of an optical beam incident on a mirror moving at the velocity of sound [Yariv 1996].

Brillouin scattering is subdivided into two processes: spontaneous and stimulated. A light scattering process is spontaneous if the fluctuations of the refractive index that cause the light scattering are thermally excited. Conversely, a light scattering process is stimulated when the fluctuations are induced by the presence of a light field [Boyd, 2003].

In order to make a visual comparison, Fig. 1-1 is presented to illustrate the spectrum of the Rayleigh-center, Rayleigh-wing, Raman and Brillouin spontaneous light scattering, in most general circumstances.

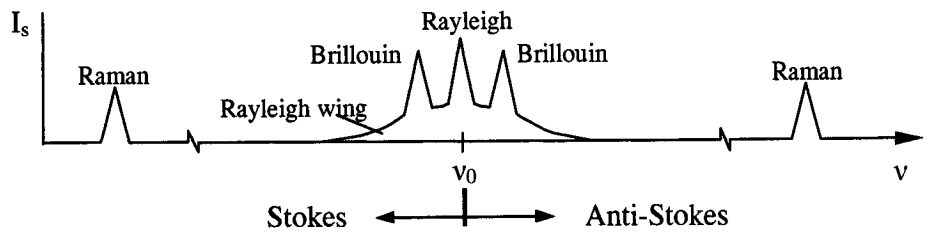

Fig. 1-1 A typical spontaneous light scattering spectrum [Boyd 2003].

1.3 Acoustic wave and Spontaneous Brillouin scattering

1.3.1 Acoustic wave propagation in a medium

Acoustic waves come from pressure (hence density) fluctuations in the medium. In this section we discuss acoustic wave propagation in the specific medium of an optical fiber.

Assume an optical fiber is isotropic, viscous and compressible. The corresponding dielectric permittivity fluctuations of the fiber under a density variation can be expressed as:

$$\Delta\varepsilon = \frac{\partial\varepsilon}{\partial\rho}\Delta\rho\,, \tag{1-3}$$

where ρ is the density of the medium.

The mean squared fluctuation in the dielectric constant is

$$\left\langle \Delta\varepsilon^2 \right\rangle = \gamma_e^2 \frac{\left\langle \Delta\rho^2 \right\rangle}{\rho_0^2}, \tag{1-4}$$

where

$$\gamma_e = \rho \frac{\partial \varepsilon}{\partial \rho} \tag{1-5}$$

is defined as the electrostrictive constant.

The density variation can be presented by

$$\Delta\rho = \left(\frac{\partial \rho}{\partial p}\right)_s \Delta p + \left(\frac{\partial \rho}{\partial s}\right)_p \Delta s\,, \tag{1-6}$$

here pressure p and entropy s are the independent variables. The first term describes adiabatic density fluctuations (acoustic waves), which leads to Brillouin scattering. The second term describes adiabatic fluctuation (entropy or temperature fluctuation), which leads to Rayleigh scattering [Boyd 2003]. In thermal equilibrium, thermally generated phonons are the main source of internal pressure variations, which are usually small. This is why spontaneous Brillouin scattering is weak.

An optical fiber can be considered to be a thin and long cylinder. The pressure fluctuations involve small displacements of a unit volume along the fiber. The relationship between pressure and volume is given:

$$\Delta p = -K \frac{\Delta V}{V}, \tag{1-7}$$

where K is the bulk modulus. This pressure transmitted to adjacent volume elements propagates according to the d'Alembert wave equation:

$$\nabla^2 p - \frac{\rho}{K} \frac{\partial^2 p}{\partial t^2} = 0\,. \tag{1-8}$$

Since K=7.37x10^{10} Pa and ρ=2.21 x10^3 kg/m^3 for fused silica at room temperature and atmospheric pressure, the acoustic wave velocity is $v_A = \sqrt{\frac{K}{\rho}}$ =5775 m/s.

The density variation induced by the pressure wave has the form

$$\Delta\rho = -\frac{1}{2}[\rho(z,t)e^{i(\omega_B t - k_B Z)} + c.c]\,, \tag{1-9}$$

where ω_B is the angular velocity and $\boldsymbol{k}_B$ the wave vector of the acoustic wave.

1.3.2 Light wave scattered by acoustic wave

When an incident light wave of frequency ν_p (wave vector $\boldsymbol{k_p}$) strikes an acoustic wave with frequency ν_B (wave vector $\boldsymbol{k_B}$) the incident wave scatters from the acoustic wave at a new frequency ν_s (wave vector $\boldsymbol{k_s}$), which satisfies the Bragg condition for energy and momentum conservation:

$$\nu_P - \nu_S = \nu_B, \tag{1-10}$$

$$\boldsymbol{k}_p - \boldsymbol{k}_S = \boldsymbol{k}_B. \tag{1-11}$$

where the dispersion relations are $k_p = \frac{\omega_p}{c} n_p$, $k_s = \frac{\omega_s}{c} n_s$ and $k_B = \frac{\omega_B}{V_A}$; c is the velocity of light and V_A is the acoustic wave velocity.

In general, the thermally induced acoustic wave has no preferred propagation direction. The three waves have a relation as shown in Fig. 1-2.

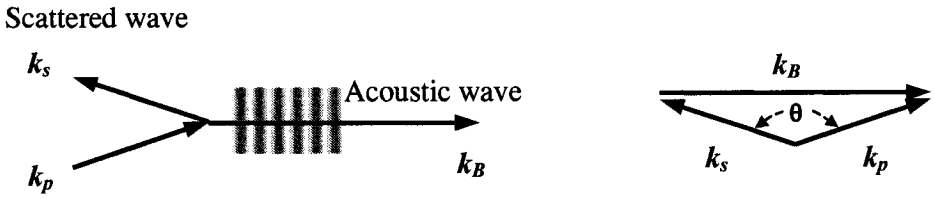

(a) (b)

Fig. 1-2 Momentum vector representations of the photon-phonon interactions in Brillouin scattering. The subscripts p, s, and B denote the incident, scattered and acoustic waves, respectively.

From the triangle relation we have

$$\omega_B = V_A |\boldsymbol{k}_B| \cong 2V_A |\boldsymbol{k}_p| \sin\left(\frac{\theta}{2}\right). \tag{1-13}$$

An optical fiber is a waveguide, which guides light along the longitudinal axis of the fiber. Based on Eq.(1-13) the Brillouin shift is zero at $\theta = 0$ (forward scattering) and can only happen at $\theta = \pi$ (back scattering). Therefore,

$$\nu_B = \frac{\omega_B}{2\pi} = \frac{2nV_A}{\lambda_p} \quad . \tag{1-14}$$

1.4 Stimulated Brillouin scattering

Stimulated Brillouin scattering (SBS) was first observed by Chiao *et al.*, who discovered that the acoustic waves that initiate Brillouin scattering could be produced from incident light waves [Chiao *et al.* 1964]. This was the start of extensive studies in SBS.

1.4.1 Electrostriction and stimulated Brillouin scattering

Electrostriction is the tendency of materials to become compressed in the presence of an electric field [Boyd 2003, p.411].

The electrostrictive pressure can be expressed as a function of the electric field

$$p_{el} = -\gamma_e \frac{E^2}{8\pi}, \tag{1-15}$$

where γ_e is the electrostrictive coefficient having the form

$$\gamma_e = \rho_0 \frac{\partial \varepsilon}{\partial \rho} = n^4 \varepsilon_0 p_{12}, \tag{1-16}$$

where ρ_0 is the average density of the material, n is the refractive index, ε_0 is the dielectric constant and p_{12} is the longitudinal photo-elastic coefficient, which is important for Brillouin scattering as it relates the mechanical strain in the axial direction to the radial electric field.

The pressure within an optical fiber generated by an inhomogeneous electric field results in periodic fluctuations, which correspond to periodic refractive index fluctuations in the medium. The density fluctuations result from a pressure variation $\Delta p = K\Delta\rho / \rho$ and a variation of the dielectric susceptibility

$$\Delta\chi = \frac{\gamma_e}{\varepsilon_0}\frac{\Delta\rho}{\rho} \,. \tag{1-17}$$

Stimulated Brillouin scattering is due to the density variation of the optical fiber induced by the input light waves. Fig. 1.3 shows such a SBS process in the probe-pump configured Brillouin sensor. The probe wave (Stokes wave) ν_s is launched into one fiber end A and the pump wave ν_p is launched into the opposite fiber end B. They counter-propagate and interfere to generate a propagating acoustic wave. As the waves interact and propagate, the amplified Stokes wave is detected at end A while the depleted pump wave is detected at end B.

The bottom part of Fig.1.3 illustrates the processes in the fiber. The interference of the pump and probe contains a frequency component at the difference frequency ν_p - ν_s (the so-called "beat frequency"). If this beat frequency matches the sound wave frequency, then the sound wave amplitude dramatically increases via the electrostriction effect. Probe and pump waves interact with the acoustic wave (which functions like a moving Bragg grating) through Bragg diffraction. Meanwhile the pump wave combined with the sound wave tends to reinforce the Stokes wave. Therefore, the Stokes wave is 'amplified' and the pump wave is 'depleted' by such positive feedback.

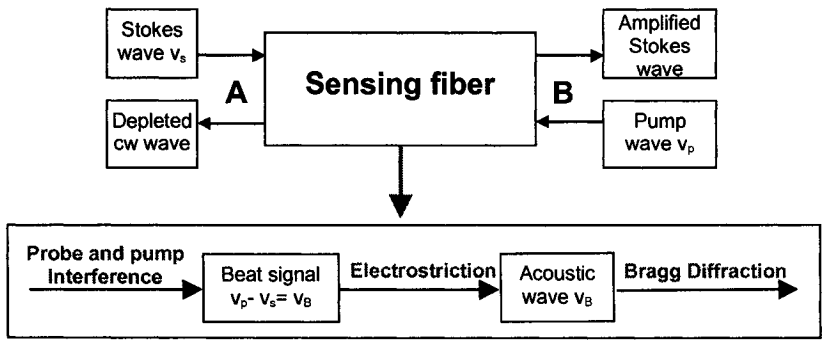

Fig. 1-3 Stimulated Brillouin scattering process in a probe-pump Brillouin sensor.

Figure1-4 illustrates that the interaction between the probe (Stokes) and pump waves ultimately generates an acoustic wave through electrostriction.

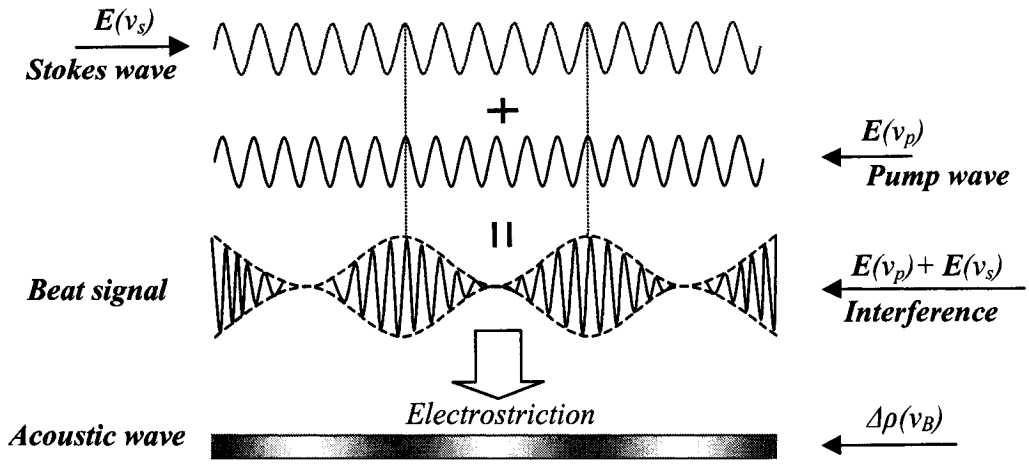

Fig. 1-4 Generation of an acoustic wave by electrostriction.

1.4.2 Coupled wave equations

The physical process of Brillouin amplification can be thought of as a nonlinear interaction between the probe and pump waves through an acoustic wave. The beat field resulting from the interference of pump and Stokes waves enhances the thermally induced acoustic wave through the process of electrostriction. The acoustic wave periodically varies the refractive index along the fiber, which scatters the pump wave through Bragg diffraction. The scattered light suffers a frequency up or down shift depending on its direction due to the Doppler effect induced by the index grating traveling at the acoustic velocity.

From Maxwell's equations and the Navier-Stokes equation for the acoustic field in the optical medium, we can derive three equations to describe the SBS process using the slowly varying envelope approximation [Kaiser and Maier 1972; Horiguchi *et al.* 1989; Afshaarvahid and Munch 2001]

$$\left(\frac{\partial}{\partial z}-\frac{n}{c}\frac{\partial}{\partial t}\right)E_p = ig_1 Q E_s - \frac{1}{2}\alpha E_p, \tag{1.18-1}$$

$$\left(\frac{\partial}{\partial z}+\frac{n}{c}\frac{\partial}{\partial t}\right)E_s = -ig_1 Q^* E_p + \frac{1}{2}\alpha E_s, \tag{1.18-2}$$

$$\left(\frac{\partial}{\partial t}+\Gamma\right)Q = -ig_2 E_p E_s^*, \tag{1.18-3}$$

where E_p, E_s and Q are the pump, Stokes, and acoustic fields, respectively; α is the linear fiber attenuation coefficient, and g_1 and g_2 are coupling coefficients related to the Brillouin gain coefficient $g_B = \frac{2g_1 g_2}{\Gamma_1}$. The complex detuning parameter is $\Gamma = \Gamma_1 + i\Gamma_2$, $\Gamma_1 = \frac{1}{2\tau}$ is the damping rate, τ is phonon lifetime (10ns for silica fiber). $\Gamma_2 = 2\pi(\nu - \nu_B)$ is the detuning frequency, and ν is the beat frequency.

The SBS dynamics in a single mode fiber can be described by the following equations for the pump and the Stokes intensities [Chen and Bao 1998]

$$\left[\frac{n}{c}\left(\frac{\partial}{\partial t}\right)+\frac{\partial}{\partial z}\right]I_p = \left(-\alpha - g_B I_s\right)I_p, \tag{1-19-1}$$

$$\left[\frac{n}{c}\left(\frac{\partial}{\partial t}\right)-\frac{\partial}{\partial z}\right]I_s = \left(-\alpha + g_B I_s\right)I_p, \tag{1-19-2}$$

where I_p and I_s are the pump and Stokes wave intensities in the fiber.

Neglecting the time dependence of the system and the dynamic response of acoustic waves, we can derive the steady state coupling equations as follows [Pannell *et al.*1993]:

$$\frac{dI_P}{dz} = -\alpha I_p - g_B I_s I_p, \tag{1-20-1}$$

$$\frac{dI_s}{dz} = \alpha I_s - g_B I_s I_p. \tag{1-20-2}$$

Agrawal has presented an incorrect solution for the above in his book "*Nonlinear Fiber Optics*" [Agrawal 1995]. Chen and Bao gave the correct solutions for the steady state SBS both analytically and numerically [Chen and Bao 1998]. The exact solution is left in integral form since there was no closed form solution for the integral:

$$\Sigma(z) = \sqrt{\left(\Sigma_0^2 - \Delta_0^2\right)\exp\left\{\left(g_B/\alpha\right)\left[\Delta(z) - \Delta_0\right]\right\} + \Delta^2(z)}\ , \tag{1-21-1}$$

$$\int_{\Delta_0}^{\Delta(z)} \frac{dx}{\sqrt{\left(\Sigma_0^2 - \Delta_0^2\right)\exp\left\{\left(g_B/\alpha\right)\left[x - \Delta_0\right]\right\} + x^2}} = -\alpha z\ , \tag{1-21-2}$$

where $\Delta = I_p - I_s$ and $\Sigma = I_p + I_s$, Δ_0 and Σ_0 are the corresponding values at the origin ($z = 0$).

1.4.3 Brillouin spectrum

The diagram in Fig. 1.5 illustrates how a Brillouin spectrum is acquired. During the measurement, the probe frequency is fixed and the pump frequency is scanned. For every beat frequency, a time domain waveform along the entire fiber is obtained. The Brillouin frequency spectra are collectively formed by those waveforms.

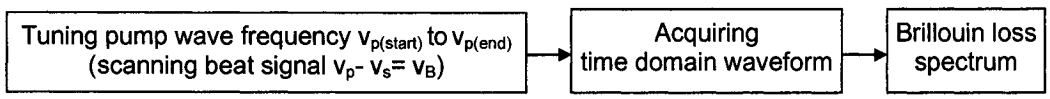

Fig. 1-5 Acquisition of Brillouin loss spectra from SBS process.

Since the Brillouin scattering process is not instantaneous, the scattered intensity varies over a frequency range that is symmetric about the Brillouin frequency ν_B (Equation 1-14). The maximum scattered intensity occurs at the Brillouin frequency ν_B, which is determined by fitting the raw data points with a profile [Bao *et al.* 1993a; Horiguchi *et al.* 1995].

For low-intensity, continuous-wave input light waves, the resulting Brillouin gain spectrum has a Lorentzian shape given by

$$g_B(\nu) = \frac{g_{B\max}}{1 + 4\left(\dfrac{\nu - \nu_B}{\Delta\nu_B}\right)^2}, \tag{1-22}$$

The maximum gain coefficient is

$$g_{B\max} = \frac{2\pi\,\gamma^2}{c\varepsilon_0^2\lambda_p^2\rho_0\Delta\nu_B\,V_A\,n}\,, \tag{1-23}$$

where λ_p is the laser wavelength, ρ_0 is the unperturbed fibre density, V_A is the acoustic velocity in silica, and $\Delta\nu_B$ is the Brillouin linewidth.

A Brillouin spectrum is shown in Fig. 1-6. The maximum gain coefficient is normalized to 1.

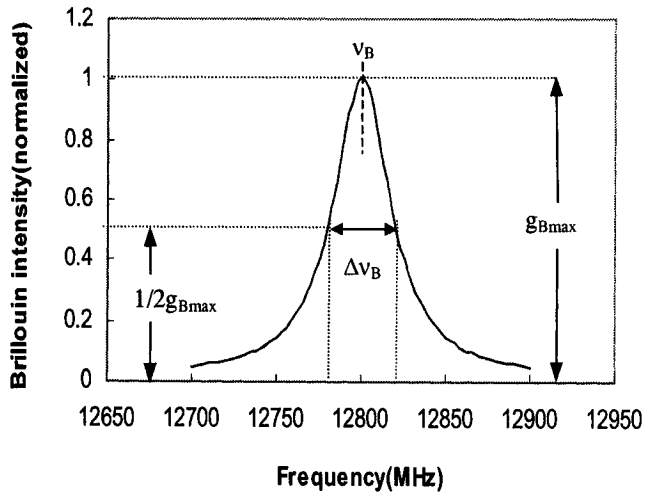

Fig. 1-6 A Lorentzian shaped Brillouin spectrum.

1.5 Temperature and Strain measurement through Brillouin spectrum analysis

It was found that the Brillouin frequency shift increases linearly with strain [Horiguchi *et al.* 1989a] and temperature [Kurashima, *et al.* 1990a]. The relation is generally described by the following equations [Horiguchi, *et al.* 1995]:

$$T = C_{\nu T}\left[\nu_B - \nu_{B0}\right] + T_0\,, \tag{1-24}$$

$$\varepsilon = C_{\nu\varepsilon}\left[\nu_B - \nu_{B0}\right] + \varepsilon_0\,, \tag{1-25}$$

where ε and T are the strain and temperature, respectively. $C_{\nu T} = \left[\frac{\partial \nu_B}{\partial T}\right]_{\varepsilon}$ is the temperature coefficient and $C_{\nu\varepsilon} = \left[\frac{\partial \nu_B}{\partial \varepsilon}\right]_{T}$ is the strain coefficient. The initial strain ε_0 and temperature T_0 are usually determined experimentally for a specific fiber being used.

The measurable parameters from a Brillouin scattering spectrum include

- Brillouin frequency: ν_B,
- Brillouin spectrum linewidth: $\Delta\nu_B$,
- Brillouin intensity: $P_0 \propto g_{B\max}$

As previously mentioned, ν_B is the frequency corresponding to the peak intensity of the spectrum. It is the most accurately measurable parameter. The Brillouin linewidth, $\Delta\nu_B$, is the full width at half maximum (FWHM) of the spectrum.

Besides the parameters of the Brillouin spectrum, another important parameter is the location of a point of interest along the sensing fiber. Location Z can be determined by measuring traveling time Δt of the pulse in the fiber:

$$Z = \frac{\Delta t \cdot c}{2n}, \tag{1-26}$$

where c is the speed of light in vacuum and n is the refractive index of the optical fiber. In the Brillouin sensing system, Z depends on the time for a pulse to reach that location plus the return time to the detector. Therefore, the ½ factor means that light requires only ½ Δt to reach position Z.

An example of strain measurement (at room temperature) on a PANDA PM fiber is shown in Fig. 1-7. Two Brillouin spectra were plotted. ν_{B1} is the Brillouin frequency at 0 με, and ν_{B2} is the Brillouin frequency under an applied strain. The Brillouin frequency was up-shifted about 9.6 MHz as the response to a 125 με strain applied to the fiber.

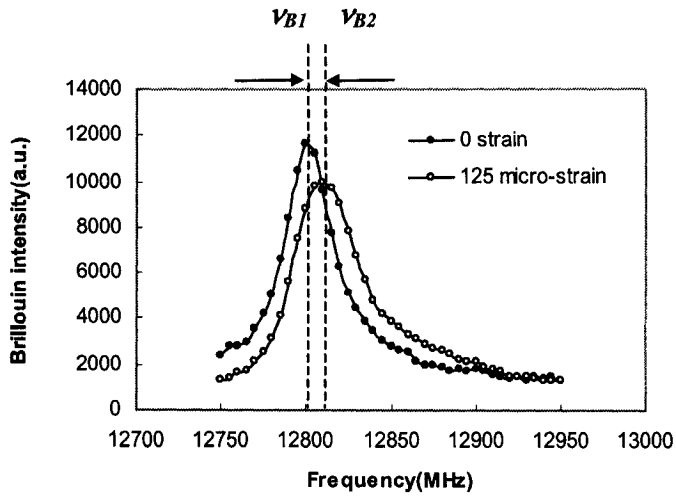

Fig.1-7 Brillouin frequency shift due to a strain applied in a PANDA fiber.

Chapter 2

Review of Distributed Brillouin Sensing Technologies

2.1 Brillouin optical time domain analysis (BOTDA)

Horiguchi and his colleagues reported the first distributed sensor [Horiguchi, *et al.* 1989a; Horiguchi and Tateda 1989] based on Brillouin scattering. A relevant patent was filed by Nippon Telegraph and Telephone (NTT) in the same year [Horiguchi, *et al.* 1989b, US patent number 4,997,227]. They showed a linear dependence of the Brillouin frequency shift of an optical fiber to an applied strain. It combined the techniques of OTDR and an early Raman distributed sensor [M.C.Farries *et al.* 1984], and applied them to stimulated Brillouin scattering. The method was named Brillouin optical time domain analysis (BOTDA). The system included two Nd:YAG CW lasers operated at 1319nm. A short pump pulse was generated through an Acoustic-Optic Modulator (AOM)). During the measurement the pulse was sent into one end of the sensing fiber and a CW wave into the other end as shown in Fig.2-1 while the frequency difference

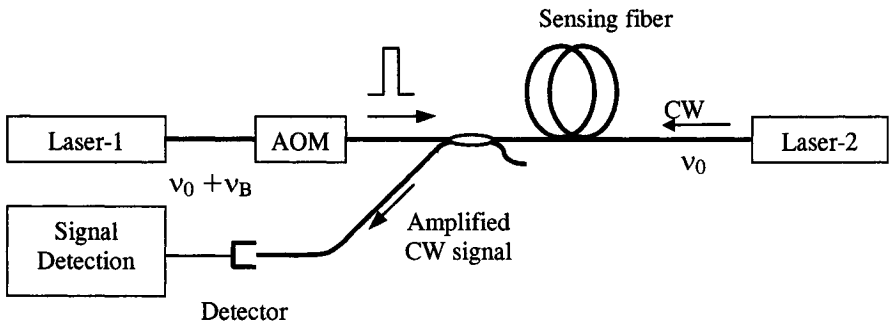

Fig. 2-1 Gain based BOTDA configuration

between the two beams was tuned across a range of several GHz, the CW wave experienced power amplification when the beat frequency of the two light waves matched the Brillouin frequency of the fiber. The gain as a function of fiber position was determined by the time dependence of the detected CW light wave. With the BOTDA approach, Kurashima *et al.* demonstrated distributed temperature measurement on a 1.2

km long optical fiber with a 3°C temperature resolution and a 100 m spatial resolution using NTT's BOTDA system [Kurashima, *et al.* 1990]. Culverhouse *et al.* reported a linear dependence of Brillouin shift due to temperature in a single mode fiber using a Fabry-Perot interferometer at the University of Kent in England. They found that two different fibers, which had different core refractive indices, had different temperature frequency coefficients, 6.4 MHz/°C and 2.67 MHz/°C [Culverhouse, *et al.* 1989]. Bao *et al.* at the University of Kent significantly improved the performance, achieving a 22 km sensing distance with a 1°C temperature resolution and a 10 m spatial resolution [Bao, *et al.* 1993a].

A milestone in the development of BOTDA was the use of Brillouin loss based distributed sensing rather than Brillouin gain. In the loss-based approach [Bao, *et al.* 1993b], the pulsed beam amplifies at the expense of the CW wave; therefore the intensity of the CW wave is reduced. The pulse amplification enables sensing of much longer fibers with equivalent or possibly better signal-to-noise ratios.

Using the Brillouin loss technique, Bao *et al.* measured a 32 km sensing length with a 1°C temperature resolution and a 5 m spatial resolution. Shortly afterward, they achieved a 5 m spatial resolution and a 20 με strain resolution in a 22 km optical fiber [Bao, Webb and Jackson 1994a]. They also first reported the Brillouin loss based simultaneous strain and temperature measurement using two side-by-side parallel optical fiber sections; one section subjected to both strain and temperature while the other was subjected to temperature only [Bao, *et al.* 1994a]. The corresponding strain, temperature, spatial resolutions were 20 με and 2°C and 5 m respectively. Finally, Bao *et al.* measured a record-setting 51 km sensing length with a 5 m spatial resolution and 1°C temperature measurement resolution [Bao *et al.* 1995].

2.2 Brillouin optical time domain reflectometry (BOTDR)

Kurashima and colleagues at NTT introduced a configuration known as Brillouin optical time domain reflectometry (BOTDR), which uses coherent detection of spontaneous Brillouin scattered light rather than detecting a Brillouin amplification signal.

A spatial resolution of 100 m and a frequency accuracy of 3.6 MHz (corresponding to ~ 3°C) was reported [Kurashima *et al.* 1992; Horiguchi *et al.* 1992]. In their system configuration, a fraction of pump light provided a local oscillator signal in the coherent detector. The Brillouin scattered light is beat against a local oscillator light wave, and the beat signal is observed by means of an electrical spectrum analyzer. Since the output beat signal is proportional to the scattered light intensity as well as to the local oscillator light intensity, a high signal to noise ratio can be obtained. The configuration is illustrated in Fig. 2-2.

The system had the advantage of requiring access to only one end of the sensing fiber. The drawback is that the spontaneous Brillouin scattering signal is much weaker than that of BOTDA.

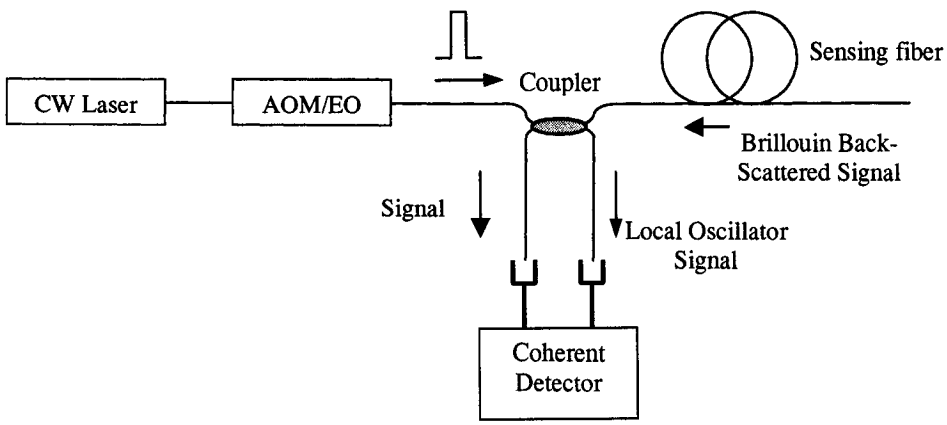

Fig. 2-2 BOTDR coherent detection system.

Shimizu *et al.* at NTT modified their early BOTDA to BOTDR by adding a frequency shifter and a second acoustic-optic modulator (AOM) in a ring configuration. By shifting the frequency at the Brillouin frequency, a lower bandwidth detector could be used in the BOTDR system [Shimizu, *et al.* 1993]. The advantages were: lower cost and better frequency stability due to one laser and minimization of signal distortion from pump depletion or pulse amplification [Horiguchi, *et al.* 1995].

The BOTDR system proposed by NTT [Horiguchi, *et al.* 1989b] was commercialized as the AQ8602 Optical Fiber Strain/Loss Analyzer by Ando Electric

Company, Ltd. (the latest model is AQ8603). The unit has a 40 με strain measurement resolution and 1 m spatial resolution [Technical Data Sheet of AQ8603, Ando Electric Co., Ltd. 2005]

2.3 Single laser BOTDA

Niklès *et al.* at the Metrology Lab (MET-EPFL) of the Swiss Federal Institute of Technology, Switzerland, developed a distributed Brillouin sensor consisting of a single laser [Niklès, *et al.* 1994, Niklès, *et al.* 1996]. A $LiNbO_3$ intensity electro-optic modulator (EOM) was used in the design. The light source was a 1.32 μm diode-pumped single frequency Nd: YAG laser. Through a coupler the light was divided into two portions. One was sent into the sensing fiber while the other one was launched into the EOM, which was driven by a microwave generator.

When a single frequency lightwave is modulated at a frequency ν_m, the modulation gives new frequency lines symmetrically distributed around the incident light or carrier frequency ν_0 in the spectrum, called modulation sidebands. When the modulation frequency ν_m is equal to the Brillouin frequency ν_B, the first-order sidebands can interact with the incident lightwave through a Brillouin scattering process, provided that they propagate in opposite directions [Niklès, *et al.* 1997].

The researchers of the MET-EPFL replaced the 1.32 μm laser with a 1.55 μm laser. Therefore an Erbium-Doped Fiber Amplifier (EDFA) could be deployed in the system.

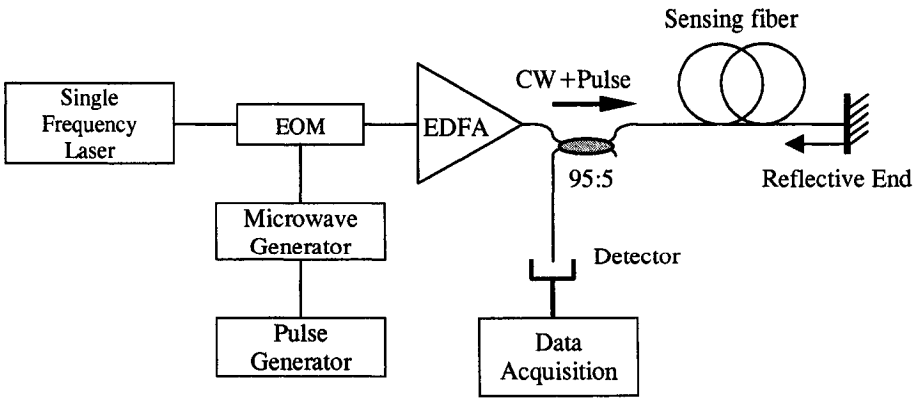

Fig. 2-3 Single laser, single-ended BOTDA system

They also designed the system using a single ended sensing fiber [Fellay, *et al.* 1997]. 1°C temperature resolution, 20 $\mu\varepsilon$ strain resolution, and 1 m spatial resolution were reported for a 10 km sensing fibers. The simplified configuration of this system is shown in Fig.2-3.

2.4 Brillouin optical frequency domain analysis (BOFDA)

Figure 2-4 shows the configuration of a distributed fiber optic sensor based on a Brillouin optical frequency domain analysis (BOFDA) system reported by the Lehrstuhl für Allgemeine Elektrotechnik und Elektrooptik (AEEO) at Ruhr-University, Germany [Garus, *et al.* 1997].

BOFDA is based on the measurement of a complex baseband transfer function, which relates the amplitudes of counter-propagating pump and Stokes waves along a sensing fiber. The lasers and fibers are the same as in the previously described approaches. An amplitude EOM was used to modulate the light of the probe laser with a variable modulation frequency f_m. The output signals were fed to a network analyzer to determine the baseband transfer function of the sensing fiber. The digitized output signal of the network analyzer was fed to a signal processor to get the inverse fast Fourier transform (IFFT). It was reported that the initial test results with the BOFDA system on a 1 km sensing fiber were 3 m spatial resolution, 1.5°C temperature resolution and 40 $\mu\varepsilon$ strain resolution [Garus, *et al.* 1997].

A BOFDA system is similar to a BOTDA system in sensing length and spatial resolution. Since the discrete Fourier transform induces additional averaging effects for uncorrelated noise signals, the noise level of a BOFDA system is lower than that of a BOTDA system for the same total measurement time. Two drawbacks of the BOFDA system include the relatively long measurement time (since BOFDA system needs more effective averaging time) and the requirement that temperature and strain must be constant during the measurement, which is impossible to achieve in a field test.

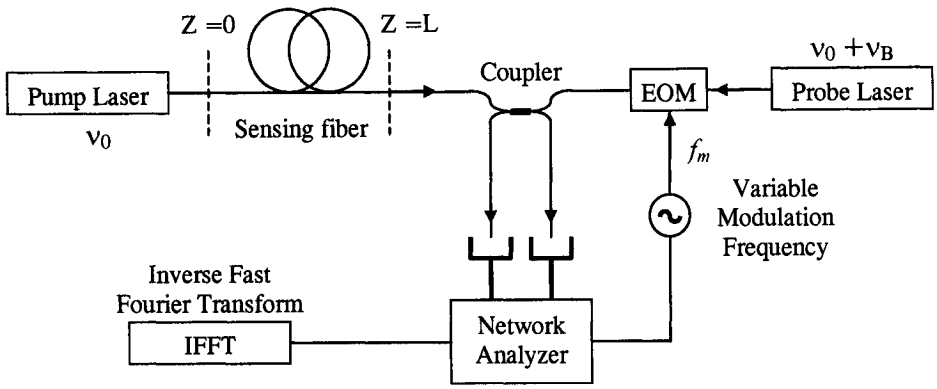

Fig. 2-4 Basic BOFDA configuration.

2.5 Spontaneous Brillouin scattering-based distributed temperature sensing systems

Using a short-pulse-width laser source at a wavelength of 1.5 μm, a 35 cm spatial resolution and 4.3 ℃ temperature resolution were achieved over a 1 km single mode fiber with distributed temperature sensing based on spontaneous Brillouin scattering system as reported by Kee *et al.* at the Optoelectronics Research Center (ORC), University of Southampton, UK, in 2000 [Kee *et al.* 2000b]. They measured the temperature dependence of the Landau–Placzek ratio (the ratio of the intensities of the Rayleigh and the spontaneous Brillouin signals) in their system. In 2001, Maughan *et al.* at ORC reported a calibrated 27-km distributed fiber temperature sensor based on microwave heterodyne detection of spontaneous Brillouin backscattered power. It had a spatial resolution at 20m and a temperature resolution of 3.4°C over 27 km of optical fiber [Maughan *et al.* 2001a].

2.6 Correlation-based Brillouin sensing approach

Researchers at the University of Tokyo introduced a technique to improve the spatial resolution for distributed Brillouin sensing [Hotate and Hasegawa 1999, Tanaka and Hotate 2002]. This is the so called Correlation-Based Continuous-Wave technique [Hotate and Tanaka 2001]. It used simultaneously frequency-modulated lightwaves instead of pulsed lightwaves for locally exciting stimulated Brillouin scattering. SBS was generated at a position where the two lightwaves are highly correlated. A spatial resolution of 1 cm (for 1000 με) has been reported [Hotate and Tanaka 2002].

The basic measurement system is shown in Fig.2-5. A CW 1.55 μm distributed feedback (DFB) laser diode was used as light source for both probe and pump. The laser was modulated by a sinusoidal wave with a frequency f_m. The output light beam from the laser was divided by a 50:50 coupler into two beams: the first beam entered EOM-1 as probe, and the second entered EOM-2 as pump. These two counter propagating beams created a series of beat peaks (called correlation peaks) along the fiber as they were modulated with an identical frequency, f_m. The distance between the adjacent two peaks was $d_m = v_g/2f_m$. d_m can be changed by varying the modulation frequency f_m of DFB laser.

The first beam was modulated by EOM-1 at microwave frequency v_m to generate two modulation sidebands around the optical frequency v_0 of the DFB laser [Niklès, 1996]. The lower sideband at $v_0 - v_m$ serving as the probe, propagated against pump in the fiber and reached the detector, while the upper sideband was eliminated by the optical filter.

The second beam was chopped by EOM-2 (for lock-in purpose) and amplified by passing through an erbium-doped fiber amplifier (EDFA) before entering the sensing fiber. There was a delay line added in after EOM-2 to keep the two beams in phase.

Through changing the frequency v_m of the probe modulator, the system creates a Brillouin gain spectrum. By varying the modulating frequency f_m to the laser source, the correlation peak was shifted along the fiber, and Brillouin gain spectrum was obtained as a function of position [Hotate and Tanaka 2002]. At the position where the correlation peak takes place, the frequencies of the two beams change synchronously and the frequency difference between two beams was kept constant. In this case, the Brillouin

gain spectrum takes the same shape as an intrinsic spectrum without the modulation. On the other hand, at another position where the correlation is low, the frequency of the probe relative to the pump changes continuously, and that results in suppression of the gain. Stimulated Brillouin scattering (SBS) was only triggered by interference at locations in the fiber where the sensing fiber was under strain, so that high correlation occurs between the probe and pump lightwaves at that location [Hotate and Hasegawa 1999].

The pump and probe light are launched oppositely to each other into a fiber under test. The probe obtained gain from the pump. A part of the probe passes through a 10-dB coupler and an etalon filter, which is used to eliminate light except for the probe, and is detected by a photodetector (PD). The electrical signal from the PD consists of the ac element, caused by the chopping of the pump, and the dc element. The former is extracted by a lock-in amplifier and the latter by a low pass filter. During the measurement, the following operation was repeated under the control of a computer: (1) obtain a Brillouin gain spectrum by sweeping the frequency (ν_m) of microwave applied to the EOM-1 and store the data of the gain in an oscilloscope, and (2) change the frequency f_m that determines the distributed measurement by using a nonzero correlation peak scanning a strained section.

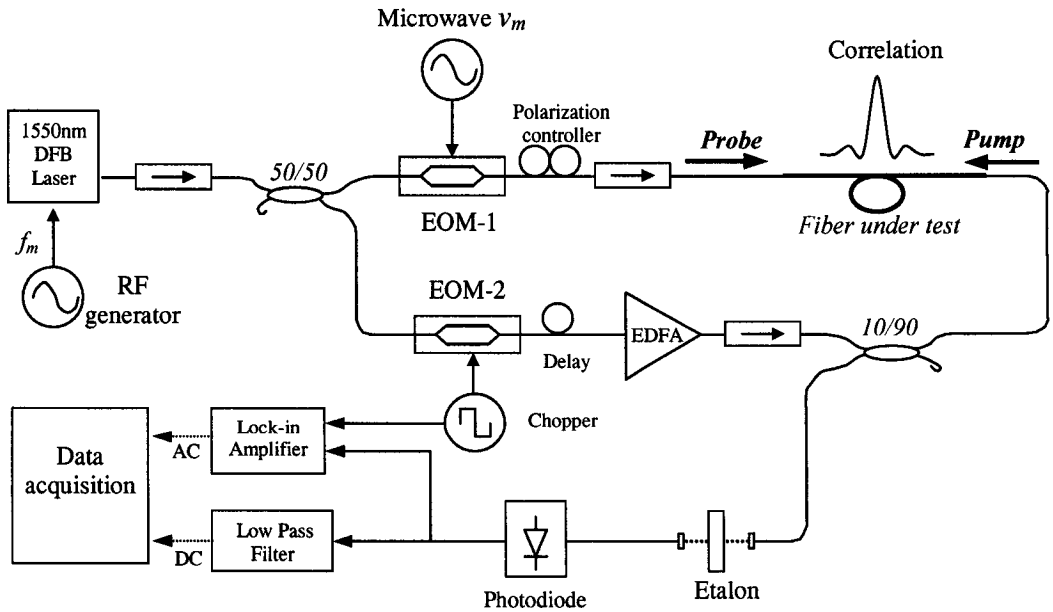

Fig. 2-5 Distributed Brillouin sensing based on the correlation technique.

Since in this technique there was no pulse being used to give location information, it used "zeroth" peak position as a reference (The "zeroth" peak is the position at which the difference of the optical path length between the pump-and-probe from the light source is equal to zero.)

The drawbacks of this approach are short sensing range and long testing time (on the order of an hour for a few meters of fiber). Because of the delay line, it would be difficult to determine the exact location of a stain section since the "zeroth" peak position could vary.

2.7 Dark pulse approach

Brown *et al.* reported a distributed sensing technique based on dark-pulse Brillouin scattering [Brown *et al.* 2005]. The sensing system was a two-laser BOTDA. In that configuration, two counter-propagated CW laser beams were used. The probe was created by switching one of the CW lightwave off for a short duration. This duration of the extinction of the Stokes light was called a "dark pulse". A 0.5 ns pulse for a 6 με strain resolution on a 100-m fiber was reported. The drawback of this approach was apparent: the large CW power levels involved may result in stimulated Brillouin scattering (SBS) if long fibers are used. A quasi-CW power of 80 mW will exceed the SBS threshold for standard fibers that are over a few hundred meters in length.

2.8 BOTDA system at the University of Ottawa

The BOTDA system at the University of Ottawa was originally designed and built by the team headed by Dr. Bao at the University of New Brunswick (UNB). It was rebuilt by the fiber optic team at the University of Ottawa in 2001.

The configuration is shown in Fig. 2-6. The light sources are two tunable Nd:YAG (neodymium-doped yttrium aluminum garnet) lasers operating at 1319 nm. The optical pulse is created by use of an electro-optic modulator (EOM) driven by a pulse generator

over a wide range of pulse widths (1 to100 ns, equivalent to 10 cm to 10 m spatial resolution). The time-domain signals are detected at certain frequency intervals to produce the Brillouin loss spectra by use of a 1-GHz bandwidth receiver and acquired via signal averaging by a 1-Gb/s digitizer.

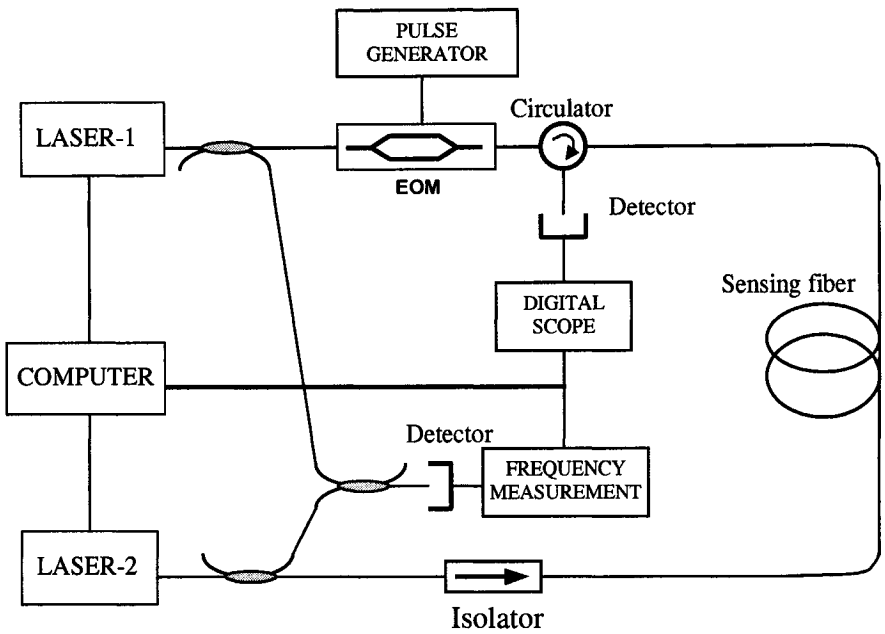

Fig. 2-6 Brillouin loss based BOTDA system developed by our group.

The system was modified by attaching two polarizing beam splitters, which made the use of polarization-maintaining fibers possible. Three major commercial PM fibers were characterized as sensing media for the first time. The resolution was 0.5°C for temperature and 7 με for strain using PANDA PM fiber [Yu *et al.* 2004a] [Yu *et al.* 2004b]. Details will be discussed in Chapter 3, 4 and 5.

2.9 Simultaneous strain and temperature measurement

Due to the cross sensitivity of Brillouin frequency to strain and temperature, it is impossible to directly differentiate strain from temperature if one only monitors the

Brillouin frequency. Early solutions to this problem suggested placing a second fiber, isolated from strain effects, adjacent to the strain-sensing fiber [Bao *et al.* 1994b]. This fiber would be used for temperature monitoring, and the frequency shift resulting from any temperature effects could then be subtracted from the combined frequency shift to determine the strain on the structure.

Subsequently, simultaneous strain and temperature measurement using single fiber has been an active research area since 1997 when Parker *et al.* resolved strain and temperature effects by simultaneously measuring noise-initiated Brillouin scattering power and frequency shift in optical fibers [Parker *et al.* 1997a, Parker *et al.* 1997b; Parker, *et al.* 1998]. To normalize the spontaneous Brillouin signal, they presented a new technique that mathematically combines the Stokes and anti-Stokes powers to produce a linear effective power. Using their technique, Parker *et al.* reported 100 με strain resolution, 4°C temperature resolution, and 40m spatial resolution over a 1.2 km sensing fiber in 1998 [Parker, *et al.* 1998].

Bao's group achieved strain and temperature resolutions of 178 με and 3.9°C respectively at a spatial resolution of 3.5 m on a 50 m PM fiber using stimulated Brillouin scattering [Smith 1999; Smith *et al.* 1999a].

The NTT group reported results of 260 με strain and 11°C temperature resolutions and a 1m spatial resolution over a 100 m fiber [Ohno *et al.* 1999]. They used a BOTDR system to detect the spontaneous Brillouin scatting.

Simultaneous measurement of strain and temperature was demonstrated also by the Optoelectronics Research Center (ORC), University of Southampton, UK. They obtained 290 με and 4°C resolution and a 10 m spatial resolution on a 15 km fiber length [Kee *et al.* 2000a]. They used the Landau–Placzek ratio (the ratio of the intensities of the Rayleigh and the spontaneous Brillouin signals) and cascaded Mach–Zehnder interferometric filters to measure both the intensity and the frequency changes in the Brillouin backscattered signal. Recently the same group reported a new approach using spontaneous Raman and Brillouin scattering to measure strain and temperature simultaneously. The magnitude of the intensity of the anti-Stokes Raman signal was used to determine the temperature. Once the temperature has been determined the strain can then be computed from the frequency measurement of the Brillouin signal. They have

achieved a temperature resolution of 6°C and a strain resolution of 150 με with a spatial resolution of 10 m for a range of 23 km [Alahbabi *et al.* 2005].

Lee *et al.* at National Chiao-Tung University (NCTU) in Taiwan used a large-effective-area nonzero dispersion-shifted fiber (LEAF) to demonstrate the simultaneous measurement of strain and temperature. A LEAF fiber has compound compositions in its core. The multipeak structure in Brillouin spectrum of this optical fiber is arises from the different acoustic velocities, which are due to different compositions or doping concentrations in the core. The two main peaks in the Brillouin spectrum were used due to the fact that they have different strain and temperature coefficients. The test results gave 5°C and 60 με resolutions and 2 m spatial resolution in a 3.7 km fiber [Lee *et al.* 2001].

Zou *et al.* in our fiber optic group at the University of Ottawa demonstrated simultaneous measurement of strain and temperature using photonic crystal fiber (PCF) [Zou *et al.* 2004a]. A PCF has a small, solid-silica core with multiple air holes typically arranged in a hexagonal lattice about the core to act as a cladding. The Brillouin spectrum of PCF showed multi-peaks due to waveguide and antiwaveguide types of sound propagation. The two main peaks in the Brillouin spectrum have different strain and temperature dependence attributed to the scattering from longitudinal acoustic waves in the Ge-doped center region and the solid pure-silica region of the core of the PCF. 1.3°C temperature resolution and 15 με strain resolution were obtained with a spatial resolution of 15 cm.

2.10 Work done by the Fiber Optics Group at the University of Ottawa

The distributed sensor based on Brillouin loss at the University of Ottawa was based on the work done at the University of New Brunswick (UNB) by Dr. Bao and her students [DeMerchant *et al.*1998; Brown *et al.* 1998]. It was an automated version of a two-laser BOTDA system rooted in the research of Dr. Bao at the University of Kent [Bao *et al.* 1993b] [Bao *et al.* 1995].

At the University of Ottawa, the Brillouin sensor was re-constructed in 2001. Over time, some components were introduced into the system such as the free space tunable attenuator. The damaged laser was repaired and the defective circulator was replaced with a new one. Most of the ST (Straight Tip) connectors on the components, which have a poor repeatability in nature, were replaced with FC/PC (Face Contact/Physical Contact) connectors.

The system has been used for field tests as well as for experimental studies in the lab, and many interesting results were published. Here I just mention a few: By using our system, strain in a nuclear reactor concrete wall [Zeng *et al.* 2002b] and a concrete bridge [Zeng *et al.* 2002c] were monitored. A steel pipeline was tested for its strain under elevated pressure [Zou *et al.* 2004a]. As for sensing technology research and development, the effect of optical phase on a distributed Brillouin sensor at centimeter spatial resolution was studied [Bao *et al.* 2004b]. Subpeaks in the Brillouin loss spectra were explained [Wan *et al.* 2005]. Simultaneous measurement of strain and temperature using photonic crystal fiber was examined [Zou *et al.* 2004a]

The BOTDA system was modified by the author to use PM fiber as a temperature and strain sensing medium in 2003. Numerous interesting results were obtained and published in Optics Letters [Yu *et al.* 2004a, Yu *et al.* 2004b, Bao *et al.* 2004, Yu *et al.* 2005, Bao *et al.* 2006]. Those works will be discussed in detail in this thesis.

Chapter 3

Polarization Maintaining Fibers and Their Application for Brillouin Scattering Sensing

In the stimulated Brillouin scattering process, the electric fields from the probe and pump waves interfere with each other to establish a beat pattern. The Fresnel-Arago Laws state in part that it is not possible for two orthogonal polarization states to interfere; hence it is only the parallel components of two coherent light waves that generate interference [Hecht 1990]. If the two fields are in randomly varying polarization states, the interference pattern also varies and exhibits reduced contrast. This could create a varying Brillouin signal intensity [Brown 2000]. In Brillouin sensing, that means the measurement accuracy is affected by the polarization states of the pump and probe light fields [Horiguchi *et al.* 1989c; Deventer and Boot 1994]. In particular, because the refractive index in (SM) single-mode fibers is inhomogeneous and sensitive to the environmental change, the polarization states of the propagating light fields are not stable. Using a polarization mode scrambler can reduce but not eliminate the polarization noise in Brillouin sensing [Zeng 2002]. Therefore, use of polarization maintaining fiber is of a great interest to improve the performance of Brillouin sensing.

3.1 Structure of SM fiber and PM fiber

3.1.1 Single mode fiber

A single mode (SM) fiber contains two distinct layers: the core (GeO_3 doped SiO_2) and the cladding (SiO_2). The core contains 80-90% of the transmitted light whereas the cladding transmits the rest. On the outside of the cladding there is a buffer coating layer (usually acrylic) to provide a bendable mechanical support and a protective barrier for the fiber. The most commonly used SM fiber is Corning SMF-28 as shown in Fig. 3-1

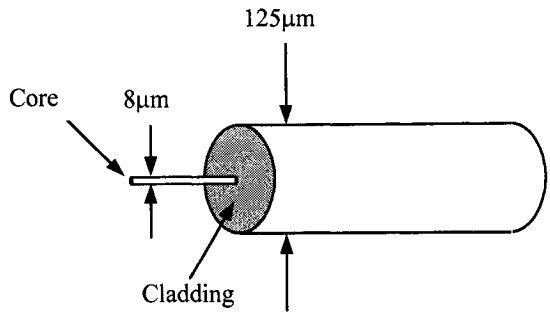

Fig.3-1 SMF-28 single mode fiber.

3.1.2 Polarization Maintaining Fibers

A polarization maintaining (PM) fiber is a highly birefringent fiber. The birefringence is induced by an internal stress either by means of an elliptical core, an elliptical cladding or with stress rods located on opposite sides of the core. Many PM fibers with different structures were designed and tested in the early days of PM fiber development [Noda *et al.* 1986]. However, only a few PM fibers have been successfully commercialized. The most commonly available PM fibers are: PANDA, Bow-tie, Tiger (elliptical cladding) and elliptical core. Since the elliptical core PM fiber has an elliptical mode field that is troublesome in mode matching to our sensing system, it was excluded from our experiments.

PANDA (Polarization-maintaining AND Absorption-reducing) fiber

PANDA fiber is fabricated by adding two stress applying rods at either side of the core as shown in Fig. 3-2 (a). The cladding is pure silica glass and the core is made of GeO_2 doped silica glass. The stress-rods contain B_2O_3 and GeO_2 doped silica glass. PANDA's slow axis passes along the center of the two stress rods whereas the fast is perpendicular to the slow axis as shown in Fig. 3-2 (b). Light travels slower along the slow axis than it does along the fast axis.

PANDA fibers are usually manufactured in the following processes [Sasaki *et al.* 1983]: First, the preforms of the stress-rods are made by the MCVD (modified chemical

vapour deposition) method. Then, two stress-rods are inserted into the two holes pre-drilled in the core preform. Finally, the assembled preform is heated to a high temperature and drawn into a fiber. Since the thermal expansion coefficient of the rods is larger than that of the core and the cladding, a stress is created as the fiber cools during the pulling process [Hosaka *et al.* 1981, Shibata *et al.* 1983]. The PANDA fiber used in our experiment was provided by Fujikura.

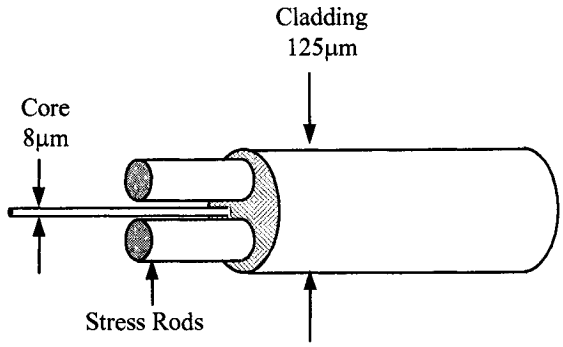

a) Structure of PANDA fiber.

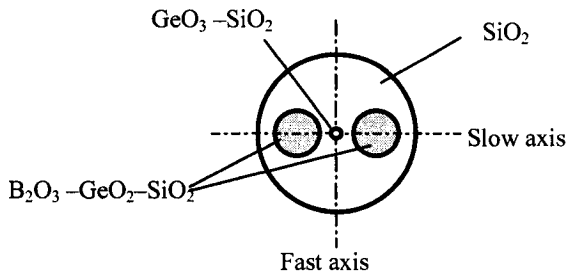

b) Cross section of a PANDA fiber.

Fig. 3-2 PANDA fiber

Bow-tie Fiber

Bow-tie fiber is similar in structure to PANDA fiber except that the stress-rods have a "bow tie"-shaped cross section as shown in Fig.3-3. The stress rods in Bow-tie fiber are made by a gas-phase-etching process. First, a B_2O_3 layer is deposited on the inside of a silica tube by MCVD. Second, the part of the layer on either side of the tube is removed

by gas etching. Third, a layer of pure silica is deposited on the top of partially B_2O_3 etched tube. Fourth, the tube is heated up to high temperature, and the tube collapse into a solid preform. The partially etched B_2O_3 doped region forms the bow-tie shaped stress rods [Stolen *et al.* 1982, Birch *et al.* 1982]. The Bow-tie fiber was commercialized by Fibercore Ltd., in Southampton, England in 1983.

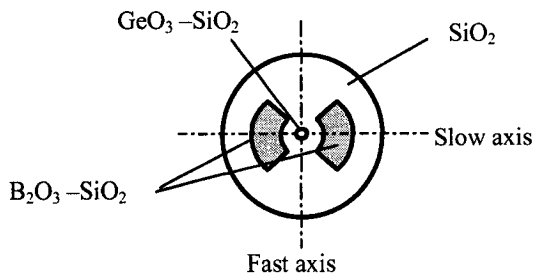

Fig. 3-3 Cross section of a bow-tie fiber.

Tiger Fiber (Elliptical cladding fiber)

Elliptical cladding fiber is one of the oldest PM fibers [Ramaswamy *et al.* 1979]. Tiger is the commercial name of elliptical cladding fiber manufactured by 3M [Data sheet, 3 M 2001]. It features circular core and cladding sections, surrounded by a second cladding (an elliptical stress-applying region), with a circular outer diameter. The structure is as shown in Fig.3-4.

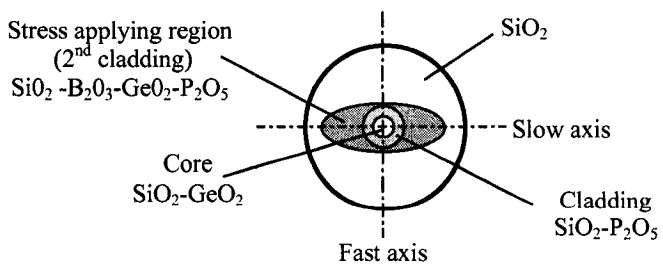

Fig. 3-4 Cross section of a Tiger fiber.

Tiger fiber is made by a so-called "shaped cladding" method [3M catalog 2001]. A circular layered preform is prepared by the MCVD. Then the cross section of the preform is made into a drum-like shape by removing part of the material on the opposite side of the preform. The preform then is then heated and pulled into a thin, long fiber. The second cladding has a lower softening point than that of the core and the first cladding layer. Therefore it is pressed into an elliptical shape during the heating and pulling process because the outsider glass is forced to be a circular shape by its surface tensions. The thermal expansion coefficients are different for core and claddings therefore the core is subject to a stress resulting in birefringence.

Table 3.1 Listed birefringence and transmission loss of the selected PM and SM fibers [Noda *et al.* 1986].

Table 3-1 Birefringence and Transmission Loss of Selected PM and SM fibers.

Types	Birefringence	Loss (dB/km)	Wavelength (nm)
PANDA	5.9×10^{-4}	0.3	1300
Bow-Tie	6.7×10^{-4}	1.0	820
Elliptical -cladding (Tiger)	4.7×10^{-4}	1.0	633
Single mode fiber	10^{-6}	0.4	1310

3.2 Properties of Polarization Maintaining Fibers

Owing to birefringence in the PM fibers' core induced by stress rods or the elliptical cladding, PM fibers maintain the polarization state of linearly polarized light that is launched into the fiber core along one of its principal axes as shown in Fig. 3-2(a). If the input light beam is aligned off-axis, the output polarization state will be arbitrary as shown in Fig. 3-2(b). Consequently, both the linearly polarized probe and pump waves must be aligned with either the slow or fast axis for Brillouin sensing applications.

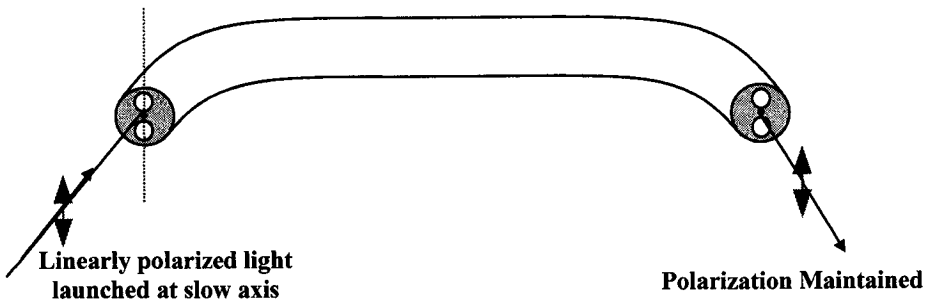

Fig. 3-5 (a) Linearly polarized light aligned with slow axis.

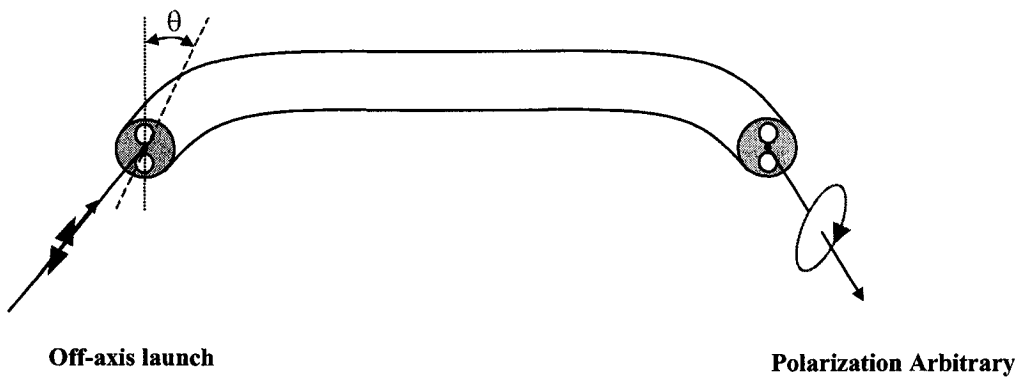

Fig. 3-5 (b) Linearly polarized light aligned off-axis into PM fiber.

The important parameters of PM fibers are [Agrawal 1997]:

Birefringence, defined as

$$B = \left| n_x - n_y \right|. \tag{3-1}$$

where n_x and n_y are the refractive indices of the two principal axes.

Beat length, defined as

$$L_B = \lambda / B, \tag{3-2}$$

where B=10^{-6}~10^{-7} and B=5x10^{-4} in SM fiber and PM fiber, at λ=1319 nm, L_B is ~1.3-13 m and ~1 cm for SM fiber and PM fiber, respectively.

Extinction ratio (ER), defined as

$$ER(dB) = 10 \times \log_{10}\left(\frac{P_{\max}}{P_{\min}}\right), \tag{3-3}$$

where P_{max} and P_{min} are the maximum and minimum transmitted powers respectively after light passes a rotating polarizer. Commercial PM fibers usually have an ER of about 40dB. If they are connectorized, their ER drops. For most applications, including sensing, 20dB ER is a minimum requirement. ER is a measure of how well the fiber can maintain the linearity of the polarized light wave.

3.3 Polarizing Beam splitter

In our BOTDA system, two pigtailed polarizing beam splitters were used in order to use PM fibers. A polarizing beam splitter (PBS) is formed by coating the hypotenuse face of an isosceles right angled prism with a number of thin-film dielectric layers and then cementing it to an identical prism as shown in Fig. 3-6(a). The optical thickness of each layer and the refractive indices of the thin-film materials are chosen such that the reflectance of the p-polarized component of the electric-field vector approaches zero while the reflectance of the s-polarized component remains high [Pezzaniti and Chipman 1994]. The cube is pigtailed by butt coupling a single-mode fiber input and two PM fibers outputs. The pigtailed polarization beam splitter used in our sensing system is illustrated in Fig. 3-6(b).

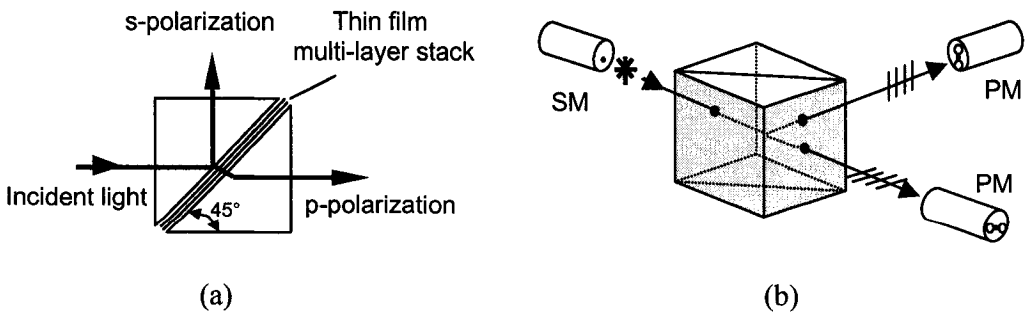

Fig. 3-6 (a) Structure of polarizing beam splitter cube;
(b) Pigtailed polarizing beam splitter.

3.4 Optical circuit attached to the BOTDA for using PM fibers

Figure 3-7 shows the BOTDA configuration for using PM fibers in our lab. On the left-side of the dashed line is the standard configuration (see Fig. 2-6 in Chapter 2) for using an SM sensing fiber. The right side is the optical circuit attached for using a PM sensing fiber. The input of the PBS was an SM fiber. Two outputs were PM fibers. One of the connector's key-ways was aligned with the slow axis, and the other was aligned with the fast axis. The polarization controller rotated the light into s-polarization or p-polarization corresponding to transmission or reflection of the PBS. A pair of PBS at each side of the sensing fiber guarantees that the probe and pump light waves had the same polarization when counter-propagating in the PM fiber.

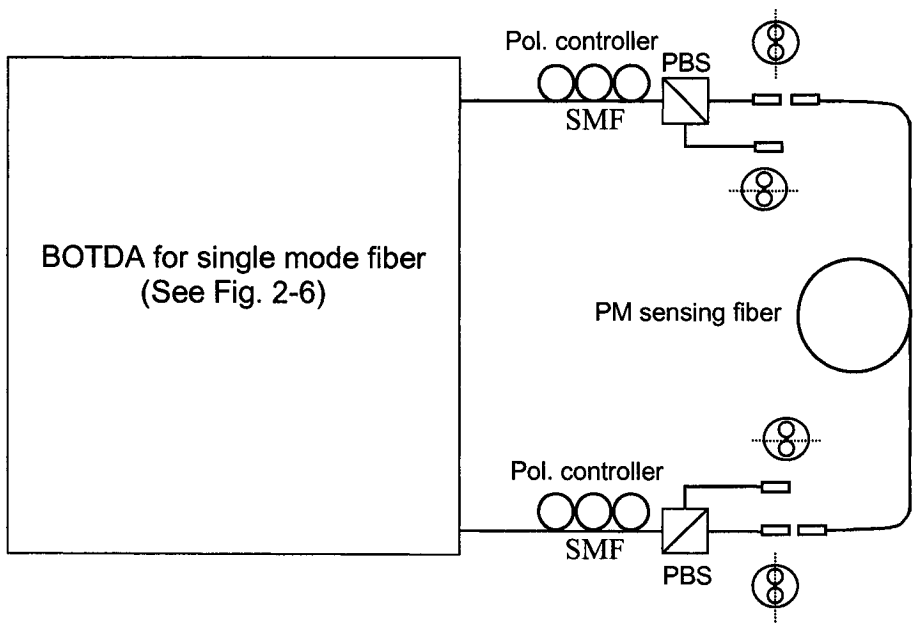

Fig. 3-7 Configuration of BOTDA using PM fiber as the sensing medium.

3.5 Comparisons of SM and PM fiber in Brillouin scattering

The residual birefringence in single-mode fibers along with environmental variations such as temperature and strain both cause the light polarization to vary randomly along the fiber. Therefore, a polarization scrambler is needed to reduce the polarization mode dispersion effect if one uses single mode fiber.

For PM fiber, if the polarizations of the two counter-propagated beams are aligned, the Brillouin scattering efficiency is maximum and uniform along the fiber. Fig. 3-8 shows the waveforms of an SM fiber (in grey) and a PM fiber section (in black) inserted in the middle of an SM fiber. Compared with the single-mode, the Brillouin loss profile of PM fiber clearly shows a more uniform loss over its fiber length.

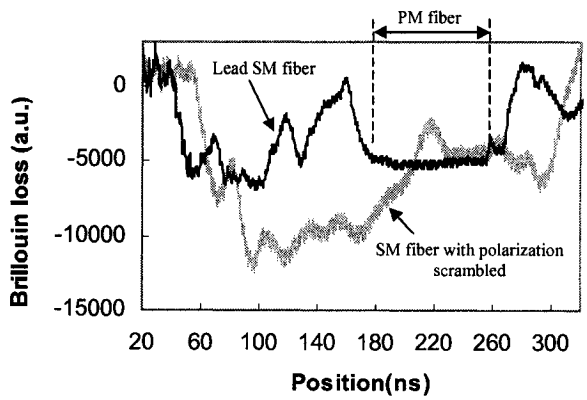

Fig. 3-8 Waveforms of SM and PM fiber (in a 10 m section).

Chapter 4

Temperature dependence of Brillouin frequency, intensity and bandwidth in PANDA, Bow-tie and Tiger PM fibers

[This chapter is adapted from the paper published in OPTICS LETTERS, 29, 17-19 (2004)]

4.1 Introduction

A distributed Brillouin sensor can be used for structural health monitoring to measure the cracks in civil structures. In field tests, both temperature and strain are unknown. If only the Brillouin frequency is measured, two fibers are needed [Bao *et al.* 1994], one to detect the temperature and the other to detect the strain. In practice, it is difficult to install a second temperature-sensing fiber that is totally isolated from the strain.

A few studies on measuring temperature and strain simultaneously in one fiber with a distributed fiber sensor have been reported [Parker *et al.* 1997, Smith *et al.* 1999, Kee *et al.* 2000]. A hundred to a few hundred micro-strain and a temperature resolution of a few degrees with a spatial resolution of a few to a few tens of meters have been achieved. One of the major limitations in spatial, temperature, and strain resolution is related to the intensity fluctuation induced by variation of the polarization states along single-mode fibers, which is caused by polarization mode dispersion (PMD), unless the principal state of polarization (PSP) is launched. However, the PSP changes with temperature, strain, and stress along the fiber length. This introduces higher-order PMD. As a result, the Brillouin interaction between two counter-propagating beams fluctuates along the various positions of single-mode fibers. The polarization-maintained fibers can be considered as a fiber with only a first-order PMD effect in the fiber. Its two polarization-maintaining (PM) states are equivalent to two PSPs. If we launch into one of the PSPs of the PM fiber, there is no polarization variation and less power fluctuation, and the PSP is a weak function of temperature. Even with the temperature and strain variations along the PM fibers, the intensity fluctuation caused by the variation of the polarization states from

temperature and strain is not as strong as in the case of the single-mode fiber. With the Brillouin intensity and frequency shift measurements, we can achieve simultaneous temperature and strain sensing with high accuracy.

Although Smith *et al.* used a PM fiber (3M Tiger) as a sensing fiber [Smith *et al.* 1999a] no polarizing device was used for the connection between the single-mode and PM fibers. The Brillouin gain signal fluctuated as in the single-mode fiber. In this study we launched the input light along one PM axis of a PM fiber to propagate pump and probe waves. The three most common PM fibers, PANDA, Bow-tie, and Tiger PM fibers were used in this experiment to characterize the dependence of the Brillouin loss spectrum on temperature for its frequency, intensity, and bandwidth.

For PM fibers the refractive index of two orthogonal axes, i.e., the slow axis and the fast axis, is different. The difference in the Brillouin frequency shift for the slow axis and the fast axis can be described as

$$\Delta \nu_{Bsf} = \frac{2V_a}{\lambda}(n_{slow} - n_{fast}), \tag{4.1}$$

where n_{slow} and n_{fast} are the refractive index of slow axis and fast axis respectively. V_a is the speed of the acoustic wave. λ is the optical wavelength. Take λ=1310 nm, V_a ~6000 m/s, $\Delta n = n_{slow} - n_{fast} = 4\text{x}10^{-4}$, then $\Delta \nu_{Bsf}$ =3.66 MHz. This number is similar to what we measured in PANDA, Bow-tie and Tiger fibers.

4.2 Experiment setup

The Brillouin sensing system was described in Fig. 3-5. The PM fibers under test were placed in a bench-top environment chamber (ESPEC ETC-3) which has a temperature constancy of $\pm 0.5\,^{\circ}$C. The experimental setup is as shown in Fig. 4-1.

All PM fibers used in our experiment have been tested to have ER $\geq$25 dB. When the PM fiber was connected to the system, the polarization was measured to yield an ER of 20 dB for each connector and each axis. For each type of PM fiber, two pieces of fiber were tested in the experiment. The input power for the cw beam was 5 mW, and the pulse power was 6 mW. The pulse width was 2 ns, which is equivalent to a 20-cm spatial resolution.

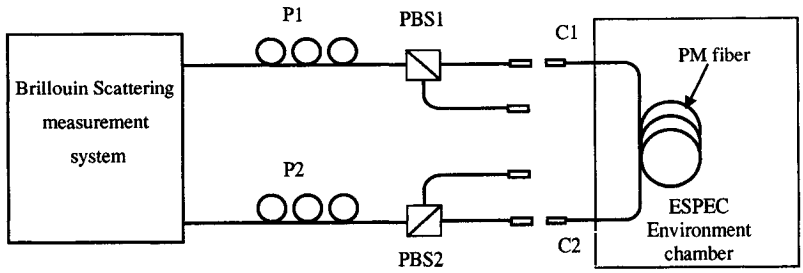

Fig. 4-1 Set-up for Brillouin scattering measurement of PM fibers

4.3. Results and discussion

Figure 4-2 shows the Brillouin frequency shift versus temperature for three PM fibers. The temperature coefficient is C_{vT} =1.37MHz/°C for PANDA fiber at both the slow and the fast axis. The frequency difference between the fast and the slow axis is $\Delta\nu_{Bsf}$ =3.6 MHz. The spectrum bandwidth is shown in Fig. 4-3. The bandwidth decreases from 49.5 MHz at –60°C to 29.2 MHz at 80°C, corresponding to $\Delta\nu/\Delta T$= -0.146MHz/°C. The normalized Brillouin scattering intensity increases with temperature as shown in Fig. 4-4. Both Figs. 4-3 and 4-4 show the dependence of the slow axis for PANDA, fast axis for Bow-tie and Tiger. The behavior of the slow axis is the same as that of the fast axis.

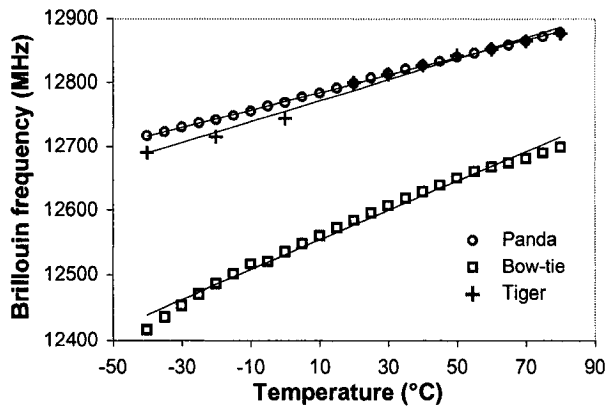

Fig. 4-2 Temperature dependence of Brillouin frequency shift of PANDA, Bow-tie and Tiger PM fibers at fast axis.

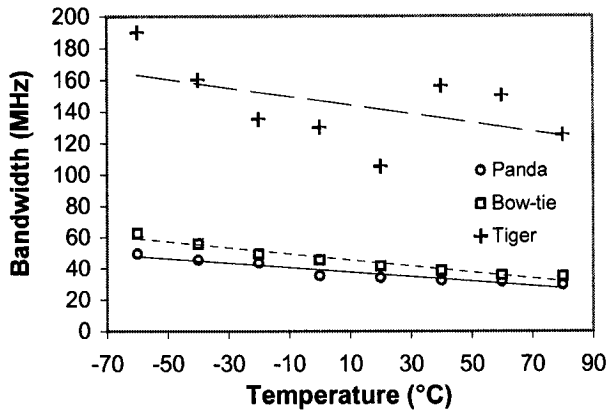

Fig. 4-3. Temperature dependence of Brillouin bandwidth in PM fibers (slow axis for PANDA, fast axis for Bow-tie and Tiger).

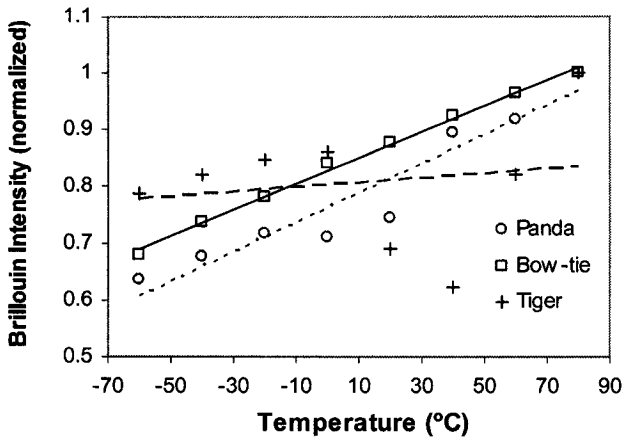

Fig. 4-4 Temperature dependence of Brillouin intensity (The maximum intensity at 80 ° C is normalized to 1) for the three PM fibers (slow axis for PANDA, fast axis for Bow-tie and Tiger).

It was noticed that the Brillouin frequency shift of the Bow-tie PM fiber was lower than that of the single-mode fiber (12.6 versus 12.8 GHz at 20℃). The temperature coefficient $C_{\upsilon T} = 2.30$ MHz/ ° C was almost twice that of the single-mode fiber for the same wavelength. One can see that for Bow-tie fiber, there is a deviation of Brillouin frequency from linearity at low and high temperature. That was caused by the polyvinyl

chloride jacket. One of the PANDA fibers in a loose tube showed similar behavior for Brillouin frequency measurement. Among the three PM fibers, only the Bow-tie fiber had a thick jacket (0.9-mm polyvinyl chloride).

To show the relationship between the slow axis and the fast axis, the Brillouin frequency shift was measured from 0 to 40 °C, as shown in Fig. 4-5. Two straight lines are parallel with the same slope of 2.34 MHz/ °C and are separated by 2.9 MHz.

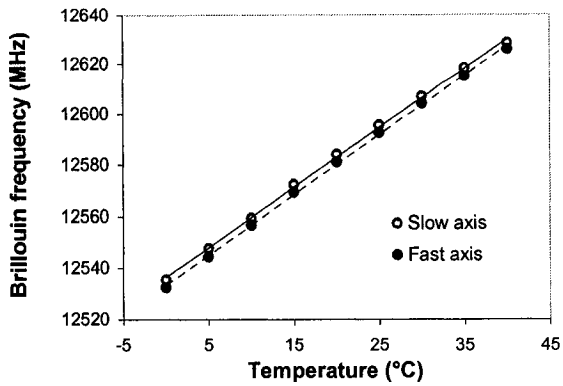

Fig. 4-5 Temperature dependence of Brillouin frequency shift of Bow-tie fiber between fast and slow axis.

Both the PANDA and the Bow-tie PM fibers have a linear temperature dependence on the Brillouin bandwidth and intensity, as shown in Figs. 4-3 and 4-4.

From Figs. 4-2 to 4-4 we see that the Tiger fiber had higher fluctuation in frequency, intensity, and bandwidth than PANDA and Bow-tie fiber. Tiger fiber had a temperature coefficient of C_{vT} =1.66 MHz/ °C, the difference between the slow and fast axes was 4.3 MHz (averaged). If taking a close look at the Brillouin frequency versus distance plot as shown in Fig. 4-6, one can see that the Brillouin frequency of Tiger fiber goes up and down over the distance. However, the Brillouin frequency versus distance for the PANDA and Bow-tie is relative flat and smooth although the three fibers were tested under the same conditions.

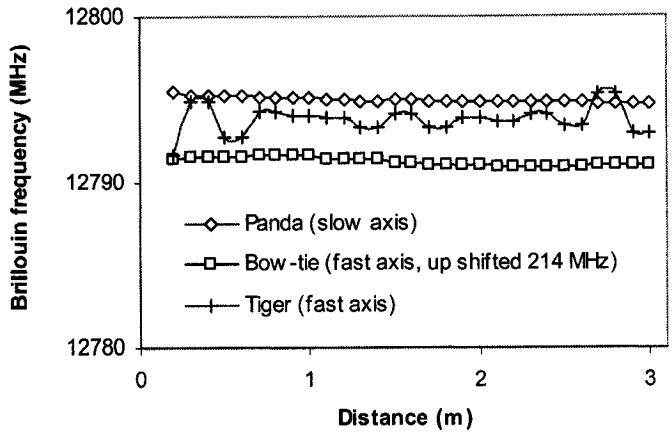

Fig. 4-6 Comparison of time traces (at 20℃) flatness for the three PM fibers (Bow-tie is up shifted 214MHz for comparison)

Fig. 4-7 shows the normalized Brillouin spectra at 20℃ for PANDA (peak at 12795 MHz; BW≈34 MHz), Bow-tie (peak at 12581 MHz; BW≈41 MHz) and Tiger (peak at 12798 MHz; BW ≥300 MHz) fibers. We found that the Brillouin spectrum of the Tiger fiber was asymmetric so that its peak frequency obtained by curve fitting was higher than that apparent in Fig.4-7. Its peak intensity is only half that of the Bow-tie and PANDA fibers and the BW is 7–9 times broader than those of Bow-tie and PANDA fibers. This unique feature of Tiger fiber may be attributed to its elliptical cladding structures.

As we learned from a reported study [Yu *et al.* 2002] on a circular double cladding SM fiber, the thermal stress (due to differences in thermal expansion coefficients of the layers) across the double cladding fiber could induce a local distribution of longitudinal acoustic waves and densities, which in turn affects the behavior of the Brillouin frequency shift and Brillouin bandwidths. Tiger fiber's structure is more complicated than that of the double cladding SM fiber. It is believed that because of the irregular transverse shape of the second cladding (Fig.3-4) in a Tiger fiber, there exist many acoustic modes corresponding to very close Brillouin frequencies. Thus the laser beam excites all acoustic modes at the same time. Each of these acoustic modes has its own

Brillouin frequency and bandwidth. Therefore, a Brillouin spectrum of Tiger fiber shows a broad bandwidth with low peak intensity.

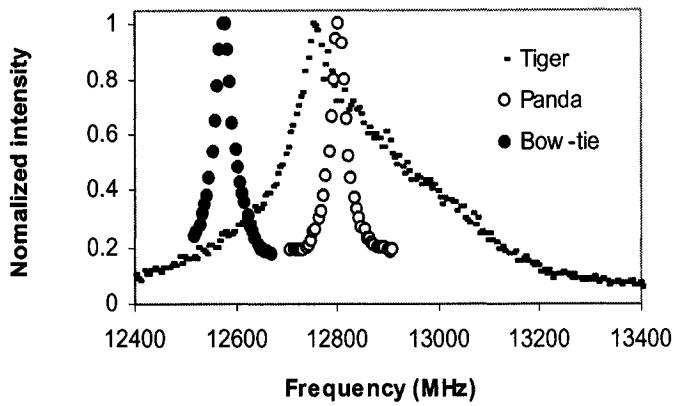

Fig. 4-7 Normalized Brillouin spectra of unstrained PANDA, Bow-tie and Tiger fiber at 20℃.

The asymmetry of the Tiger fibre's Brillouin spectrum can be attributed to input power drift. For the spectrum of Tiger fiber in Fig.4-7, it took 9 minutes to scan the beat frequency from 12400 MHz to 13400 MHz with a step of 5 MHz. During that period of time, the input pump (or probe) power drifted. As a result, an asymmetric Brillouin spectrum was obtained. Compared to Tiger fiber, the time to obtain the spectrum of PANDA or Bow-tie fiber was much shorter (with same step size), requiring only 1 to 3 minutes (depending on the frequency range).

The deviation from the linear fit for the Tiger fiber is the largest among the three PM fibers for the Brillouin frequency, intensity, and bandwidth measurement, as shown in Tables 4-1 and 4-2. The Bow-tie fiber is the most promising candidate for distributed Brillouin temperature sensing. Its temperature measurement uncertainties for the Brillouin frequency are ~1.5 ℃ at a 20 cm spatial resolution, as shown in Table 4-2. The thick jacket induces the high error at low and high temperatures for the Bow-tie fiber.

Table 4-1 Temperature dependence of frequency $\Delta\nu_B$, intensity ratio and bandwidth BW.

PM fiber type	PANDA (slow axis)	Bow-tie (fast axis)	Tiger (fast axis)
$\nu_{B(slow)}$ (MHz) at 20℃	12799.2	12584.0	12799.6
$\nu_{B(fast)}$ (MHz) at 20℃	12794.8	12581.0	12793.6
$\nu_{B(slow)} - \nu_{B(fast)}$	3.6	2.9	4.3
$C_{\nu T}$ (MHz/°C)	1.37	2.30	1.66
Intensity ratio (P_{tiger}=1)	1.9	5.9	1
C_{pT} (%/°C)	0.26	0.23	0.04
BW at 20℃ (MHz)	33.7	41.5	300
C_{BwT} (MHz/°C)	0.15	0.20	0.20

Note: C_{pT} is the intensity coefficient and C_{BwT} is the bandwidth coefficient.

Table 4-2 Standard error (StdErr) of measurement (– 40°C to + 80°C) and the equivalent temperature uncertainty ΔT for PM fibers.

PM fiber type	PANDA (slow axis)	Bow-tie (fast axis)	Tiger (fast axis)
StdErr of BS Freq. (MHz)	0.56	3.20	3.14
ΔT (℃)	0.3	1.4	1.9
StdErr of BS Freq. (MHz) (0 ~40℃)	0.3	0.3	2.7
ΔT (℃)	0.2	0.1	1.2
StdErr of Normalized P_B	1.5%	0.3%	4.3%
ΔT (℃)	5.8	1.3	106
StdErr of BW (MHz)	0.82	0.83	6.92
ΔT (℃)	5.5	4.2	77.2

4.4 Summary

The temperature dependence of the Brillouin loss spectrum for three PM fibers has been studied for their temperature coefficients of the Brillouin frequency shift, intensity, and bandwidth for the first time to our knowledge. The highest temperature measurement uncertainty for the Brillouin frequency shift is 0.3°C (PANDA), for Brillouin intensity it is 1.3°C (Bow-tie), and for the Brillouin bandwidth it is 4.2°C (Bow-tie) at a 20 cm spatial resolution. The Brillouin frequency at 20°C for the fast axis of the PANDA, Bow-tie, and Tiger PM fibers is 12794.8, 12581.0, and 12793.6 MHz, respectively. The Brillouin frequency difference between the fast and slow axes among the three PM fibers is between 2.9 and 4.3 MHz.

Chapter 5

Strain dependence of Brillouin frequency, intensity, and bandwidth in polarization-maintaining fibers

[This chapter is adapted from the paper published in OPTICS LETTERS, 29, 1065-1067(2004)]

5.1 Introduction

In this chapter we present experimental results on the strain dependence of frequency, intensity and bandwidth (BW) of the Brillouin loss spectrum for the PM fibers in the temperature range 0 to 50°C.

In single-mode fibers the Brillouin frequency and intensity have been found to be linearly proportional to both strain and temperature [Bao *et al.* 1994b, Alahbabi *et al* 2004]. The Brillouin spectrum's bandwidth, however, was reported to be unchanged with strain [Niklès *et al.* 1997].

In our experiment, it was found that these parameters, frequency, intensity, and BW, are linearly dependent on strain for PANDA and Bow-tie PM fibers. Our results suggest that all three parameters of a Brillouin spectrum may be used with either a slow or a fast axis for distributed strain measurement.

5.2 Experiment

The Brillouin loss sensing system is described in Chapter 3. The setup of the strain-temperature test is shown in Fig.5-1. The PM fiber was wound around two pulleys. One pulley was fixed, and the other was movable along a rail. The fiber was glued onto the movable pulley and was pulled away from the fixed pulley during the strain measurement. The pulleys and PM fiber on the rail were sealed in a temperature chamber. For temperatures below room temperature we used dry ice and for temperatures above room temperature we used an electrical heating strip.

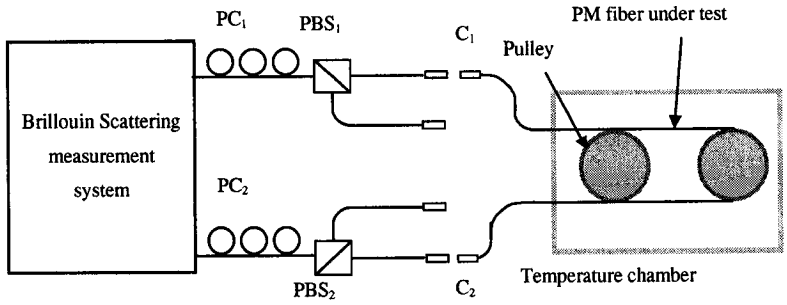

Fig. 5-1. Setup for strain measurement of PM fibers using Brillouin sensor.

We used 20-dB extinction ratio PM fibers to preserve the linear polarization state of the input light. The pulse width was 2 ns, corresponding to 0.2 m spatial resolution. The average number of time traces to produce a 25–30 dB signal-to-noise ratio (SNR) for measurement of the Brillouin loss spectrum was 2000.

The PM fibers used in this experiment are the same fibers used for the temperature dependence measurement as discussed in Chapter 4. The length of the strained fiber was 1.57 m, and the input powers were 5 and 6 mW for cw and pulsed beams, respectively. Both PANDA and Tiger fibers were 0.25 mm bare fibers (acrylate coated), and the Bow-tie fiber was a 0.9 mm jacketed fiber. We verified the extinction ratio of the PM fibers during the test and no ER change was observed while the fibers were strained (by as much as 500 με for PANDA and Tiger fibers and 1200 με for Bow-tie fiber). The pulse width was 2 ns, and the average number of time traces was 2000 to produce a 25–30 dB signal-to-noise ratio (SNR) for measurement of the Brillouin loss spectrum.

5.3 Results and discussion

The Brillouin frequencies of the slow and fast axes in the PANDA fiber are linearly dependent on strain with the same slope (0.077 ± 0.002 and 0.075 ± 0.002 MHz/με, respectively), as shown in Fig. 5-2. Thus either the slow or the fast axis can be used for strain measurement.

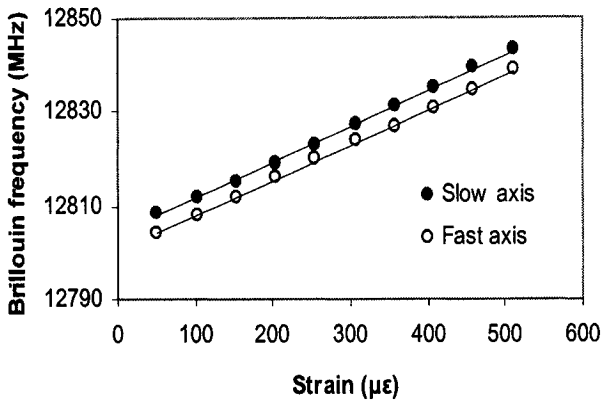

Fig. 5-2 Strain dependence of Brillouin frequency at slow and fast axis of PANDA fiber at room temperature 23°C.

The Brillouin frequency of the fast axis of the PANDA fiber is measured as a function of strain in the temperature range 0°C to 50°C (Fig.5-3(a)); it shows a linear relationship, with an average slope of 0.077 ±0.002 MHz/με. Similarly, the Bow-tie fiber (Fig.5-4(b)) Brillouin frequency in the temperature range 0°C to 43°C shows an average slope of 0.024 ±0.002 MHz/με.

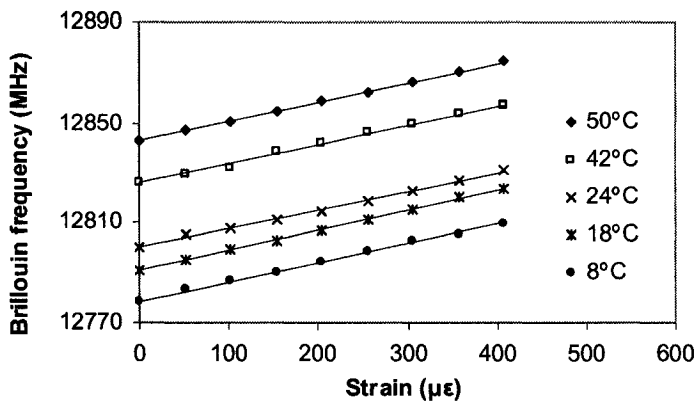

(a)

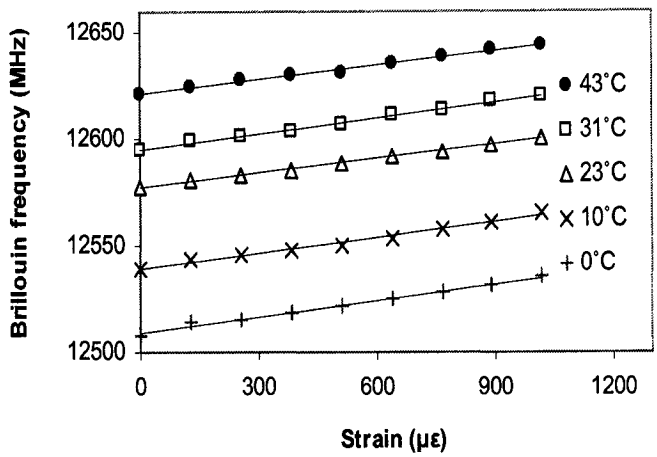

(b)

Fig. 5-3 Strain dependence of Brillouin frequency at different temperatures for (a) PANDA fibers at fast axis; (b) Bow-tie fiber at fast axis.

Like the Brillouin frequency, the BW and the intensity of the Brillouin profile exhibit a linear relationship to the strain over the same temperature range, as shown in Fig. 5-4. Although the BW and the intensity of the Brillouin spectrum have a linear relationship to the strain for both Bow-tie and PANDA fibers, the trend of the Bow-tie fiber is quite different from that of PANDA fiber. The intensity increases and the BW decreases with strain over the temperature range 0°C to 43°C, as shown in Fig. 5-5.

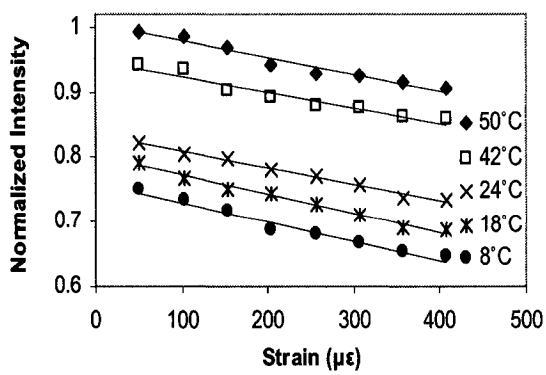

(a)

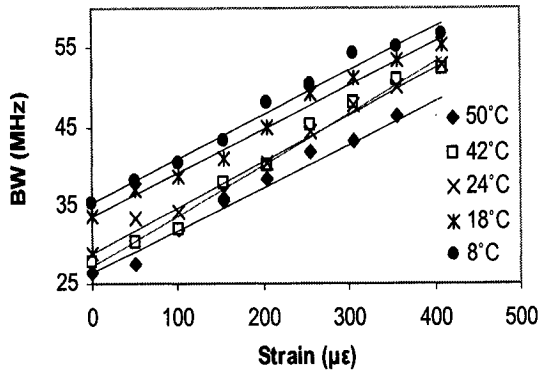

(b)

Fig. 5-4 In a PANDA fiber: (a) Strain dependence of intensity normalized to biggest value at 50°C; (b) Strain dependence of BW.

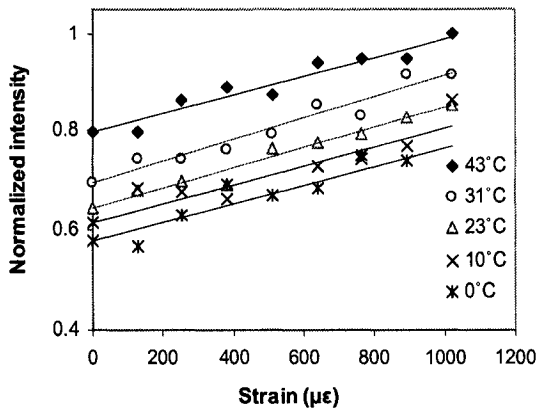

(a)

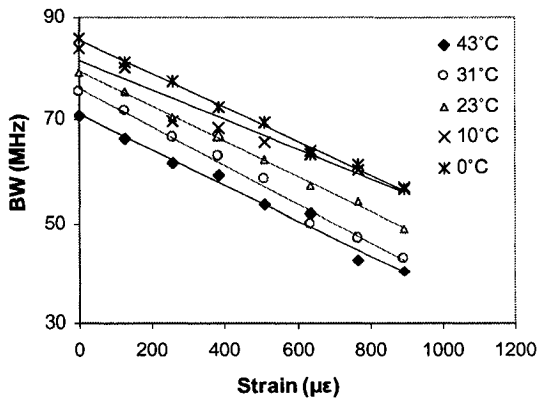

(b)

Fig. 5-5 In Bow-tie fiber: (a) Strain dependence of intensity normalized to biggest value at 43°C; (b) Strain dependence of BW.

The slopes of intensity–strain linear curves are the same (within experimental error) in the range of temperatures used in the experiment. The strain dependence of the Brillouin intensity for the slow axes of PANDA and Bow-tie fibers resembles a similar linear relationship with the same slope (within experimental error) for the fast axis, as demonstrated in Fig. 5-6. In Fig. 5-6, to show the linear trend we averaged the intensity–strain results for the slow and the fast axes of PANDA and Bow-tie fibers over the temperature range. For both fibers the intensity values that correspond to the slow axis were bigger than those of the fast axis, a result that we attribute to the extra connector and polarizing beam splitter insertion loss of the fast axis. Note that the unstrained BW of the Bow-tie fiber in Fig. 5-5(b) is bigger than that in zero strain (see Fig. 4-7,Chapter 4) because of the residual strain in the poly(vinyl chloride) jacket of the Bow-tie fiber after the first elongation. However, this outcome does not affect our measurements because only the slope and the variation with respect to a reference condition are measured in our system.

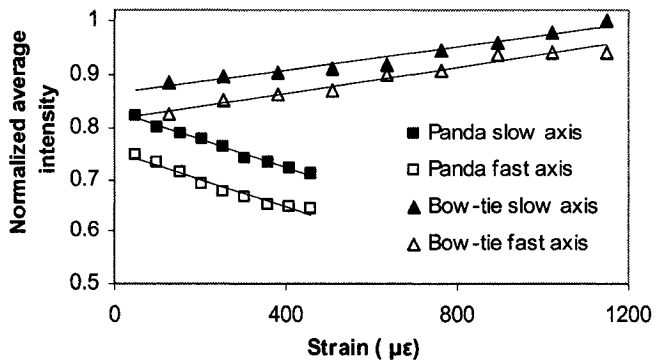

Fig. 5-6 Strain dependence of Brillouin intensity (normalized to highest value in Bow-tie slow axis) averaged over the range of temperature for PANDA and Bow-tie fibers.

As we can see from Figs. 5-4(a) and 5-5(a), the intensity of Brillouin spectrum of the Bow-tie fiber increase while the PANDA fiber's intensity decrease with strain. One can understand this result by examining the structures of the PANDA and the Bow-tie fibers (as depicted in Fig. 5-8) and the ways in which these structures change under stress. When a PANDA fiber is stretched, the mode confinement factor is affected because the two stress rods are pressed into the core. The rods degrade the guiding properties and boundary conditions for mode field propagation, leading to increased attenuation. In the case of Bow-tie fiber, the penetration of the two rods into the core is more nearly uniform because of the circular shape of the internal surface of the two rods (Fig. 5-7 (b)).

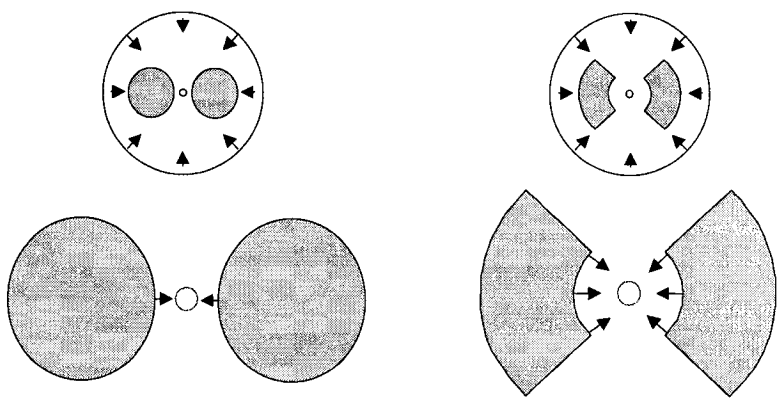

(a) PANDA. (b) Bow-tie.

Fig. 5-7 Structure of PANDA (a) and Bow-tie (b) PM fibers and their stress applying parts. Applied forces are shown for elongated fiber.

Thus the pressure does not change the boundary conditions for mode field propagation but simply decreases the core's cross section as the fiber is elongated if the stress is not large, as in our experimental condition. These constant boundary conditions result in higher power density and accordingly in higher Brillouin loss for strained Bow-tie fibers. Assuming that for low-power input pump and pulse the integral of the Brillouin spectrum over all frequencies is a constant [Nikles *et al.* 1997]

$$\int_0^{\infty} g_B(\nu)\, d\nu = \int_0^{\infty} g_B \frac{\left(\frac{\Delta\nu_B}{2}\right)^2}{(\nu-\nu_B)^2 + \left(\frac{\Delta\nu_B}{2}\right)^2} d\nu = \pi\, g_B\, \Delta\nu_B \tag{5-1}$$

where g_B is the peak gain (or loss), $\Delta\nu_B$ is the bandwidth.

The decrease (increase) of intensity in the PANDA (Bow-tie) fibers as a function of strain results in an increase (decrease) of Brillouin BW, as shown in Figs. 5-4 and 5-5. This result indicates that the Brillouin intensity and the BW are not independent parameters and that the linear relationships in Figs. 5-4 and 5-5 are valid only for a limited range of strain or temperature.

It was noticed that the ratio of strain to Brillouin intensity showed more fluctuations than that of strain to Brillouin frequency. This was because the laser we used was frequency stabilized (with a drift of a few tens of kilohertz), i.e., the laser intensity fluctuates to compensate for frequency drift to produce high-frequency stabilization [Lipson *et al.* 1995].

The strain coefficients (slopes) of Brillouin frequency, intensity ratio, and BW for three PM fibers are listed in Table 5-1. For comparison, the results for single-mode fiber [Alahbabi *et al* 2004] are also included.

Table 5-1 Average Strain Coefficients of Brillouin Frequency, Normalized Intensity and Bandwidth (0°C to +50°C).

Fiber type	PANDA	Bow tie	Tiger	SM
C_ν^ε (MHz /με)	0.077 ±0.002	0.024 ±0.002	0.091 ±0.005	0.048 ±0.03
C_P^ε (%/με)	-0.027 ±0.002	0.020 ±0.003	0.01 ±0.004	-0.0009
C_B^ε(MHz/με)	0.058 ±0.003	-0.031 ±0.002	-	-

No strain dependence on BW of Tiger fiber was observed because of the broad Brillouin spectrum. The standard errors of measurements and corresponding strain uncertainties are listed in Table 5-2. Overall, the PANDA fiber has the highest strain measurement accuracy, *i.e.*, 7, 25, and 19 με for Brillouin frequency, BW, and intensity, respectively.

Table 5-2 Average Standard Errors of Measured Parameters and Corresponding Strain Uncertainty (0°C to +50°C).

Fiber type	PANDA	Bow-tie	Tiger
StdErr Frequency (MHz)	0.54	0.85	1.57
Strain uncertainty ($\mu\varepsilon$)	7	36	19
StdErr Normalized Intensity (%)	0.7	2.4	1.2
Strain uncertainty ($\mu\varepsilon$)	25	124	110
StdErr BW (MHz)	1.1	1.6	-
Strain uncertainty ($\mu\varepsilon$)	19	53	

5.4 Summary

The strain dependence of the Brillouin gain–loss spectrum for PANDA, Bow-tie, and Tiger polarization-maintaining fibers has been studied in the range 0°C to 50°C. We found a linear relationship between the strain and the Brillouin frequency, intensity, and bandwidth for PANDA and Bow-tie fibers. For PANDA fiber at 20 cm spatial resolution, Brillouin frequency gives 7 με uncertainty, which is the highest accuracy among three parameters, whereas the Brillouin bandwidth gives 19 με uncertainty. Tiger fiber is not a good candidate for strain sensing using Brillouin sensor due to its broad bandwidth.

Chapter 6

Simultaneous strain and temperature measurements with PM fibers and their error analysis

[This chapter is adapted from the paper published in OPTICS LETTERS, 29, 1342-1344 (2004)]

6.1 Introduction

In chapter 4 and 5, the temperature and strain dependence of Brillouin frequency, intensity, and bandwidth in PM fibers have been studied. Once the temperature and strain coefficients become available, with the measured parameters in Brillouin spectra we can obtain the strain and temperature simultaneously with PM fibers.

Brillouin frequency shift is sensitive to changes in both temperature and strain in SM fibers [Bao *et al.* 1994]. This leads to a problem common in many sensors: one cannot distinguish a change in the strain or the temperature experienced by the fiber. Neglecting the temperature effect leads to substantial errors in strain measurements. For simultaneous measurement of temperature and strain, a few results have been reported in SM fibers with Brillouin frequency and intensity [Park *et al.* 1998, Smith *et al.* 1999, Kee *et al.* 2000]. However, because of polarization mode dispersion (PMD) [Chen *et al.* 1999, Yu *et al.* 2004a] of SM fiber, the polarization state varies randomly along the SM fiber. It is impossible to separate the state of polarization changes induced by the temperature and strain from the dynamic features caused by PMD. As a result, the intensity measurement uncertainty increased in addition to the laser power fluctuation for simultaneous temperature and strain measurement with SM fiber using intensity and Brillouin frequency.

It is known that PM fibers allow the light to travel in one polarization state if the input light is launched into one of the PM fiber axes. As a result, the PMD-induced fluctuation can be minimized, and the power fluctuation is attributed only to the laser source. Because of the minimization of polarization fluctuation in the power, we can possibly achieve a spatial resolution on the scale of centimeters for simultaneous

temperature and strain sensing with PM fibers. SM fibers can have a spatial resolution only on the scale of meters for simultaneous temperature and strain sensing.

We have used three types of PM fiber, PANDA, Bow-tie and Tiger, to measure strain coefficients at various temperatures for the Brillouin intensity, frequency, and bandwidth as presented in Chapter 4 and 5, and then we calculated the temperature and strain uncertainty. With three measurable parameters for the Brillouin scattering spectrum—intensity, bandwidth, and frequency—there are three options for simultaneous temperature and strain sensing: (1) intensity and frequency, (2) intensity and bandwidth, and (3) bandwidth and frequency. For the second option the Brillouin intensity integral over frequency is a constant over the complete frequency range if the input power is not very high (below the stimulated Brillouin scattering threshold), so the intensity and the bandwidth are two related parameters. However, within a limited temperature and strain range (within our measurement range) we can ignore the correlation between the intensity and the bandwidth; hence the intensity and the bandwidth can be considered two independent parameters for simultaneous temperature and strain sensing. Although we have learned that Tiger fiber is not be a good candidate for sensing, for comparison purpose we still list results for the Tiger fiber in this chapter.

6.2 Simultaneous measurement of strain and temperature

First, we used intensity and frequency shift as known parameters, which yielded the following for temperature and strain variation [Smith *et al.* 1999]:

$$\Delta T = \frac{\Delta\nu \cdot C_P^{\varepsilon} - C_\nu^{\varepsilon} \cdot \Delta P}{C_P^{\varepsilon} \cdot C_\nu^{T} - C_\nu^{\varepsilon} \cdot C_P^{T}}, \tag{6.1-a}$$

$$\Delta\varepsilon = \frac{\Delta\nu \cdot C_P^{T} - C_\nu^{T} \cdot \Delta P}{C_\nu^{\varepsilon} \cdot C_p^{T} - C_p^{\varepsilon} \cdot C_\nu^{T}}, \tag{6.1-b}$$

where $\Delta\nu$ and ΔP are the frequency and relative intensity variations induced by strain and temperature change and $C_\nu^{\varepsilon} = \left[\frac{\partial\nu}{\partial\varepsilon}\right]_T$, $C_\nu^{T} = \left[\frac{\partial\nu}{\partial T}\right]_\varepsilon$, $C_P^{\varepsilon} = \left[\frac{\partial P}{\partial\varepsilon}\right]_T$ and $C_P^{T} = \left[\frac{\partial P}{\partial T}\right]_\varepsilon$ are the

temperature and strain coefficients of the frequency and intensity. If we ignore the uncertainty in the temperature and strain coefficients for Brillouin frequency and intensity, and account for only the uncertainty induced by the Brillouin frequency and intensity, we can determine the maximum errors for the temperature and strain measurements as follows:

$$\delta(\Delta T)_{\max} = \frac{\left|\delta(\Delta\nu)\cdot C_P^{\varepsilon}\right| + \left|C_\nu^{\varepsilon}\cdot\delta[\Delta P]\right|}{\left|C_\nu^{\varepsilon}\cdot C_P^{T} - C_P^{\varepsilon}\cdot C_\nu^{T}\right|}, \tag{6.1-c}$$

$$\delta(\Delta\varepsilon)_{\max} = \frac{\left|\delta(\Delta\nu)\cdot C_P^{T}\right| + \left|C_\nu^{T}\cdot\delta(\Delta P)\right|}{\left|C_\nu^{\varepsilon}\cdot C_P^{T} - C_P^{\varepsilon}\cdot C_\nu^{T}\right|}. \tag{6.1-d}$$

If we assume that the probability distributions for ΔT and Δε are Gaussian functions, we can calculate the rms values for ΔT and Δε as follows: in all the rms value calculations we ignored the uncertainty of temperature and strain coefficients for Brillouin frequency, bandwidth and intensity.

$$\text{rms}(\Delta T) = \sqrt{\left(\frac{rms(\Delta\nu)\cdot C_P^{\varepsilon}}{C_P^{\varepsilon}\cdot C_\nu^{T} - C_\nu^{\varepsilon}\cdot C_P^{T}}\right)^2 + \left(\frac{C_\nu^{\varepsilon}\cdot rms(\Delta P)}{C_P^{\varepsilon}\cdot C_\nu^{T} - C_\nu^{\varepsilon}\cdot C_P^{T}}\right)^2}, \tag{6.1-e}$$

$$\text{rms}(\Delta\varepsilon) = \sqrt{\left(\frac{rms(\Delta\nu)\cdot C_P^{T}}{C_P^{\varepsilon}\cdot C_\nu^{T} - C_\nu^{\varepsilon}\cdot C_P^{T}}\right)^2 + \left(\frac{C_\nu^{T}\cdot rms(\Delta P)}{C_P^{\varepsilon}\cdot C_\nu^{T} - C_\nu^{\varepsilon}\cdot C_P^{T}}\right)^2}. \tag{6.1-f}$$

Similarly, using frequency and bandwidth we have:

$$\Delta T = \frac{\Delta\nu\cdot C_B^{\varepsilon} - C_\nu^{\varepsilon}\cdot\Delta B}{C_B^{\varepsilon}\cdot C_\nu^{T} - C_\nu^{\varepsilon}\cdot C_B^{T}}, \tag{6.2-a}$$

$$\Delta\varepsilon = \frac{\Delta\nu\cdot C_B^{T} - C_\nu^{T}\cdot\Delta B}{C_\nu^{\varepsilon}\cdot C_B^{T} - C_B^{\varepsilon}\cdot C_\nu^{T}}, \tag{6.2-b}$$

where ΔB are the variations of the Brillouin bandwidth due to temperature and strain. $C_B^{\varepsilon} = \left(\partial B / \partial \varepsilon\right)_T$ and $C_B^{\varepsilon} = \left(\partial B / \partial T\right)_{\varepsilon}$ are the temperature and strain coefficients of the bandwidth. The maximum errors and rms values for the temperature and strain measurements are given by the following:

$$\delta\left(\Delta T\right)_{\max} = \frac{\left|\delta(\Delta\nu)\cdot C_B^{\varepsilon}\right| + \left|C_{\nu}^{\varepsilon}\cdot\delta(\Delta B)\right|}{\left|C_B^{\varepsilon}\cdot C_{\nu}^{T} - C_{\nu}^{\varepsilon}\cdot C_B^{T}\right|}, \tag{6.2-c}$$

$$\delta\left(\Delta\varepsilon\right)_{\max} = \frac{\left|\delta(\Delta\nu)\cdot C_B^{T}\right| + \left|C_{\nu}^{T}\cdot\delta(\Delta B)\right|}{\left|C_{\nu}^{\varepsilon}\cdot C_B^{T} - C_{\nu}^{T}\cdot C_B^{\varepsilon}\right|}, \tag{6.2-d}$$

$$\text{rms}\,(\Delta T) = \sqrt{\left(\frac{rms(\Delta\nu)\cdot C_B^{\varepsilon}}{C_{\nu}^{\varepsilon}\cdot C_B^{T} - C_B^{\varepsilon}\cdot C_{\nu}^{T}}\right)^2 + \left(\frac{C_{\nu}^{\varepsilon}\cdot rms(\Delta B)}{C_{\nu}^{\varepsilon}\cdot C_B^{T} - C_B^{\varepsilon}\cdot C_{\nu}^{T}}\right)^2}, \tag{6.2-e}$$

$$\text{rms}(\Delta\varepsilon) = \sqrt{\left(\frac{rms(\Delta\nu)\cdot C_B^{T}}{C_{\nu}^{\varepsilon}\cdot C_B^{T} - C_B^{\varepsilon}\cdot C_{\nu}^{T}}\right)^2 + \left(\frac{C_{\nu}^{T}\cdot rms(\Delta B)}{C_{\nu}^{\varepsilon}\cdot C_B^{T} - C_B^{\varepsilon}\cdot C_{\nu}^{T}}\right)^2}. \tag{6.2-f}$$

If we use bandwidth and intensity, we have

$$\Delta T = \frac{\Delta B\cdot C_P^{\varepsilon} - C_B^{\varepsilon}\cdot\Delta P}{C_P^{\varepsilon}\cdot C_B^{T} - C_B^{\varepsilon}\cdot C_P^{T}}, \tag{6.3-a}$$

$$\Delta\varepsilon = \frac{\Delta B\cdot C_P^{T} - C_B^{T}\cdot\Delta P}{C_B^{\varepsilon}\cdot C_P^{T} - C_P^{\varepsilon}\cdot C_B^{T}}. \tag{6.3-b}$$

The maximum errors and rms values for the temperature and strain measurements as follows:

$$\delta\left(\Delta T\right)_{\max} = \frac{\left|\delta(\Delta B)\cdot C_P^{\varepsilon}\right| + \left|C_B^{\varepsilon}\cdot\delta(\Delta P)\right|}{\left|C_P^{\varepsilon}\cdot C_B^{T} - C_B^{\varepsilon}\cdot C_P^{T}\right|}, \tag{6.3-c}$$

$$\delta(\Delta\varepsilon)_{max} = \frac{\left|\delta(\Delta B)\cdot C_P^T\right| + \left|C_B^T\cdot\delta(\Delta P)\right|}{\left|C_B^\varepsilon\cdot C_P^T - C_V^\varepsilon\cdot C_B^T\right|} . \quad (6.3\text{-d})$$

$$\text{rms}(\Delta T) = \sqrt{\left(\frac{rms(\Delta B)\cdot C_P^\varepsilon}{C_P^\varepsilon\cdot C_B^T - C_B^\varepsilon\cdot C_P^T}\right)^2 + \left(\frac{C_B^\varepsilon\cdot rms(\Delta P)}{C_P^\varepsilon\cdot C_B^T - C_B^\varepsilon\cdot C_P^T}\right)^2} , \quad (6.3\text{-e})$$

$$\text{rms}(\Delta\varepsilon) = \sqrt{\left(\frac{rms(\Delta B)\cdot C_P^T}{C_P^\varepsilon\cdot C_B^T - C_B^\varepsilon\cdot C_P^T}\right)^2 + \left(\frac{C_B^T\cdot rms(\Delta P)}{C_P^\varepsilon\cdot C_B^T - C_B^\varepsilon\cdot C_P^T}\right)^2} . \quad (6.3\text{-f})$$

6.3 Experiment and results

The experiment setup was described in Fig.5-1, Chapter 5.

The Brillouin frequency was measured as a function of strain over the temperature range 8°C to 50°C for the fast axis PANDA fiber. It showed a linear relationship with an average slope of 0.077 MHz/με in Fig. 5-3(a). The same test was done for fast axis of a Bow-tie from 0°C to 43°C, with an average slope 0.023 MHz/με as shown in Fig. 5-3(b). The bandwidth and intensity of the Brillouin spectrum exhibited a linear relationship with respect to strain over the same temperature range, as shown in Figs. 5-4 (a) and (b) for the PANDA fiber. When the same measurement was done for the Bow-tie fiber, it was observed that the Brillouin intensity increased, but the bandwidth decreased as a function of increasing strain as shown in Fig. 5-5 (a) and (b).

Clearly the three parameters of the Brillouin spectrum are linear functions of temperature and strain, so that Eqs. (6.1) to (6.3) are valid. The temperature and strain coefficients of Brillouin frequency, intensity ratio, and bandwidth for three PM fibers

were measured and calculated as shown in Table 6-1. The strain coefficients were averaged over the measurements in the temperature range 0°C to 50°C. By substituting the parameters in Table 6-1 and the directly measured frequency, intensity, and bandwidth values into Eqs. (6.1) to (6.3), we obtained rms and maximum error values for the temperature and strain of all three PM fibers. The average strain and temperature uncertainties are listed in Table 6-2 and are calculated as shown in Figs. 5-4 and 5-5 for the measured temperature and strain. The temperature range is 0°C to 50°C, and the strain range is 0-408 με for PANDA, and 0-1021 με for Tiger fiber. As expected, the calculated rms values for temperature and strain using the intensity, bandwidth, and frequency are similar to the strain and temperature uncertainties, which are derived from the strain and temperature measurements in Figs. 5-3(a) and (b).

Table 6-1 Temperature and Strain coefficients of Brillouin frequency, intensity and bandwidth.

PM fiber type	PANDA	Bow-tie	Tiger
C_ν^T (MHz/℃)	1.37	2.30	1.66
	±0.007	±0.05	±0.07
C_P^T (%/℃)	0.26	0.23	0.04
	±0.03	±0.01	±0.09
C_B^T (MHz/℃)	-0.15	-0.20	-
	±0.02	±0.02	
C_ν^ε (MHz /με)	0.077	0.024	0.091
	±0.002	±0.001	±0.005
C_P^ε (%/με)	-0.027	0.020	0.01
	±0.003	±0.002	±0.004
C_B^ε (MHz/με)	0.058	-0.031	-
	±0.004	±0.002	

Table 6-2 Uncertainties of Temperature and Strain Calculated with Measured Brillouin Frequency (F), Intensity (P) and Bandwidth (B).

	PANDA			Bow-tie			Tiger
Property	F-P	F-B	P-B	F-P	F-B	P-B	F-P
Uncertainty of temp. (℃)	8	2	38	4	3	38	16
Uncertainty of strain ($\mu\varepsilon$)	153	39	135	237	126	195	598
Max error of ΔT (℃)	10	4	58	12	7	137	78
Max error of $\Delta\varepsilon$ ($\mu\varepsilon$)	331	82	249	741	490	1096	1308
rms(ΔT) (℃)	2	2	40	8	4	73	38
rms($\Delta\varepsilon$) ($\mu\varepsilon$)	221	43	149	414	152	567	926

6.4 Discussions

By using PM fibers we had hoped to achieve better frequency and intensity measurement accuracy, *i.e.*, better temperature and strain measurement accuracy. However, we found relative large uncertainty with a combination of intensity and frequency. We believe this is due to the nonlinear Brillouin amplification fluctuation induced by the laser power. In a SM fiber the polarization state varies randomly along the fiber length, the Brillouin loss takes the average effects between the pump and the probe polarization state variation. When the laser power fluctuates, its effect on the Brillouin loss is not obvious because of the average Brillouin loss effects induced by PMD. While in a PM fiber, the polarization directions of the pump and the probe beams remained parallel when they were launched in the same state. As a result, the Brillouin loss, i.e., nonlinear amplification, grows exponentially along the fiber length because no PMD-

induced polarization state variations existed. When the laser power varies, it causes relative larger fluctuation in the Brillouin loss.

It must be pointed out that all experiments discussed in this thesis were done at well-controlled conditions in our lab; therefore, the correlation between temperature and strain has been neglected. In the field application, however, sensing fiber must be attached to the structure. It is possible that temperature effect is coupled with strain effect. For example, a structure temperature change may generate a strain due to structure expansion (or contract). In this case, the thermal-induced strain must be taken into account.

6.5 Summary

The stain and temperature were simultaneously measured with PANDA, Bow-tie and Tiger PM fibers using frequency, intensity and BW for the first time. The expressions for simultaneous temperature and strain sensing and the maximum errors and rms values of temperature and strain measurements are derived with three combinations of the parameters: (1) intensity and Brillouin frequency, (2) bandwidth and Brillouin frequency, and (3) bandwidth and Brillouin intensity. The experiments demonstrate that simultaneous temperature and strain sensing at 20-cm spatial resolution for Brillouin frequency combined with bandwidth the strain/temperature resolutions are 39 $\mu\varepsilon$/2°C (PANDA), 126 $\mu\varepsilon$/3°C (Bow-tie), and 598 $\mu\varepsilon$/16°C (Tiger); for the Brillouin frequency combined with intensity the strain/temperature resolutions are 153 $\mu\varepsilon$/8°C (PANDA) and 237 $\mu\varepsilon$/4°C (Bow-tie); and for the bandwidth combined with intensity the strain/temperature resolutions are 135 $\mu\varepsilon$/38°C (PANDA) and 195 $\mu\varepsilon$/38°C (Bow-tie). PANDA shows the best performance.

Chapter 7

Identification of the spatial location to better than the pulse length with high strain accuracy

[This chapter is adapted from the paper published in OPTICS LETTERS, 30, 2215-2217(2005)]

7.1 Introduction

In Chapter 4, 5 and 6, we have studied the temperature and strain dependence of Brillouin scattering spectrum of PM fibers; by using the PM fiber we obtained higher (comparing to SM fiber) measurement accuracy and resolution in terms of temperature and strain simultaneously. On the other hand, identifying the location of a strain section accurately in a field test is sometimes more important than just measuring the strain changes. In this chapter we propose a novel method to identify spatial location of the boundary between two strain sections.

In a Brillouin-loss-based distributed sensor, the location information is obtained by measuring the travel time of the pulse reflected from a specific position in the sensing fiber. The location accuracy is defined as the spatial interval for a signal change from 10% to 90% or 90% to 10% of the rise or fall time, respectively. Normally, this is longer than the pulse length because of the noise involved in the signal. The minimum detectable strain or temperature length depends on a short rise or fall time, the pulse length, and the SNR (signal and noise ratio). A shorter pulse requires broadband detectors and electronics. This leads to a low SNR and poor strain accuracy. If a broader pulse is used, the strains within the pulse length may not be uniform for a small strain length. This leads to a low SNR and poor strain accuracy. Hence the Brillouin spectrum involves multiple peaks (for relative large Brillouin frequency variation) or a broadened Brillouin profile (small Brillouin frequency variation). Thus finding the boundary of two strained sections is a difficult task.

7.2 Methods used by others for strain boundary determination

Brown proposed the two-equal-height-peak method by finding the position where the Brillouin spectrum shows two equal-heights [Brown *et al.* 1999]. This position is defined as boundary between two strained sections. This method introduces errors for short pulses due to the fact that the location of the two-equal-height spectrum depends on the input power level and the CW component (base) of the pulse (This issue will be discussed in the next chapter).

A frequency modulation method was used to deconvolute the Brillouin spectrum. For instance, Hotate and Tanaka [Hotate *et al.* 2001] reported 1 cm spatial resolution with a correlation-based Brillouin sensor. A strain of 1000 $\mu\varepsilon$ was applied with a Brillouin frequency uncertainty of 5 MHz to 6 MHz, equivalent to 100 $\mu\varepsilon$ to 120 $\mu\varepsilon$, over a limited sensing length (0.3 m).

Shi [Shi *et al.* 2003] used a 10 ns pulse, equivalent to 1 m, to get a spatial resolution of 0.2 m with a frequency bandwidth method. They used the maximum bandwidth (convolution of the Brillouin peaks from two strained sections) as the criterion to determine the boundary of two strained sections. Using this method they obtained a ~100 $\mu\varepsilon$ uncertainty for a 750 $\mu\varepsilon$ measurement. The method is actually similar to Brown's method where the difference of the two Brillouin frequencies is not big enough to show the two peaks.

A deconvolution method for a two-peak Brillouin spectrum was proposed by Afshar [Afshar *et al.* 2005a]. Because one peak Brillouin spectrum fitting represents only uniform strain or temperature. However, the measured spectrum near the boundary is the overlap of two or multiple peaks, which form a non-symmetric and broadened peak for small Brillouin frequency variation. If we use one Lorentzian peak to fit a distorted spectrum (an overlap of multiple Brillouin peaks), we will get an offset peak-frequency from the real peak-frequency. Using a multiple-peak function to fit the spectrum near a boundary of different strain sections is possible if one knew the number of peaks in the Brillouin spectrum in advance. Often this is not the case. In addition, the experimental data contains noise such as power fluctuates. It is difficult and time consuming to use a multiple-peak function to fit a distorted spectrum.

7.3 The second-order partial derivative method

Theoretically for a noiseless signal, the first-order derivative of signal with respect to position would be able to reveal the boundaries of the strained sections. Based on Brillouin loss signal changes with strain, we calculated the Brillouin loss versus position at the peak Brillouin frequency and its first-order derivative with respect to location with uniformly strained sections by use of the coupling wave equations (Eq. 2-10-1 and Eq. 2-10-2 in Chapter 2), as shown in Fig. 7-1. It can be seen that the first-order derivative of the position reveals the boundaries of the strained sections at positions of 1.0, 2.0, and 3.0 m. In the theoretical calculation, no noise is included; hence the first-order derivative is adequate.

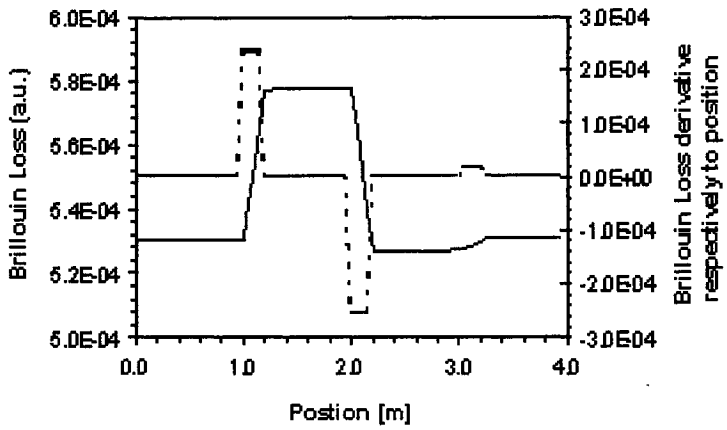

Fig.7-1 Brillouin loss (solid line) and its 1st order derivative (dashed line).

For experimental data, we propose a mixed second-order partial derivative of the Stokes intensity (Brillouin loss signal) with respect to frequency and location to identify the boundary for different Brillouin frequencies. The second-derivative procedure has been used in spectroscopic signal processing to find the peaks of a spectrum (second derivative of amplitude with respect to frequency). Here, the derivative is relative to frequency and location, rather than frequency alone, because the distributed Brillouin sensor needs both location and spectrum information related to strain or temperature. The reason for using the mixed second order derivative is to remove the noise from intensity fluctuations. Detailed discussion will be presented in the section 7.5.

7.4 Experiment setup and considerations

A PANDA fiber was used in the experiment as the strain-sensing fiber. The fiber was passed around a pulley with bearings and wrapped and glued to a post. The post was pulled away from the pulley to create a uniform strain on the fiber as shown in Fig. 5-1. The length of the strained sections was physically measured to be 157 cm. The pulse width was 2 ns.

For PM fiber, we can get a 30 dB SNR (signal to noise ratio) by averaging 2000 waveforms for pulses of 1-3 ns. This can resolve a minimum Brillouin frequency shift of 1-1.5 MHz. If a single mode fiber were used, the minimum detectable strain would be larger than that of the PM fiber, unless more averaging is introduced, which adds to the measurement time. For a SM fiber at the same power level and averaging number (2000), we could get a SNR of only ~25 dB. This means a minimum Brillouin frequency of ~2 MHz, unless we increase the number of waveforms averaged.

7.5 Results and analysis

As the spectrum evolves from unstrained to strained fiber, there is a maximum change in Brillouin frequency and Stokes intensity at the strain boundary. At the peak frequency of the unstrained section of 12,800 MHz, the Stokes intensity drops from the unstrained section to the strained section. Fig. 7-2 shows Stokes intensity in three experiments: Strain-1, Strain-2, and Strain-3. The corresponding Brillouin frequency differences between the strained and the unstrained sections are 1.2, 8.4, and 15.4 MHz, respectively. In principle, the first-order derivative of the Stokes intensity with respect to the position at a given frequency is able to reveal the boundary. However, its SNR is low due to the Stokes intensity fluctuation caused by digitizer quantization (rounding) error and input laser power fluctuation.

To minimize the error in finding the boundary, we first calculated the relative change for two consecutive frequencies, the first-order derivative of the Stokes intensity with respect to frequency:

$$\alpha(\nu,z)=\frac{P(\nu+\Delta\nu_{scan},z)-P(\nu,z)}{\Delta\nu_{scan}}, \tag{7.1}$$

where $P(\nu,z)$ is the Stokes intensity near peak frequency and $P(\nu+\Delta\nu_{scan})$ is the

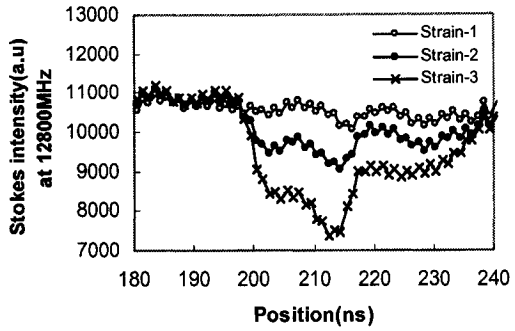

Fig. 7-2 Stokes intensity vs. position for Strain-1, Strain-2 and Strain-3.

intensity at $\nu + \Delta\nu_{scan}$. $\Delta\nu_{scan}$ is the laser frequency scanning step size. Obviously, $\alpha(\nu,z)$ has much smaller fluctuation as shown Fig. 7-3. Note the $\Delta\nu_{scan}$ was 5 MHz in our experiment.

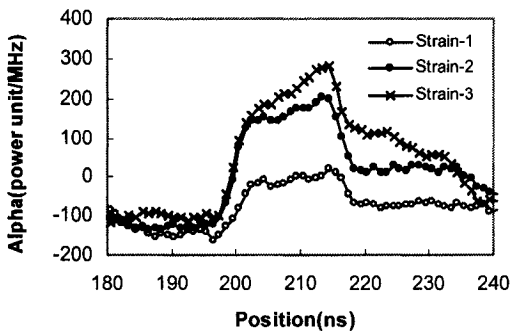

Fig. 7-3 Alpha (1st derivative of Stokes intensity respect to frequency) versus position for Strain-1, Strain-2 and Strain-3.

Then we calculated the 2nd order partial derivative of the Stokes intensity with respect to frequency and position:

$$\beta(\nu,z) = \frac{\Delta\alpha(\nu,z)}{\Delta z} = \frac{\alpha(\nu,z+\Delta z)-\alpha(\nu,z)}{\Delta z}, \qquad (7.2)$$

where Δz is the step size of the digitizer. The plot of $\beta(\nu, z)$ versus position z is shown in Fig. 7-4 for Brillouin frequency for Strain-1, Strain-2 to Strain-3 corresponding of

1.2, 8.4 and 15.4 MHz respectively. We see a positive peak ($\alpha(\nu, z)$ increasing), and a negative peak ($\alpha(\nu, z)$ decreasing) corresponding to the start and end of the strained section. The SNR of $\beta(\nu, z)$ is about 6 dB, much higher than that of the first-order derivative of Stokes intensity with respect to position. We used a quadratic fitting method to find the peak position at both sides of the maximum, so that it gives a more accurate location. The first boundary location was measured as 200 ns for the three strain cases, and the second boundary location was measured as 216.5 ns for Strain-1 and 216.0 for both Strain-2 and Strain-3. Knowing the two boundaries, the length of the strained section was thus calculated as 16.5 ns (=165 cm) for Strain-1 and 16 ns (160 cm) for both Strain-2 and Strain-3. Comparing to the actual length of the strained section, 157 cm, we see that the accuracy is within one to two digitizing steps, which is equivalent to 5 cm to 10 cm.

Once two boundaries were found we then applied one peak fitting method for the Lorentzian shape of the Brillouin spectrum at the middle point of two boundaries. This will allow us to find the central Brillouin frequency and to get the strain for this section. It is assumed that between two boundaries the strain is uniformly distributed. The accuracy of the boundary measured by this method depends on the SNR, the scanning frequency step, $\Delta\nu_{scan}$, the digitizing step Δz and the frequency variation $\delta\nu$ between the two sections. For a large scanning frequency increment, $\Delta\nu_{scan} >> \delta\nu$, the accuracy in evaluating $\alpha(\nu, z)$ decreases. Although it is commonly believed that the spatial resolution is determined by pulse width, the digitizer step is the ultimate resolving factor in this method, since the recorded spatial information within the pulse width is updated at every digitized step.

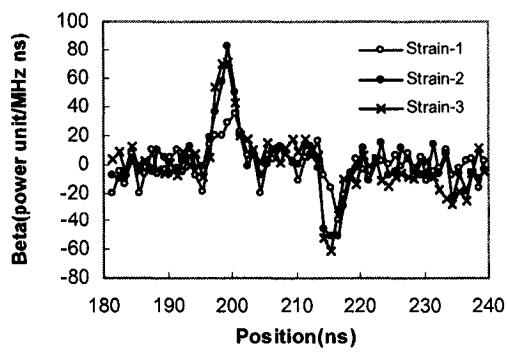

Fig. 7-4 $\beta(\nu, z)$ versus position for Strain-1 Strain-2 and Strain-3.

Figure 7-5 shows the strain distribution measured by a sensor with the boundary identification method as Strain-1, Strain-2, and Strain-3 corresponding to strain levels of 16, 108 and 200 με. The dial-gauge measurements are also plotted as Strain-1', Strain-2' and Strain-3' corresponding strain levels 19, 114 and 217 με.

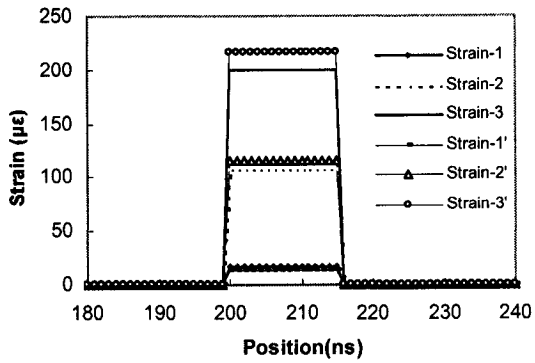

Fig. 7-5 Strain distribution Strain-1, Strain-2 and Strain-3 measured by sensor using boundaries identification method and the dial-gauge measurements Strain-1', Strain-2' and Strain-3'.

Note that the strain measurement accuracy of the dial-gauge is 6 με. The distributed sensor has a frequency measurement accuracy of 1.2 MHz, equivalent to 13 με. The difference between the distributed sensor and dial gauge reading is within the sum of uncertainties (±21 με) attributed to both methods. Since this method is not iterative but a rather simple calculation (all the peak fitting methods use iteration approach), it is suitable for implementation to the real time measurement.

7.6 Summary

The second-order partial derivative of the Stokes signal with respect to frequency and position shows a maximum or minimum at the boundary between two different strained sections. This idea is used to locate the boundary of different strain regions. Using this method can improve the location accuracy to ½ to 1/4 of the pulse length with a 1.2 MHz minimum detectable Brillouin frequency between the two sections. This method is relatively simple, and therefore can be deployed in the sensing system to detect the location of a boundary between two strained sections.

Chapter 8

Influence of transient phonon relaxation on the Brillouin loss spectrum of nanosecond pulses

[This chapter is adapted from the paper published in OPTICS LETTERS, 31, 888-890(2006)]

8.1 Introduction

In this chapter, we study the influence of transient phonon relaxation on the Brillouin loss spectrum, and the physics of Brillouin signal cross talk near the boundary of two strained sections. The transient phonon is observed when the pulse width is shorter than the phonon relaxation time in a Brillouin scattering sensing system.

For a pump-probe based distributed Brillouin sensor system, when the probe signal consists of the pulse and DC component, the Brillouin loss spectral width can be much narrower than the pulse spectrum [Bao *et al.* 1999, Lecoueche *et al.* 2000]. The advantage of this approach is a high signal-to-noise ratio, which leads to better temperature-strain accuracy. To our knowledge there has been no research conducted on the phonon relaxation time (or the acoustic field decay time) affected by the DC level of the probe signal and pump power in the Brillouin loss spectrum at a pulse width shorter than the natural phonon lifetime (~10 ns).

We conducted experimental and theoretical studies of the effects of the pump and the DC levels of the probe on the acoustic field for a short pulse (~10 ns), by studying the Brillouin loss spectrum at the boundaries of two or three temperature and strain sections in the sensing fibers. We demonstrated, for what is believed to be the first time, that when a 2 ns pulse is used the probe and the pump interact with the acoustic field, resulting in a longer relaxation time. This induces an AC power increment in the Brillouin loss spectrum in the next fiber region with a distance much larger than the pulse length. This can cause a problem for a distributed sensor in determining the strain-temperature boundary, and for central Brillouin peak fitting to a multiple peak convolution, and it affects temperature and strain accuracy. The measured saturation power of the pump and

probe waves of nanosecond pulses is ~4 mW, which is much lower than the stimulated Brillouin scattering threshold.

The prolonged phonon relaxation time, defined as τ_{decay}, depends on the pump and DC levels of the pulsed probe signal. This was detected by an AC coupled optical receiver. τ_{decay} was measured with two temperature sections of a PANDA fiber at the end of the first fiber section from the maximum Brillouin loss signal ($\nu_1-\nu_2=\nu_{B1}$), decreasing to minimum Brillouin loss in section-2 ($\nu_1-\nu_2\neq\nu_{B2}$). The boundary was determined using the second-order derivative described in Chapter 7. Note that ν_1 and ν_2 are the frequencies of the pump and probe lasers, respectively. ν_{B1} and ν_{B2} are the Brillouin frequencies for fiber sections-1 and -2, respectively. The Brillouin loss signal shows saturation of ~4 mW for pump power at 2 ns pulse width with a power of 2.5 $\pm$0.5 mW for the probe.

For the DC level effect on the acoustic field, we have found a minimum phonon relaxation time corresponding to a moderate DC level, if the DC level is higher or lower than this value, then the relaxation time is increased for single-mode (SM) fiber. The same trend is found for increasing pump power; a minimum phonon relaxation time occurs at ~3 mW.

8.2 Observation of the transient phonon field and its decay

Consider two PM fiber sections with different Brillouin frequencies ν_{B1} and ν_{B2}. When the pump and probe frequency difference is ν_{B1}, a strong phonon field is created as the pulse propagates along section-1. Even after the pulse passes section-1 and goes to section-2, the phonon field at ν_{B1} is still sustained by the interaction of the probe DC level and pump signals. When the CW power or the DC level is increased, the acoustic wave does not decay naturally. Rather, it is driven by the CW pump and the DC level of the probe after passage of the pulse. This process can be seen in the Brillouin loss signal when $\nu_1-\nu_2=\nu_{B1}$ (Fig.8-1): the ν_{B1} component is seen at time 228 ns (section-2), which is 12 ns from the boundary at 216 ns. This time difference is larger than the 2 ns pulse width and the natural phonon lifetime of ~10 ns.

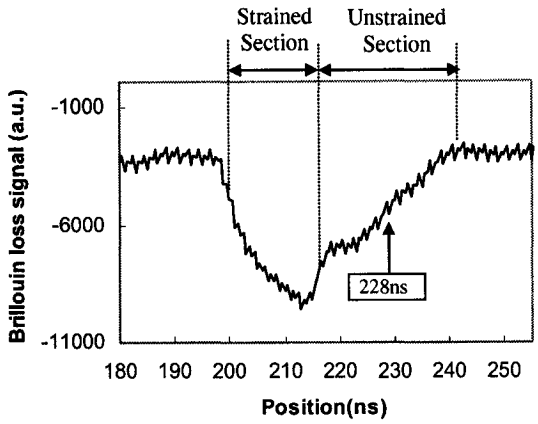

Fig. 8-1 Brillouin loss signal versus position for a PM Panda fiber when $\nu_1-\nu_2 = \nu_{B1}$=12830 MHz. The strained section is between 200 and 216 ns.

The experimental setup [Yu *et al.* 2005] was similar to that described in chapter 5. The DC level was determined by the extinction ratio (ER), the pulse/DC level ratio, an ER of 14 dB, power P_{probe}~2.5 mW, and P_{pump}=3 mW. 1.6 m Panda PM fiber was stretched by 400 μs, with a small strain gradient between the strained and loose fiber. The equivalent Brillouin frequency shift was ~31 MHz. The acoustic field at section-1 interacts with the CW pump before reaching the minimum Brillouin loss at 240 ns, which gives τ_{decay} as 240–216 ns=24 ns.

8.3 The effect of the CW pump power to the transient phonon relaxation

We also studied the correlations between the CW pump power and the acoustic field relaxation, as well as the pump power saturation and the Brillouin loss signal. A 10 m Panda PM fiber with a loose 1.2 mm tube was used in two sections: length L_1=5 m in an environment chamber of −45℃ (ν_{B1}=12670 MHz), and length L_2=5 m at room temperature (ν_{B2} =12790 MHz). The Brillouin loss signal versus position at different pump powers is plotted in Fig. 8-2. The small positive peak at the input end is due to the reflection at the connector. At low pump power, the reflection of the probe pulse is added

to the pump power as a positive peak. As the pump power increases for a fixed probe power, the reflection of the probe is smaller than the pump power. The Brillouin loss signal shows saturation at a pump power of ~4 mW. Note that this saturation power is much lower than the stimulated Brillouin scattering threshold for a 2 ns pulse, which occurs at a few hundred milliwatts. This means that the optimized pump power for the distributed sensor should be ~4 mW for a pulse width of 1 ns to 5 ns.

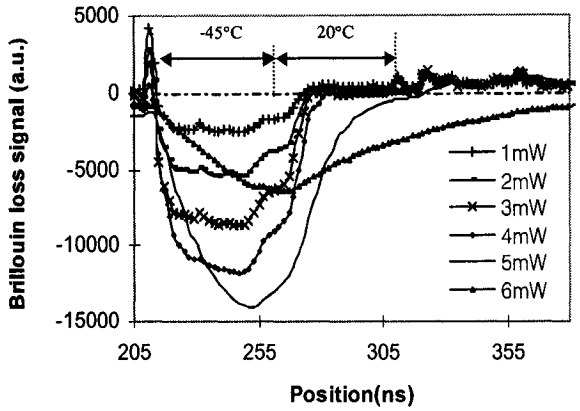

Fig. 8-2 Brillouin loss signal versus position at ν_{B1} =12760 MHz with different pump powers for a 2 ns pulse.

Figure 8-3 represents the measured τ_{decay} at different pump powers for a pulse power of 2.3 mW and an ER of 14 dB. As the Brillouin loss signal is proportional to the acoustic wave, we can measure the Brillouin loss signal decay to obtain the relaxation time of the acoustic wave. Acoustic waves decay as Brillouin loss signal $P=P_0 \exp(-t/\tau_{decay})$, where P_0 is the maximum Brillouin loss signal at the boundary measured at difference $\nu_1 - \nu_2 = \nu_{B1}$ =12670 MHz.

The slopes in Fig. 8-3 give the acoustic wave relaxation time at the different pump powers shown in Table 8-1. At a pump power of 3 mW, we observed an ~9 ns relaxation time, which is equivalent to an ~39 MHz Brillouin bandwidth. This bandwidth value matched well with our measured the Brillouin loss spectrum width of ~38 MHz at -45 °C. The bandwidth remains unchanged for pump power of 1mW to 6 mW, as the ER is kept constant.

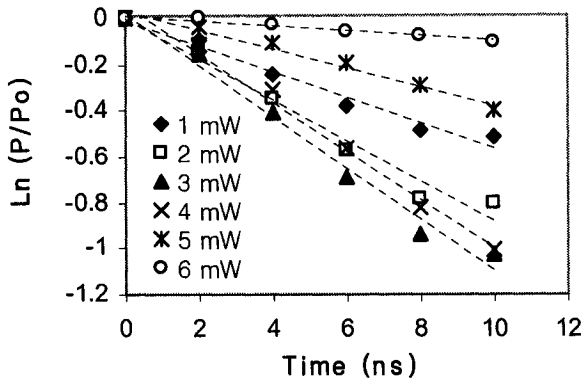

Fig. 8-3 Brillouin loss signal versus time at $\nu_1 - \nu_2 = \nu_{B1}$ for different CW pump powers.

Table 8-1 Phonon Relaxation Time τ_{decay} for PM Fiber

Pump Power (CW ,mW)	1	2	3	4	5	6
τ_{decay} **(ns)**	18.0	11.3	9.0	9.4	24.8	90.1

The prolonged acoustic field was observed in the Brillouin loss signal by an AC-coupled optical receiver in the form of AC power gain at ν_{B1} in section-2 (ν_{B2}). In the ν_{B2} section, the returned pump signal includes ν_{B2} and was added to the probe DC level signal interaction with a prolonged acoustic field at ν_{B1}. Therefore ν_{B1} appeared in the spectrum corresponding to a time delay at section-2 for a distance much longer than the pulse length and the natural phonon relaxation time. ν_{B2} and ν_{B1} belong to different locations, arrive at the same time, and became evident in the same Brillouin loss spectrum. Hence the probe DC level interacts with the prolonged ν_{B1} field, acting as a gain in this Brillouin loss signal at ν_{B2}. We refer to this as an AC power increment to differentiate it from the peak Brillouin loss signal at ν_{B1}. This combined Brillouin loss spectrum continues to exist during τ_{decay} for the acoustic field in section-1. This process was simulated with our theoretical model [Afshar *et al.* 2005b] for AC detection of the Brillouin loss spectrum.

8.4 The effect of the DC level of the pulse on the transient phonon field

The AC power increment was studied at different DC levels of the probe (the pulse amplitude remains constant) by use of a 30 m SM fiber divided into three 10 m sections, with Brillouin frequencies ν_{B1} =12785 MHz, ν_{B2}=12820 MHz (25°C), and ν_{B3} =12850 MHz. The maximum power for the probe signal is 7 mW. The CW pump power was maintained at 4 mW. Fig.8-4 shows the Brillouin loss spectrum at section-2 for a DC level corresponding to an ER of 10 dB to 20 dB with an AC power increment occurring at 260 ns (the middle of section-2). It is clear that both the ν_{B1} and the ν_{B2} frequency components appeared in the spectrum. If we fit the central peak with a Lorentzian profile, then the Brillouin frequency will be shifted from the true peak position.

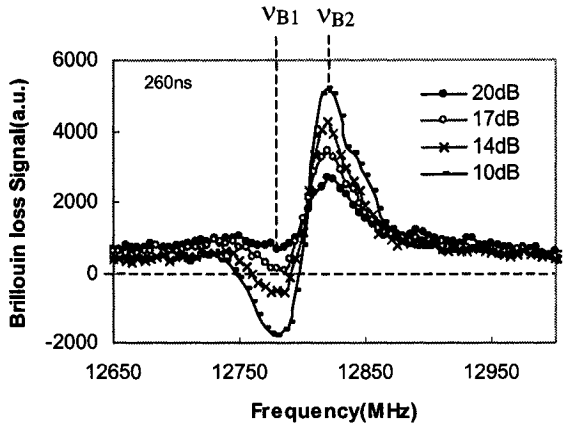

Fig. 8-4 Brillouin loss spectra at the middle of section-2 (at time 260 ns) for different ERs corresponding to probe powers of 0.1, 0.6, 3.3, and 7 mW; ν_{B1}=12780 MHz, ν_{B2} =12820 MHz, and ν_{B3}=12850 MHz.

This effect may create a drawback to the distributed Brillouin sensing, namely, fitting errors in the central Brillouin peak for the strain and temperature accuracy. Due to the negative peak, the single-peak fit will be shifted from the positive peak, while the multiple-peak fit will give two Brillouin frequencies for the related temperature and strain for this fiber section. To solve this problem, one can use the position correlation in the time domain, combined with the central frequency fitting method, and then find the

maximum Brillouin loss and Brillouin frequency for each peak for the location, instead of looking for the highest Brillouin loss signal among Brillouin peaks at a given location. This allows the removal of the different section peaks.

To study the effect of DC level on the prolonged phonon relaxation time τ_{decay} in SM fiber, we measured τ_{decay} for different ERs when $\nu_1 - \nu_2 = \nu_{B2} \approx 12820$ MHz for a pump power of 4 mW. We found a minimum τ_{decay} at a moderate DC level. When the DC level is higher or lower, τ_{decay} tends to be longer. This minimum relaxation time equivalent DC level ($\sim$14 dB) is recommended for the sensing operation. The result is shown in Table 8-2. The Brillouin loss spectral width increases with increasing ER because of the increase of the pulse component [Lecoueche *et al.* 2000]. The decay time uncertainty for SM fiber is higher than that for PM fiber because the polarization state changes in the SM fiber, which induces a Brillouin loss signal variation. This translates to decay time uncertainties of $\sim$4 ns for SM fiber and $\sim$1 ns for PM fiber.

Table 8-2 Phonon Relaxation Time τ_{decay} and Brillouin Loss Spectral Width at Different ERs for SM Fiber

ER (dB)	10	12	14	17	20
$\tau_{decay\ (ns)}$	23.8	24.0	20.6	34.5	45.2
$\Delta\nu_B$(MHz)	38	39	42	45	58

Figure 8-5 shows the calculated Brillouin loss signal at AC detection. It can be seen that the prolonged phonon fields at ν_{B1} and ν_{B2} extend to sections-2 and -3 at lengths $\geq$10 and $\geq$20 m, respectively. The Brillouin loss also extends more than the natural phonon lifetime. This agrees with the experimental observation shown in Fig. 8-3. Apparently the interaction between the DC of the probe and pump contributes to this prolonged acoustic field, which is attributed to a long phonon relaxation time. We noticed that a lower DC level of the probe corresponds to a shorter phonon relaxation time of $\sim$10 ns.

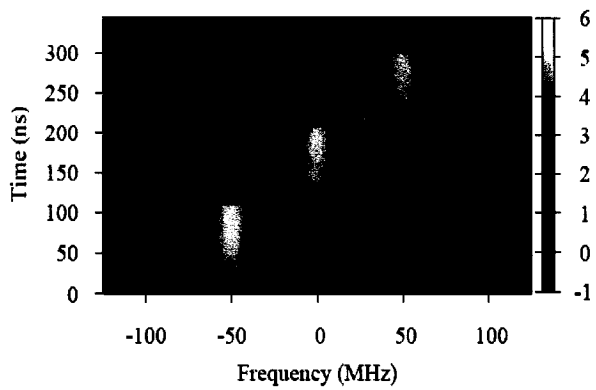

Fig. 8-5 Calculated AC pump power (Brillouin loss signal) in 3-10 m section fibers with ν_{B1} =12750 MHz, ν_{B2}=12800 MHz, and ν_{B3}=12850 MHz (ER=10 dB, P_{probe}=10 mW, P_{pump}=5 mW).

8.5 Summary

We have demonstrated prolonged acoustic field relaxation time and its dependence on the pump power and the DC level of the probe pulse, as well as its effect on the Brillouin loss spectrum. Using two- or three-section sensing fiber and varying DC levels of the probe and pump powers, we observed an AC power increment in the AC-detected signal (Brillouin loss signal) as well as a prolonged acoustic field relaxation process. This effect may create a drawback to the use of a distributed Brillouin sensor in determining the boundary of two different Brillouin frequency sections and the corresponding temperature or strain reading.

Chapter 9
Conclusions and Future work

9.1 Conclusions

Based on experimental studies of the temperature and strain dependence of the Brillouin loss spectrum for the three types of commercial PM fibers, it was found that PANDA and Bow-tie fibers are feasible for simultaneously measuring strain and temperature. Tiger fibers are not suitable for sensing applications. The expressions for simultaneous temperature and strain sensing, the maximum errors and RMS values of temperature and strain measurements have been derived using combinations of 1) power and Brillouin frequency, 2) bandwidth and Brillouin frequency, and 3) bandwidth and Brillouin power.

A 2^{nd} derivative method was proposed for the identification of strain locations with spatial location accuracy better than the pulse width. This method involves only simple data processing, which can be implemented into the control and display system in the Brillouin sensing system.

The observations and studies on the influence of the transient phonon relaxation were presented. The transient phonon field lasts longer than the phonon lifetime (~10 ns). A 90 ns phonon relaxation time for two temperature/strain sections has been observed. This prolonged relaxation time depends on the pump and probe powers, and it affects the use of a distributed Brillouin sensor in determining the boundary of two different Brillouin frequency sections and the corresponding temperature or strain reading.

9.2 Proposed future work

(1) To develop a numerical model for a deeper understanding of the transient phonon relaxation process.
(2) To build a sensing system using polarization-maintaining components.

(3) To use PM fibers for structural health monitoring as well as for early failure alarm of critical structures which require high accuracy.

(4) To implement the second derivative method in the real-time test control-display program to accurately identify strain locations.

REFERENCES

[3M catalog 2001] 3M catalog, Introduction to PM fiber, 2001.

[Afshaarvahid and Munch 2001] S. Afshaarvahid and J. Munch, "A transient, three-dimensional model of stimulated Brillouin scattering," *Journal of Nonlinear Optical Physics & Materials*, 10, 1-27 (2001).

[Afshar *et al.* 2005a] S. Afshar V., X. Bao, L. Zou and L. Chen, "Brillouin spectral deconvolution method for cm spatial resolution and high strain accuracy measurement in Brillouin sensors," *Optics Letters,* 30, 705-707 (2005).

[Afshar *et al.* 2005b] S. Afshar, V.P. Kalosha, X. Bao and L. Chen, "Enhancement of stimulated Brillouin scattering of higher-order acoustic modes in single-mode optical fiber," *Optics Letters,* 30, 2685-2687 (2005).

[Alahbabi *et al* 2004] M. Alahbabi, Y. T. Chao, and T. P. Newson, "Comparison of the methods for discriminating temperature and strain in spontaneous Brillouin-based distributed sensors," *Optics Letters,* 29, 26-28 (2004).

[Alahbabi *et al.* 2005] M. N. Alahbabi, Y. T. Cho, and T. P. Newson, "Simultaneous temperature and strain measurement with combined spontaneous Raman and Brillouin scattering," *Optics Letters*, 30, 1276-1278(2005).

[Agrawal 1995] Govind P. Agrawal, *Nonlinear Fiber Optics*, 2nd ed., Academic Press, Boston (1995).

[Agrawal 1997] Govind P. Agrawal, *Fiber-Optic Communication Systems*, 2nd ed., John Wiley & Sons, Inc. (1997).

[Bao *et al.* 1993a] X. Bao, D. J. Webb, and D. A. Jackson, "22-km distributed temperature sensor using Brillouin gain in an optical fiber," *Optics Letters*, 18, 552-554 (1993).

[Bao *et al.* 1993b] X. Bao, D. J. Webb, and D. A. Jackson, "32-km distributed temperature sensor based on Brillouin loss in an optical fiber," *Optics Letters*, 18, 1561-1563 (1993).

[Bao *et al.* 1993c] X. Bao, D. J. Webb, D. A. Jackson, "Temperature non-uniformity in distributed temperature sensor," *Electronics Letters,* 29, 976-978 (1993).

[Bao *et al.*1994a] X. Bao, D. J. Webb, and D. A. Jackson, "22 km distributed strain sensor using Brillouin loss in an optical fiber," *Optics Communications*, 104, 298-302 (1994).

[Bao *et al.* 1994b] X. Bao, D. J. Webb, and D. A. Jackson, "Combined distributed temperature and strain sensor based on Brillouin loss in an optical fiber," *Optics Letters*, 19, 141-143(1994).

[Bao *et al.* 1995] X. Bao, J. Dhliwayo, N. Heron, D. J. Webb, and D. A. Jackson, "Experimental and theoretical studies on a distributed temperature sensor based on Brillouin scattering," *Journal of Lightwave Technology*, 13, 1340-1348 (1995).

[Bao *et al.* 1999] X. Bao, A. Brown, A., DeMerchant, J. and Smith, "Characterization of the Brillouin loss spectrum of single mode fiber by use of very short (<10-ns) pulses," *Optics Letters*, 24, 510-512 (1999).

[Bao *et al.* 2001] X. Bao, M. DeMerchant, A. Brown, and T. Bremner, "Tensile and Compressive Strain Measurement in the Lab and Field with the Distributed Brillouin Scattering Sensor," *Journal of Lightwave Technology,* 19, 1689-1704 (2001).

[Bao *et al.* 2002] X. Bao, C. Huang, and X. Zeng, "Simultaneous strain and temperature monitoring of the composite cure with a Brillouin-scattering-based distributed sensor," *Optical Engineering,* 41, 1496-1501 (2002).

[Bao *et al.* 2004a] X. Bao, Q. Yu, L. Chen, "Simultaneous strain and temperature measurements with polarization-maintaining fibers and their error analysis by use of a distributed Brillouin loss system," *Optics Letters*, 29, 1342 (2004).

[Bao *et al.* 2004b] Xiaoyi Bao, Yidun Wan, Lufan Zou, and Liang Chen, "Effect of optical phase on a distributed Brillouin sensor at centimeter spatial resolution," OPTICS LETTERS,30, 827-829 (2005)

[Bao *et al.*2005a] X. Bao, Y. Wan, L. Zou, and L. Chen, "Effect of optical phase on a distributed Brillouin sensor at centimeter spatial resolution," *Optics Letters*, 30, 827-829 (2005).

[Bao *et al.* 2006] X. Bao, Q. Yu, V. P. Kalosha, and L. Chen, "The influence of transient phonon relaxation on the Brillouin loss spectrum for nanosecond pulses," *Optics Letters*, 31, 888-890 (2006).

[Barnowski *et al.* 1976] M. K. Barnowski and S. M. Jensen, "Fiber waveguides: a novel technique for investigating attenuation characteristics," *Applied Optics*, 15, 2112-2115 (1976).

[Barnowski *et al.* 1977] M. K. Barnowski and S. M. Jensen, "Optical time domain reflectometer," *Applied Optics,* 16, 2375-2379 (1977).

[Birch *et al.* 1982] R. D. Birch, M. P. Varnham, D. N. Payne, and E. J. Tarbox,, "Fabrication of polarization-maintaining fibers using gas-phase etching," *Electron Letter*, 18, 1036-1038 (1982).

[Boyd 2003] Robert W. Boyd, "Nonlinear Optics," Second Edition, Academic Press, 2003. Chapter 8 and 9.

[Brillouin 1922] L. Brillouin, "Diffusion de la lumière et des rayons par un corps transparent homogène," *Annales de Physique*, 17, 88(1922).

[Brown *et al.* 1998] A. Brown, M. DeMerchant, X. Bao, and T. Bremner, "Advances in distributed sensing using Brillouin scattering," in *Smart Structures and Materials 1998: Sensory Phenomena and Measurement Instrumentation for Smart Structures and Materials*, R.O. Claus, W.B. Spillman, Jr. Eds. *Proceedings of SPIE*, 3330, 294-300 1998.

[Brown *et al.* 1999] A. Brown, M. DeMerchant, X. Bao, and T. Bremner, "Spatial resolution Enhancement of a Brillouin-Distributed sensor using a novel signal processing method," *Journal of Lightwave Technology*, 17, 1179-1183 (1999).

[Brown 2000] Anthony W. Brown, "Development of a Brillouin Scattering Based Distributed Fiber Optic Strain Sensor," Ph.D Thesis, University of New Brunswick (2000).

[Brown *et al.* 2005] A. Brown, B. Colpitts and K. Brown, "Distributed sensor based on Dark-pulse Brillouin scattering," *Photonics Technology Letters,* 17, 1501-1503 (2005).

[Chen and Bao 1998] L. Chen and X. Bao, "Analytical and numerical solutions for steady state stimulated Brillouin scattering in a single-mode fiber," *Optics Communications*, 152 65-70 (1998).

[Chiao *et al.* 1964] R. Y. Chiao, C. H. Townes, and B. P. Stoicheff, "Stimulated Brillouin scattering and coherent generation of intense hypersonic waves," *Physical Review Letter*, 12, 562 (1964).

[Culverhouse *et al.* 1989] D. Culverhouse, F. Farahi, C .N. Pannell, and D. A. Jackson, "Potential of stimulated Brillouin scattering as sensing mechanism for distributed temperature sensors," *Electronics Letters*, 25, 913-915 (1989).

[Dakin *et al.* 1985] J. P. Dakin, J. Pratt, G.W. Bibby and J. N. Ross, "Distributed optical fiber Raman temperature sensor using a semiconductor light source and detector," *Electronics Letters,* 21, 569-570 (1985)

[Data sheet, 3 M 2001] Tiger™ Family of Polarization Control Fibers, 3 M Data sheet, (2001)

[Deventer *et al.* 1994] M. O. van Deventer and A. J. Boot, "Polarization properties of stimulated Brillouin scattering in single-mode fibers," *Journal of Lightwave Technology*, 12, 585-590 (1994).

[DeMerchant *et al.* 1998] M. DeMerchant, A. Brown, X. Bao, and T. Bremner, "Automated system for distributed sensing," in *Smart structures and Materials 1998: Sensory Phenomena and Measurement Instrumentation for Smart Structures and Materials*, R.O. Claus, W.B. Spillman, Jr. Eds. *Proceedings of SPIE*, 3330, 315-322 (1998).

[DeMerchant 2000] M. DeMerchant, "Distributed Strain Sensing for Civil Engineering Applications," Ph.D Thesis, University of New Brunswick (2000).

[DeMerchant *et al.* 2000] M. D. DeMerchant, A.W. Brown, X. Bao and T. W. Bremner, "Signal processing for a high-spatial-resolution distributed sensor," *Optical Engineering*, 39, 1632-1636 (2000).

[Farries *et al.* 1984] M. C. Farries et al., "Distributed sensing using stimulated Raman interaction in a monomode optical fiber," *Symposium of Optical fiber sensing,* Proceedings pp.121-132 (1984).

[Fellay *et al.* 1997] A. Fellay, L. Thévenaz, M. Facchini, M. Niklès, and P. Robert, "Distributed sensing using stimulated Brillouin scattering: towards ultimate resolution," *12th International Conference on Optical Fiber Sensors*, OSA Technical Digest Series 16, 324-327 (1997).

[Fellay *et al.* 2001] A. Fellay, S. Le Floch, M. Facchini, L. Thévenaz, W. Scandale, P. Robert, "Brillouin gain curve measurements in fibers at cryogenic temperatures (3 K-140 K)," *Proc. of the 6th Optical Fibre Measurement Conference*, Cambridge UK, p. 55-58

(2001).

[Garus *et al.* 1997] D. Garus, T. Golgolla, K. Krebber, and F. Schliep, "Brillouin optical frequency-domain analysis for distributed temperature and strain measurements," *Journal of Lightwave Technology*, 15, 654-662 (1997).

[Geinitz *et al.* 1999] E Geinitz, S Jetschke, U Ropke, S Schroter, R Willsch and H Bartelt, "The influence of pulse amplification on distributed fiber-optic Brillouin sensing and a method to compensate for systematic error," *Measurement and Science and Technology*, 10, 112–116 (1999).

[Hartog 1983] A. H. Hartog, "A distributed temperature sensor based on a liquid-core optical fibre," *Journal of Lightwave Technology*, 1, 498-551 (1983).

[Hecht 1990] Eugene Hecht, "Optics," Addison-Wesley Publishing Company, 2nd edition, 1990, pp. 339.

[Horiguchi *et al.* 1989a] T. Horiguchi, T. Kurashima and M. Tateda, "Tensile strain dependence of Brillouin frequency shift in silica optical fibers," *IEEE Photonics Technology Letters*, 1, 107-108 (1989).

[Horiguchi *et al.* 1989b] T. Horiguchi and M. Tateda, "Optical fiber evaluation method and system," US paten, No. 4,997,227 (1989).

[Horiguchi and Tateda 1989] T. Horiguchi and M. Tateda, "Optical-fiber-attenuation investigation using stimulated Brillouin scattering between a pulse and a continuous wave," *Optics Letters*, 14, 408-410 (1989).

[Horiguchi *et al.* 1989c] T. Horiguchi, M. Tateda, N. Shibata and Y. Azuma, "Brillouin gain variation due to a polarization-state change of the pump or Stokes fields in standard single-mode fibers," *Optics Letters*, 14, 329-331 (1989).

[Kurashima *et al.* 1992] T. Kurashima, T. Horiguchi, and M. Tateda, "Thermal effects of Brillouin gain spectra in single-mode fibers," *IEEE Photonics Technology Letters*, 10, 718-720 (1990).

[Horiguchi *et al.* 1992] T. Kurashima, T. Horiguchi, H. Izumita, S. Furukawa, and Y. Koyamada, "Brillouin optical-fiber time domain reflectometry," Proceedings of *the International Quantum Electronics Conference*, Vienna, 42-44, June 1992.

[Horiguchi *et al.* 1995] T. Horiguchi, K. Shimizu, T. Kurashima, M. Taleda, and Y. Koyamada, " Development of a distributed sensing technique using Brillouin scattering," *Journal of Lightwave Technology*, 13 1296-1302 (1995).

[Hosaka et al. 1981] T. Hosaka, K. Okamoto, T. Miya, Y. Sasaki, and T. Edahiro, "Low-loss single-polarization fibers with asymmetrical strain birefringence," *Electron Letters,* 17, 530-531(1981).

[Hotate *et al.* 1999] K. Hotate and T. Hasegawa, "Measurement of Brillouin gain spectrum distribution along an optical fiber with a high spatial resolution using a novel correlation-based technique," *13th International Conference on Optical Fiber Sensors*, Kyongju, Korea, *Proceedings of SPIE*, 3746, 337-340 (1999).

[Hotate *et al.* 2000] K. Hotate and T. Hasegawa, "Measurement of Brillouin gain spectrum distribution along an optical fiber suing a correlation-based technique-Proposal experimental and simulation," *IEICE Transactions on Electronics,* Vol. E83-C, 3, 405-412 (2000).

[Hotate *et al.* 2001] K. Hotate and M. Tanaka, "Correlation-based continuous-wave technique for optical fiber distributed strain measurement using Brillouin scattering with cm-order spatial resolution," *IEICE Transactions on Electronics,* Vol. E84-C, 12, 1823-1828 (2001).

[Hotate *et al.* 2002] K. Hotate and M. Tanaka, "Distributed fiber Brillouin strain sensing with 1-cm spatial resolution by correlation-based continuous-wave technique," *IEEE Photonics Technology Letters,* 14, 179-181 (2002).

[Kee *et al.* 2000a] H. H. Kee, G. P. Lees, and T. P. Newson, "All-fiber system for simultaneous interrogation of distributed strain and temperature sensing by spontaneous Brillouin scattering," *Optics Letters*, 25, 695-697 (2000).

[Kee *et al.* 2000b] H. H. Kee, G. P. Lees, and T. P. Newson, "Technique for Measuring Distributed Temperature with 35-cm Spatial Resolution Utilizing the Landau-Placzek Ratio," *IEEE Photonics Technology Letters,* 12, 873-875 (2000).

[Kersey 1996] A. D Kersey, "A review of recent developments in fiber optic sensor technology," *Optical Fiber Technology*, 2, 291-317 (1996).

[Krohn 2000] David A. Krohn, "*Fiber optic sensors: fundamentals and applications*," 3rd ed., The International Society for Measurement and Control (2000).

[Kurashima, *et al.* 1990a] T. Kurashima, T. Horiguchi, and M. Tateda, "Thermal effects on the Brillouin frequency shift in jacketed optical silica fibers," *Applied Optics*, 29, 2219-2222 (1990).

[Kurashima et al. 1990b] T. Kurashima, T. Horiguchi, and M. Tateda, "Distributed-temperature sensing using stimulated Brillouin scattering in optical silica fibers," *Optics Letters*, 15, 1038-1040 (1990).

[Kurashima *et al.* 1997] T. Kurashima, M. Tateda, T. Horiguchi, and Y. Koyamada, "Performance improvement of a combined OTDR for distributed strain and loss measurement by randomizing the reference light polarization state," *IEEE Photonics Technology Letters,* 9, 360-362 (1997).

[Lecoueche *et al.* 2000] V. Lecoueche, D. J. Web, C. N. Pannell, and D. A. Jackson, "Transient response in high resolution Brillouin-based distributed sensing using probe pulses shorter than the acoustic relaxation time," *Optics Letters*, 25, 156-158 (2000).

[Lee *et al.* 2001] C. C. Lee, P. W. Chiang, and S. Chi, "Utilization of a Dispersion-Shifts Fiber for Simultaneous Measurement of Distributed Strain and Temperature Through Brillouin Frequency Shift," *IEEE Photonics Technology Letters,* 13, 1094-1096 (2001).

[Li *et al.* 2003a] Yongqian Li, Fucai Zhang, and Toshihiko Yoshino, "Wide temperature-range Brillouin and Rayleigh optical-time-domain reflectometry in a dispersion-shifted fiber," *Applied Optics*, 42, 3772-3775 (2003).

[Li *et al.* 2003b]Y. Li, F. Zhang, and T. Yoshino, "Wide-Range Temperature Dependence of Brillouin Shift in a Dispersion-Shifted Fiber and Its Annealing Effect," *Journal Lightwave Technologies,* 21, 1663-1667 (2003).

[Lines 1984] M. E. Lines, "Scattering losses in optic fiber materials. I. A new parametrization," *Journal Applied. Physics* **55,** 4052–4057 (1984).

[Lipson *et al.* 1995] S.G. Lipson, H. Lipson, and D. S. Tannhauser, Optical Physics, 3rd edition, Cambridge University Press, 1995.

[Maughan *et al.* 2001a] S. M. Maughan, H. H. Kee, and T. P. Newson, "A Calibrated 27-km Distributed Fiber Temperature Sensor Based on Microwave Heterodyne Detection of Spontaneous Brillouin Backscattered Power," *IEEE Photonics Technology Letters,* 13, 511-513 (2001).

[Maughan *et al.* 2001b] S. M. Maughan, H. H. Kee, and T. P. Newson, "57-km single-ended spontaneous Brillouin-based distributed fiber temperature sensor using microwave coherent detection," *Optics Letters*, 26, 331-333 (2001).

[Moyer *et al.* 1998] R. S. Moyer, R. Grencavich, R. W. Smith, and W. J. Minford, "Design and qualification of hermetically packaged lithium niobate optical modulator," *IEEE Proceedings, 1997 Electronic Component and Technologies Conference*. pp. 425-429, San Jose, CA (1997).

[Mitsugi and Nagata. 1996] N. Mitsugi, and H. Nagata, "Hysterisis in DC-bias drift of $LiNbO_3$ optical modulators," *Engineering & Laboratory Notes, Optics & Photonics News*, 7, 6831-6832 (1996).

[Nagata 2000] H. Nagata, "DC Drift Failure Rate Estimation on 10 Gb/s X-Cut Lithium Niobate Modulators," *IEEE Photonic Technology Letter*, 12, 1477-1479 (2000).

[Nagata *et al.* 2004] H. Nogata, G. D. Feke, Y. Li and W. R. Bosenberg, " DC drift of Z-Cut $LiNbO_3$ Modulator," *IEEE Photonic Technology Letter*, 16, 1655-1657 (2004).

[Naruse *et al.* 2002] H. Naruse, M. Tateda, H. Ohno, and A. Shimada, "Dependence of the Brillouin gain spectrum on linear strain distribution for optical time-domain reflectometer-type strain sensors," *Applied Optics,* 41, 7212-7217 (2002).

[Niklès *et al.* 1994] M. Niklès, L. Thèvenaz, and P. A. Robert, "Simple distributed temperature sensor based on Brillouin gain spectrum analysis," *Proceedings of OFS'94*, Glasgow, Scotland, 138-141 (1994).

[Niklès *et al.* 1996] M. Niklès, L. Thèvenaz, and P. A. Robert, "Simple distributed fiber sensor based on Brillouin gain spectrum analysis," *Optics Letters*. 21, 758-760 (1996).

[Niklès *et al.* 1997] M. Niklès, L. Thèvenaz, and P. A. Robert, "Brillouin gain spectrum characterization in single-mode optical fibers," *Journal of Lightwave Technology*, 15, 1842-1851 (1997).

[Nishizawa *et al.* 1994] N. Nishizawa, S. Kume, M. Mori, and T. Goto, "Symmetric and asymmetric fiber optic loop mirrors for observing guided-acoustic-wave Brillouin scattering in PM fibers," *Optics Letters,* 19, 1424-1426 (1994).

[Noda *et al.* 1986] J. Noda, K. Okamoto, and Y. Sasaki, "Polarization maintaining fibers and their applications," *Journal of Lightwave Technology*, Vol. LT-4, 1071-1089 (1986).

[Ohno *et al.* 1999] H. Ohno, Y. Uchiyama, and T. Kurashima, "Reduction of the effect of temperature in a fibre optic distributed sensor used for strain measurements in civil structures." Smart Structures and Materials 1999: *Sensory Phenomena and Measurement Instrumentation for Smart Structures and Materials*, R. O. Claus and W. B. Spillman, eds., *Proceedings of SPIE*, 3670, 486-496 (1999).

[Ohsaki *et al.* 2002] M. Ohsaki, M. Tateda, T. Omatsu, H. Ohno, "Spatial resolution enhancement of distributed strain measurement using BOTDR by partially cluing optical fiber," *IEICE Transactions on Communications,* E85-B, 1636-1639 (2002).

[Othonos and Kalli] Andreas Othonos and Kyriacos Kalli, "Fiber Bragg Gratings: fundamentals and application in telecommunications and sensing," Chapter 7 Fiber Bragg Grating Sensors, Artech House Publishers, Inc., 1999.

[Parker *et al.* 1997a] T. R. Parker, M. Farhadiroushan, R. Faceed, V. A. Handerek and A. J. Rogers, "Temperature and strain dependance of the power level and frequency for spontaneous Brillouin scattering in optical fibers," *Optics Letters*, 22, 787-789 (1997).

[Parker *et al.* 1997b]. T. R. Parker, M. Farhadiroushan, V. A. Handerek and A. J. Roger, "A fully distributed simultaneous strain and temperature sensor using spontaneous Brillouin backscattering," *Photonic Technology Letter,* 9, 979-981 (1997).

[Parker *et al.* 1998] T. R. Parker, M. Farhadiroushan, R. Faceed, V. A. Handerek, and A. J. Rogers, "Simultaneous distributed measurement of strain and temperature from noise-

initiated Brillouin scattering in optical fibers," *IEEE Journal of Quantum Electronics*, 34, 654-659 (1998).

[Pannell *et al.* 1993] C. N. Pannell, S. J. Russell, and T. P. Newson, "Stimulated Brillouin scattering in optical fibers: the effects of optical amplification," *Journal of Optical Society of America B.* 4, 684-690 (1993).

[Pezzaniti *et al.* 1994] J. L. Pezzaniti and R. A. Chipman, "Angular dependence of polarizing beam-splitter cubes," *Applied Optics*, 33, 1916-1929 (1994).

[Ramaswamy *et al.* 1979] V. Ramaswamy, R.H.Stolen, M.D.Divino, and W. Pleibel,"Birefringece in elliptically clad borosilicate single-mode fibers," *Applied Optics* 18, 4080-4084 (1979).

[Ravet *et al.* 2005] F. Ravet, X. Bao, Q. Yu and L. Chen, "Criterion for sub-pulse-length resolution and minimum frequency shift in distributed Brillouin sensors," *IEEE Photonics Technology Letters,* 17,1504-1506 (2005).

[Rich *et al.* 1974] T. C. Rich, and D. A. Pinnow, "Evaluation of fiber optical waveguides using Brillouin spectroscopy," *Applied Optics*, 13 (6), 1376-1378 (1974).

[Sasaki *et al.* 1983] Y. Sasaki, T. Hosaka, K. Takada, and J. Noda, "8 km-long polarization- maintaining fiber with highly stable polarization state," *Electronics Letter,* 19, 792-794 (1983).

[Shi *et al.* 2003] B. Shi, H. Z. Xu, D. Zhang, Y. Ding, H. L Cui, J. Q. Gao & B. Chen, "A study on BOTDR application in monitoring deformation of a tunnel," Proceeding of *First International Conference on Structural Health Monitoring and Intelligent Infrastructure,* pp.1025-1027, Japan (2003).

[Shibata *et al.* 1983] N. Shibata, Y. Sasaki, K. Okamoto, and T. Hosaka, "Fabrication of polarization-maintaining and absorption-reducing fibers," *Journal of Lightwave Technology*, vol. LT-I, 38-43 (1983).

[Shimizu *et al.* 1993]] K. Shimizu, T. Horiguchi, Y. Koyamada, and T. Kurashima, "Coherent self-heterodyne detection of spontaneously Brillouin scattered light waves in a single-mode fiber," *Optics Letters*, 18, 185-187 (1993).

[Smith 1999] J. Smith, "Characterization of the Brillouin loss spectrum for simultaneous distributed sensing of strain and temperature," M.Sc. thesis, University of New Brunswick (1999).

[Smith *et al.* 1999a] J. Smith, A. Brown, M. DeMerchant, and X. Bao, "Simultaneous Distributed Strain and Temperature Measurement," *Applied Optics*, 38, 5372-5378 (1999).

[Song *et al.* 2005] K.Y. Song, M.G. Heraaez, L. Thevenaz, "Observation of pulse delaying and advancement in optical fibers using stimulated Brillouin scattering," *Optics Express*, 13, 82-88 (2005).

[Specifications of AQ8603] Optical Fiber Strain Analyzer, Ando Electric Co., Ltd. Tokyo, Japan. (2005); http://ando.co.kr/up_data/pds_board/pds/tm-aq8603spec.pdf.

[Stolen *et al.* 1982] R. H. Stolen, R. E. Howard, and W. Pleibel, "Substrate tube lithography for optical fibers," Electronics Letter, 18, 764-764 (1982).

[Tanaka and Hotate 2002] M. Tanaka and K. Hotate, "Application of Correlation-based Continuous-Wave Technique for Fiber Brillouin Sensing to Measurement of Strain Distribution on a Small Size Material," *Photonics Technology Letters*, 14, 675-677 (2002).

[Udd 1991] "Fiber Optic Sensors, An Introduction for Engineers and Scientists, " Edited by E. Udd, John Wiely & Sons, Inc., 1991Series.

[Udd 1995] E. Udd, "An overview of fiber-optic sensors," *Review of Scientific Instrumentation*, 66, 4015-4030 (1995).

[Waddy *et al.* 2003] D. Waddy, L. Chen, and X. Bao, "A dynamic PMD emulator," *IEEE Photonics Technology Letters,* 15, 534-536 (2003).

[Wan 2004] Yidun Wan, "Theoretical Study of the Coherent Brillouin Scattering Based Fiber Sensor," Master thesis, University of Ottawa (2004).

[Wan *et al.* 2005] Yidun Wan, Shahraam Afshar V., Lufan Zou, Liang Chen, and Xiaoyi Bao, "Subpeaks in the Brillouin loss spectra of distributed fiber-optic sensors," *Optics Letters* 30,1099-1101 (2005)

[Yariv 1996] A. Yariv, "Optical Electronics in Modern Communications," 5th Edition, pp. 478, Oxford University Press Inc., New York, New York (1996).

[Yu *et al.* 2002] J. W. Yu, Y. Park and K. Oh, "Brillouin frequency shifts in silica optical fiber with the double cladding structure," *Optics Express*, 10, 996-1004 (2002).

[Yu *et al.* 2004a] Q. Yu, X. Bao and L. Chen, "Temperature dependence of Brillouin frequency, power, and bandwidth in panda, bow-tie, and tiger polarization-maintaining fibers," *Optics Letters*, 29,17-19 (2004).

[Yu *et al.* 2004b] Q. Yu, X. Bao, L. Chen, "Strain dependence of Brillouin frequency, intensity, and bandwidth in polarization-maintaining fibers," *Optics Letters*, 29, 1605-1067 (2004).

[Yu *et al.* 2005] Q. Yu, X. Bao, F. Ravet and L. Chen, "A simple method to identify the spatial location better than the pulse length with high strain accuracy," *Optics Letters*, 30, 2215-2217 (2005).

[Zeng *et al.* 2002a] X. Zeng, X. Bao, C.Y. Chhoa, T. W. Bremner, A. W. Brown, M. D. DeMerchant, G. Ferrier, A. L. Kalamkarov, and A. V. Georgiades, "Strain measurement in a concrete beam by use of the Brillouin-scattering-based distributed fiber sensor with single-mode fibers embedded in glass fiber reinforced polymer rods and bonded to steel reinforcing bars," *Applied Optics,* 41, 5105-5114 (2002).

[Zeng *et al.*2002b] X. Zeng, X. Bao, Q. Yu, G. Ferrier, and G. Wu, "Structural health monitoring of a nuclear reactor wall with a distributed Brillouin sensor", in *proceedings of the 1st World Congress on Biomimetics and Artificial Muscles*, Albuquerque, USA, Dec. 9-11, 2002.

[Zeng *et al.* 2002c] X. Zeng, Q. Yu, G. Ferrier, X. Bao, R. E. Steffen, and M. Bowman, "Strain Measurement of the Load Test on the Rollinsford Bridge Using the Distributed Brillouin Sensor", *1st International Workshop on Structural Health Monitoring of Innovative Civil Engineering Structures,* Winnipeg, Canada, 2002.

[Zeng 2002] X. Zeng, "Characterization and Application of Brillouin Scattering Based Distributed Fiber Optic Sensor," Master thesis, University of Ottawa (2002).

[Zou *et al.* 2004a] L. Zou, X. Bao, S. Afshar V., and L. Chen , "Dependence of the Brillouin frequency shift on strain and temperature in a photonic crystal fiber," *Optics Letters*, 29, 1485-1487 (2004).

[Zou *et al.* 2004b] L. Zou, G. A. Ferrier, S. Afshar V., Q. Yu, L. Chen, and X. Bao, "Distributed Brillouin scattering sensor for discrimination of wall-thinning defects in steel pipe under internal pressure," *Applied Optics*, 43, 1583-1588 (2004).

Appendix A

Statistics formulas

(Index from SigmaPlot® User's Manual, 2001)

Mean

The arithmetic mean, or average, of all the cells in the column, excluding the missing values.

This is defined by: $$\bar{x} = \frac{1}{n}\sum_{i=1}^{n} x_i$$

Standard Deviation

The sample standard deviation is defined as the square root of the mean of the square of the differences from their mean of the data samples x_i in the column. Missing values are ignored.

$$s = \sqrt{\frac{1}{n-1}\sum_{i=1}^{n}(x_i - \bar{x})^2}$$

Standard Error

The standard error is the standard deviation of the mean. It is the sample standard deviation divided by the square root of the number of samples. For sample standard deviation s:

$$StdErr = \frac{s}{\sqrt{n}}$$

where n is the sample size.

Note: The standard errors are estimates of the uncertainties in the estimates of the regression_coefficients (analogous to the standard error of the mean). The true regression coefficients of the underlying population generally fall within about two standard errors of the observed sample coefficients.

Appendix B

Curriculum Vita

Full name Qinrong Yu

Education

B.Sc. Changchun Institute of Optics and Fine Mechanics Changchun, China (1982)

M.Sc. Changchun Institute of Optics and Fine Mechanics Changchun, China (1988)

M.Sc. Washington University, St. Louis, Missouri, USA (1996)

Ph.D University of Ottawa, Ottawa, Canada (2001-present); Supervisors: Dr. Xiaoyi Bao and Dr. Liang Chen

List of publications

Journals

1) Xiaoyi Bao, ***Qinrong Yu***, V. P. Kalosha, and Liang Chen, "The influence of transient phonon relaxation on the Brillouin loss spectrum for nanosecond pulses," *Optics Letters*, 31, 888-890 (2006).
2) ***Qinrong Yu***, Xiaoyi Bao, Fabien Ravet, and Liang Chen, "A simple method to identify the spatial location better than the pulse length with high strain accuracy," *Optics Letters*, 30, 2215-2217 (2005).
3) Fabien Ravet, Xiaoyi Bao, ***Qinrong Yu,*** and Liang Chen, "Criterion for Sub-Pulse-Length Resolution and Minimum Frequency Shift in Distributed Brillouin Sensors," *IEEE Photonic Technologies Letter*, 17, 1504-1507 (2005).
4) ***Qinrong Yu***, Xiaoyi Bao, and Liang Chen, "Strain dependence of Brillouin frequency, intensity, and bandwidth in polarization-maintaining fibers," *Optics Letters*, 29, 1605-1067 (2004).

5) ***Qinrong Yu***, Xiaoyi Bao, and Liang Chen, "Temperature dependence of Brillouin frequency, power, and bandwidth in panda, bow-tie, and tiger polarization-maintaining fibers," *Optics Letters*, 29,17-19 (2004).
6) Xiaoyi Bao, ***Qinrong Yu***, and Liang Chen, "Simultaneous strain and temperature measurements with polarization-maintaining fibers and their error analysis by use of a distributed Brillouin loss system," *Optics Letters*, 29, 1342-1344 (2004).
7) Lufan Zou, Graham A. Ferrier, Shahraam Afshar V., ***Qinrong Yu***, Liang Chen, and Xiaoyi Bao, "Distributed Brillouin Scattering Sensor for Discrimination of Wall-Thinning Defects in Steel Pipe under Internal Pressure," *Applied Optics*, 43, 1583 (2004).
8) Ziyi Zhang, Xiaoyi Bao, ***Qinrong Yu,*** and Liang Chen, "Fast States of Polarization and PMD Drift in Submarine Fibers," *IEEE Photonic Technologies Letter,* 18, 1034-1036 (2006).
9) Ziyi Zhang, Xiaoyi Bao, ***Qinrong Yu***, and Liang Chen, "Time Evolution of PMD Due to Tides and Sun," accepted by *Fiber Optics Technologies* (2006).

Conferences

1. Xiaoyi Bao, ***Qinrong Yu***, Fabien Ravet and Liang Chen, "A simple method to identify the spatial location complication due to the transient phonon relaxation on the Brillouin loss spectrum (Invited Paper)." *SPIE* Structure Health monitoring and Smart Materials, San Diego, USA, March 2006.
2. Xiaoyi Bao, Lufan Zou, ***Qinrong Yu***, Graham A. Ferrier, Fabien Ravet, and Liang Chen, "Distributed Strain and Temperature Sensor Application in Structure Health Monitoring with Centimeter Spatial Resolution," *Proceedings of International Symposium on advances & Trends in Fiber Optics & Applications.* Chongqing, China, Oct.11-15, 2005.
3. ***Qinrong Yu***, Xiaoyi Bao, and Liang Chen, "Simultaneous strain and temperature measurements with polarization-maintaining fibers in distributed Brillouin loss

system," Oral presentation at *SPIE*, Structure Health monitoring and Smart Materials, San Diego, USA, March 2004.

4. Lufan Zou, G. A. Ferrier, Shahraam Afshar V., ***Qinrong Yu***, and Xiaoyi Bao, "Distributed Brillouin scattering sensor as structural health monitoring system for pipeline integrity monitoring," *Proceedings of 16th International Conference on Optical Fiber* Sensors, 2003.
5. Z. Liu, Graham A. Ferrier, Xiaoyi Bao, Xiaodong Zeng, ***Qinrong Yu***, and A. Kim, "Brillouin Scattering Based Distributed Fiber Optic Temperature Sensing for Fire Detection," *Proceedings of 7th International Symposium on Fire Safety Science*, Worcester, Massachusetts, USA, June 2002.
6. Xiaodong Zeng, ***Qinrong Yu***, Graham A. Ferrier, and Xiaoyi Bao, "Strain and temperature monitoring of a concrete structure using a distributed Brillouin scattering sensor," *Proceedings of the 1st International Workshop on Structural Health Monitoring of Innovative Civil Engineering Structures,* Winnipeg, Canada, 2002.
7. Xiaodong Zeng, ***Qinrong Yu***, Graham A. Ferrier, Xiaoyi Bao, R. E. Steffen, and M. Bowman, "Strain Measurement of the Load Test on the Rollinsford Bridge Using the Distributed Brillouin Sensor," *Proceedings of the 1st International Workshop on Structural Health Monitoring of Innovative Civil Engineering Structures,* Winnipeg, Canada, 2002.
8. Xiaodong Zeng, Xiaoyi Bao, ***Qinrong Yu***, Graham A. Ferrier, and Guilin Wu, "Structural health monitoring of a nuclear reactor wall with a distributed Brillouin sensor," *Proceedings of the 1st World Congress on Biomimetics and Artificial Muscles*, Albuquerque, USA, Dec. 9-11, 2002.
9. Xiaodong Zeng, Xiaoyi Bao, Graham A. Ferrier, ***Qinrong Yu***, R. E. Steffen, and M. Bowman, "Load Test of the Rollinsford Bridge Using the Distributed Brillouin Sensor," *Proceedings of the 1st World Congress on Biomimetics and Artificial Muscles*, Albuquerque, USA, Dec. 9-11, 2002.

Posters

- Yidun Wan, Ou Chen, ***Qinrong Yu***, Shahraam Afshar V., and Xiaoyi Bao, "A Distributed Fiber Optics Sensor System for Health Monitoring," *9th Annual Conference of ISIS Canada*, Halifax, Canada, April 2004.
- ***Qinrong Yu***, G. Ferrier, Shahraam Afshar V., Ou Chen, and Xiaoyi Bao, "Polarization maintaining fiber & fiber Bragg gratings for simultaneous measurement of strain and temperature," poster session, *7th Annual Conference of ISIS Canada*, May 2002
- Graham A. Ferrier, Shahraam Afshar V., Xiaodong Zeng, ***Qinrong Yu***, and Xiaoyi Bao, "Distributed temperature and strain sensing of concrete structures using stimulated Brillouin scattering in optical fibers," poster session, 7th Annual Conference of ISIS Canada, May 2002. Received prize for "Most Creative Poster".

Patent

- Xiaoyi Bao, ***Qinrong Yu***, Lufan Zou, and Liang Chen, "Methods to measure strain and temperature simultaneously," Patent filed in 2004 through University of Ottawa.

Temperature dependence of Brillouin frequency, power, and bandwidth in panda, bow-tie, and tiger polarization-maintaining fibers

Qinrong Yu, Xiaoyi Bao, and Liang Chen

Fiber Optics Group, Department of Physics, University of Ottawa, Ottawa, Ontario K1N 6N5, Canada

Received June 13, 2003

We report a study of the temperature dependence of the Brillouin gain and loss for three different kinds of commercial polarization-maintaining fibers for the first time to our knowledge. The Brillouin frequency differences between the fast and slow axes are independent of the temperature, varying between 2.9 and 4.3 MHz. Using 2-ns pulses (equivalent to a spatial resolution of 20 cm), we find that the temperature coefficients for the relative Brillouin power at a wavelength of 1310 nm are 0.26%/°C (panda fiber), 0.23%/°C (bow-tie fiber), and 0.04%/°C (tiger fiber); the temperature coefficients for the Brillouin frequency are 1.37 MHz/°C (panda), 1.66 MHz/°C (tiger), and 2.30 MHz/°C (bow-tie). The temperature coefficients for the Brillouin gain bandwidth are 0.15 MHz/°C (panda), 0.20 MHz/°C (bow-tie), and 0.22 MHz/°C (tiger). © 2004 Optical Society of America

OCIS codes: 060.2370, 290.5830.

A distributed Brillouin sensor can be used for structural health monitoring to measure the cracks in civil structures. In field tests, both temperature and strain are unknown. If only the Brillouin frequency is measured, two fibers are needed,[1] one to detect the temperature and the other to detect the strain. In practice, it is difficult to install a second temperature-sensing fiber that is totally isolated from the strain.

A few studies on measuring temperature and strain simultaneously in one fiber with a distributed fiber sensor have been reported.[2–4] A hundred to a few hundred microstrain and a temperature resolution of a few degrees with a spatial resolution of a few to a few tens of meters have been achieved. One of the major limitations in spatial, temperature, and strain resolution is related to the intensity and power fluctuation induced by variation of the polarization states along the single-mode fibers, which is caused by polarization mode dispersion (PMD), unless the principal state of polarization (PSP) is launched. However, the PSP changes with temperature, strain, and stress along the fiber length. This introduces higher-order PMD. As a result, the Brillouin interaction between two counterpropagating beams fluctuates along the various positions of single-mode fibers. The polarization-maintained fibers can be considered the first-order PMD effect in the fiber. Two polarization-maintaining (PM) states are equivalent to two PSPs. If we launch into one of the PSPs of the PM fiber, there is no polarization variation and less power fluctuation, and the PSP is a weak function of temperature. Even with the temperature and strain variations along the PM fibers, the intensity fluctuation caused by the variation of the polarization states from temperature and strain is not as strong as in the case of the single-mode fiber. With the Brillouin power and frequency shift measurements, we can achieve simultaneous temperature and strain sensing.

Although Smith *et al.* [3] used PM fiber as a sensing fiber, no polarizing device was used for the connection between the single-mode and PM fibers. The Brillouin gain signal fluctuated as in the single-mode fiber. In this Letter we launch the input light to one PM axis of PM fiber to propagate pump and probe waves. The three most common PM fibers, panda, bow-tie, and tiger PM fibers,[5] are used in this experiment to characterize the Brillouin gain spectrum on temperature dependence for its frequency, power, and bandwidth.

For PM fibers the refractive index of two orthogonal axes, i.e., the slow axis and the fast axis, is different. The difference in the Brillouin frequency shift at the slow axis and the fast axis can be described as

$$\Delta\nu_{\mathrm{Bsf}} = \frac{2\nu_a}{\lambda}\left(n_{\mathrm{slow}} - n_{\mathrm{fast}}\right),$$

where n_{slow} and n_{fast} are the refractive indices of the slow and the fast axis, respectively; ν_a is the speed of the acoustic wave; and λ is the optical wavelength. Take $\lambda = 1310$ nm, $\nu_a \sim 6000$ m/s, and $\Delta n = n_{\mathrm{slow}} - n_{\mathrm{fast}} = 4 \times 10^{-4}$; then, $\Delta\nu_{\mathrm{BsF}} = 3.66$ MHz. This number is similar to what we measured in bow-tie, panda, and tiger fibers.

The extinction ratio (ER) of a PM fiber is a measure of the PM fiber's ability to maintain the linear polarization state of the input light. It is defined as ER = $-10\log(P_x/P_y)$, where P_x and P_y are the minimum and maximum power, respectively, measured through a polarizer. A low ER represents an elliptical polarization state. Through our experiments we maintained an ER of >20 dB.

The experimental setup is modified from that of Ref. 1 by the addition of two pigtailed polarizing beam splitters for launching the light into either the slow or the fast axis of the PM fibers, as shown in Fig. 1. The wavelength of the light source is 1310 nm. One of the connector's key ways is aligned with the slow

0146-9592/04/010017-03$15.00/0

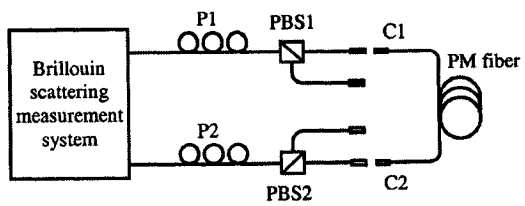

Fig. 1. Setup for the Brillouin scattering measurement of PM fibers. P1, P2, polarization controllers; PBS1, PBS2, polarizing beam splitters; C1, C2, connectors.

axis, and the other is aligned with the fast axis. When the PM fiber is connected to the system, the polarization is measured to yield an ER of >20 dB for each connector and each axis. With a polarization controller the input optical power can be launched into the sensing PM fiber at either the slow or the fast axis for both the pulsed and the cw beams.

All PM fibers used in our experiment have an ER of >25 dB. The temperature chamber's accuracy is ±0.5 °C. The input power for the cw beam is 5 mW, and the pulse power is 6 mW. The pulse width is 2 ns, which is equivalent to a 20-cm spatial resolution.

Figure 2 shows the Brillouin frequency shift versus the temperature for three PM fibers. The temperature coefficient is $C_{\nu T} = 1.37$ MHz/°C for panda fiber at both the slow and the fast axis. The frequency difference between the fast and the slow axis is $\Delta\nu_{\mathrm{BsF}} = 3.6$ MHz. The spectrum bandwidth is shown in Fig. 3. The bandwidth decreases from 49.5 MHz at −60 °C to 29.2 MHz at 80 °C, corresponding to $\Delta\nu/\Delta T = -0.146$ MHz/°C. The normalized Brillouin scattering power increases with temperature as shown in Fig. 4. Both Figs. 3 and 4 show the dependence of the fast axis only. The behavior of the slow axis is the same as that of the fast axis.

The temperature dependence of the Brillouin frequency is plotted in Fig. 2. The Brillouin shift of the bow-tie PM fiber at 20 °C is lower than that of the single-mode fiber (12.6 versus 12.8 GHz). The temperature coefficient $C_{\nu T} = 2.30$ MHz/°C is almost twice that of the single-mode fiber for the same wavelength. The deviation from linearity at low and high temperature is believed to be caused by the polyvinyl chloride jacket, because one of the panda fibers is in a loose tube that shows similar behavior for Brillouin frequency measurement. Among the three PM fibers, only the bow-tie fiber has a thick jacket (0.9-mm polyvinyl chloride).

To show the relation between the slow axis and the fast axis, the Brillouin frequency shift is measured from 0 to 40 °C, as shown in Fig. 5. Two straight lines are parallel with the same slope of 2.34 MHz/°C and are separated by 2.9 MHz. Both the panda and the bow-tie PM fibers have a linear temperature dependence on the Brillouin bandwidth and power, as shown in Figs. 3 and 4.

Tiger PM fiber is also called elliptical inner-clad or oval inner-clad fiber, because it has an elliptical cladding. From Figs. 2–4 we see that the tiger fiber has higher fluctuation in frequency, power, and bandwidth than panda and bow-tie fiber. Tiger fiber has a temperature coefficient of $C_{\nu T} = 1.66$ MHz/°C, the difference between the slow and fast axes is 4.3 MHz (averaged). The Brillouin gain spectrum for the tiger PM fiber is asymmetric and much wider (105 MHz) than

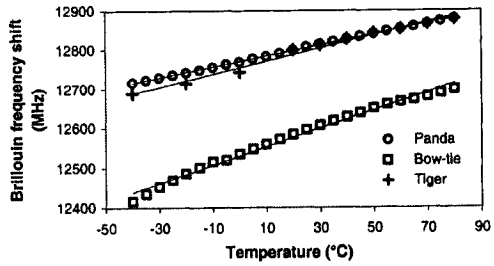

Fig. 2. Temperature dependence of the Brillouin frequency shift of panda, bow-tie, and tiger PM fibers at the fast axis.

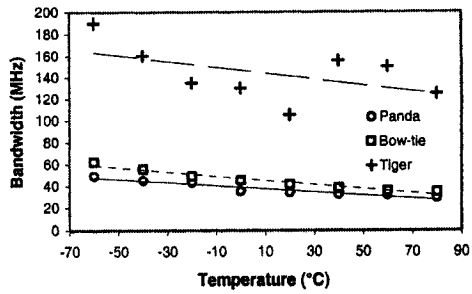

Fig. 3. Temperature dependence of the Brillouin bandwidth in PM fibers (slow axis for panda and fast axis for bow-tie and tiger).

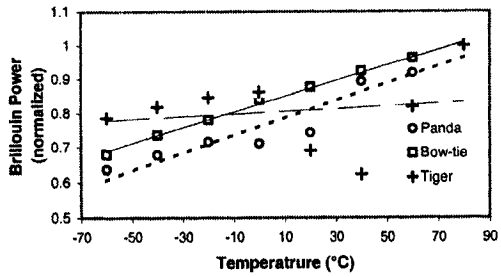

Fig. 4. Temperature dependence of the Brillouin power (the maximum power at 80 °C is normalized to 1) for the three PM fibers (slow axis for panda and fast axis for bow-tie and tiger).

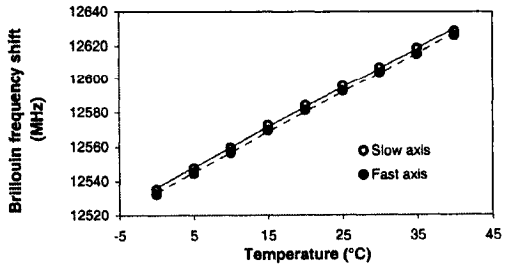

Fig. 5. Temperature dependence for the Brillouin frequency shift of the bow-tie fiber between the fast axis and the slow axis.

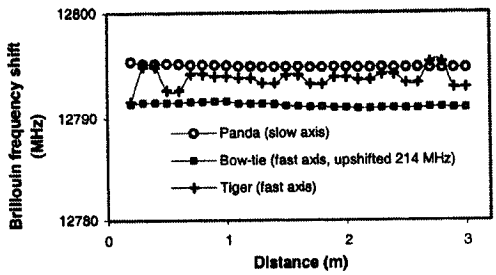

Fig. 6. Comparison of time trace (at 20 °C) flatness for the three PM fibers (bow-tie is upshifted 214 MHz for comparison).

Table 1. Temperature Dependence of the Frequency $\Delta\nu_B$, Power Ratio, and Bandwidth

PM Fiber Type	Panda (Slow Axis)	Bow-Tie (Fast Axis)	Tiger (Fast Axis)
$\Delta\nu_{B(\text{slow})}$ (MHz) at 20 °C	12799.2	12584.0	12799.6
$\Delta\nu_{B(\text{fast})}$ (MHz) at 20 °C	12794.8	12581.0	12793.6
$\Delta\nu_{B(\text{slow})} - \Delta\nu_{B(\text{fast})}$	3.6	2.9	4.3
$C_{\nu T}$ (MHz/°C)	1.37	2.30	1.66
Power ratio ($P_{\text{tiger}} = 1$)	1.9	5.9	1
C_{pT} (%/°C)[a]	0.26	0.23	0.04
Bandwidth at 20 °C (MHz)	33.7	41.5	105
C_{BwT}(MHz/°C)[b]	0.15	0.20	0.20
Average $\Delta\nu_{\text{BsF}}$(MHz)	3.6	2.9	4.3

[a] C_{pT} is the power coefficient.
[b] C_{BwT} is the bandwidth coefficient.

Table 2. Standard Error (StdErr) of Measurement (−40–80 °C) and the Equivalent Temperature Uncertainty ΔT for PM Fibers

PM Fiber Type	Panda (Slow Axis)	Bow-Tie (Fast Axis)	Tiger (Fast Axis)
StdErr of Brillouin scattering frequency (MHz)	0.56	3.20	3.14
ΔT (°C)	0.3	1.4	1.9
StdErr of Brillouin scattering frequency (MHz) (0–40 °C)	0.3	0.3	2.7
ΔT (°C)	0.2	0.1	1.2
StdErr of normalized P_B	1.5%	0.3%	4.3%
ΔT (°C)	5.8	1.3	106
StdErr of bandwidth (MHz)	0.82	0.83	6.92
ΔT (°C)	5.5	4.2	77.2

both the panda and the bow-tie PM fibers. The gain spectrum resembles the superposition of many Brillouin spectra at the measurement point representing 0.5 ns in time and 5 cm in length. When we take a close look at the Brillouin frequency versus location, we notice the noiselike time trace in comparison with the flat Brillouin frequency for the panda and bow-tie PM fibers, as shown in Fig. 6, even though the temperature is constant within this section of the fiber. For a constant temperature we should get one Brillouin frequency, as in the cases of bow-tie and panda fibers; however, with tiger fibers it seems to be an inhomogeneous broadening, which may be induced by the nonuniformity of the core and cladding materials through the fabrication of the tiger fiber by the pressed preform method.[5] This may also explain the nonlinear relation of the Brillouin power and bandwidth to the temperature.

As a result, the deviation from the linear fit for the tiger fiber is the largest among the three PM fibers for the Brillouin frequency, power, and bandwidth measurement, as shown in Tables 1 and 2. The bow-tie fiber is the most promising candidate for distributed Brillouin temperature sensing; its temperature measurement uncertainties for the Brillouin frequency are ~1.5 °C at a 20-cm spatial resolution, as shown in Table 2. The thick jacket induces the high error at low and high temperatures for the bow-tie fiber. Although the panda fiber also has a flat Brillouin frequency response, as shown in Fig. 6, its Brillouin bandwidth and power uncertainties are higher than those of the bow-tie fiber, which is caused by the Brillouin frequency's being close to that of the single-mode fiber, because we use single-mode fiber as the input and output transmission fibers, as shown in Fig. 1. The bow-tie fiber's Brillouin frequency is far from that of the single-mode fiber. If we use panda fiber for the input, output, and sensing fibers, we should get similar temperature uncertainties for both the panda and bow-tie PM fibers.

In summary, the temperature dependence of the Brillouin gain and loss spectrum for three PM fibers has been studied for their temperature coefficients of the Brillouin frequency shift, power, and bandwidth for the first time to our knowledge. The highest temperature measurement accuracy for the Brillouin frequency shift is 0.33 °C (panda), for Brillouin power dependence it is 1.27 °C (bow-tie), and for the Brillouin bandwidth it is 4.24 °C (bow-tie) at a 20-cm spatial resolution. The Brillouin frequency at 20 °C for the fast axis of the panda, bow-tie, and tiger PM fibers is 12.795, 12.581, and 12.794 GHz, respectively. The Brillouin frequency difference between the fast and slow axes among the three PM fibers is between 2.9 and 4.3 MHz.

Q. Yu's e-mail address is qinrong_yu@yahoo.ca.

References

1. X. Bao, D. J. Webb, and D. A. Jackson, Opt. Lett. **19,** 141 (1994).
2. T. R. Parker, M. Farhadiroushan, V. A. Handerek, and A. J. Roger, IEEE Photon. Technol. Lett. **9,** 979 (1997).
3. J. Smith, A. Brown, M. DeMerchant, and X. Bao, Appl. Opt. **38,** 5372 (1999).
4. H. H. Kee, G. P. Lees, and T. P. Newson, Opt. Lett. **25,** 695 (2000).
5. J. Noda, K. Okamoto, and Y. Sasaki, J. Lightwave Technol. **4,** 1071 (1986).

Strain dependence of Brillouin frequency, intensity, and bandwidth in polarization-maintaining fibers

Qinrong Yu, Xiaoyi Bao, and Liang Chen

Fiber Optics Group, Department of Physics, University of Ottawa, Ottawa, Ontario K1N6N5, Canada

Received March 25, 2004

The strain dependence of the Brillouin gain–loss spectrum for PANDA, bow-tie, and tiger polarization-maintaining fibers has been studied in the range 0 to 50 °C. We found a linear relationship between the strain and the Brillouin frequency, intensity, and bandwidth for PANDA and bow-tie fibers. For PANDA fiber at 20-cm spatial resolution, Brillouin frequency gives 7-$\mu\epsilon$ uncertainty, which is the highest accuracy among three parameters, whereas the Brillouin bandwidth gives 19-$\mu\epsilon$ uncertainty. © 2004 Optical Society of America

OCIS codes: 060.2370, 290.5830.

In single-mode fibers the Brillouin frequency and intensity have been found to be linearly proportional to both strain and temperature.[1,2] The Brillouin spectrum's bandwidth (BW), however, although it changes with temperature, is reported to be unchanged with strain.[3] Polarization-maintaining (PM) fiber, because of its high birefringence, has been used as a polarization mode dispersion emulator.[4] We believe that the birefringence property of PM fiber could be utilized for a more sensitive distributed strain sensor compared with regular single-mode fibers, particularly with a Brillouin gain–loss-based distributed sensor because of its matched polarization states for pump and probe waves. Brillouin scattering in PM fibers has been used to generate squeezed light with a fiber loop mirror[5]; however, no strain or temperature of the Brillouin spectrum was measured. We have studied temperature properties of Brillouin loss spectra of PM fibers.[6] With PM fiber we launched linearly polarized light into the slow axis of PM fiber for both pump and probe beams; because the PM fiber preserves the polarization state, the Brillouin loss or gain is maximum in every position of the PM fibers.

In this Letter we report our experiments on the strain dependence of intensity, BW, and frequency of the Brillouin loss spectrum for three PM fibers in the temperature range 0 to 50 °C. Brillouin loss is measured with the pump signal after interaction with the probe signal (pulsed).

We found that these parameters are linearly dependent on strain for PANDA and bow-tie PM fibers. We were able to obtain a strain accuracy of 7 $\mu\epsilon$ with PANDA fiber at 20-cm spatial resolution at the Brillouin frequency. Our results suggest that all three parameters of a Brillouin spectrum, i.e., frequency, intensity, and BW, may be used with either a slow or a fast axis for distributed strain measurement.

For the experiment we used a modified version of the 1310-nm Brillouin gain–loss sensing system described in Refs. 6 and 7 (Fig. 1). Two polarization controllers, PC_1 and PC_2, were installed to connect two pigtailed polarizing beam splitters, PBS_1 and PBS_2, respectively. A polarizing beam splitter has one input (single mode) and two output (PM) fibers to which the sensing fiber can be connected and aligned to either the slow or the fast axis. This configuration is designed to guarantee that both probe (pulse) and pump (cw) light are launched into the same axis of PM fiber, which will maintain the maximum Brillouin amplification in the PM fibers. The PM fiber is wound around two pulleys. One pulley is fixed, and the other is movable along a rail. The fiber is glued onto the movable pulley and is pulled away from the fixed pulley during the strain measurement. The pulleys and PM fiber on the rail are sealed in a temperature chamber. For temperatures below room temperature we used dry ice and for temperatures above room temperature we used an electrical heating strip.

We used 20-dB extinction ratio PM fibers to preserve the linear polarization state of the input light. The extinction ratio of PM fibers did not change while the fibers were strained (by as much as 500 $\mu\epsilon$ for PANDA and tiger fibers and 1200 $\mu\epsilon$ for bow-tie fiber). The pulse width was 2 ns, corresponding to 0.2-m spatial resolution. The average number of time traces to produce a 25–30-dB signal-to-noise ratio (SNR) for measurement of the Brillouin loss spectrum was 2000. The measurement time was 5 min.

The length of the strained fiber was 1.57 m, and the input powers were 5 and 6 mW for cw and pulsed beams, respectively. PANDA and tiger fibers were 0.25-mm bare fibers, and bow-tie fiber was a 0.9-mm jacketed fiber. Figure 2 shows the normalized Brillouin spectrum at 20 °C for unstrained PANDA (peak, 12 795 MHz; BW, 34 MHz), bow-tie (peak, 12 581 MHz; BW, 41 MHz) and tiger (peak, 12 798 MHz; BW, >300 MHz) fibers. We found that

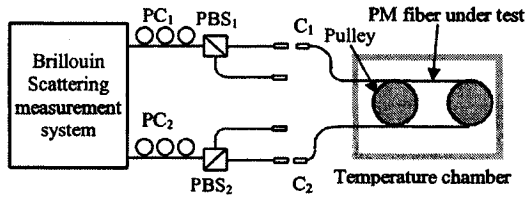

Fig. 1. Setup for Brillouin scattering measurement of PM fibers.

0146-9592/04/141605-03$15.00/0

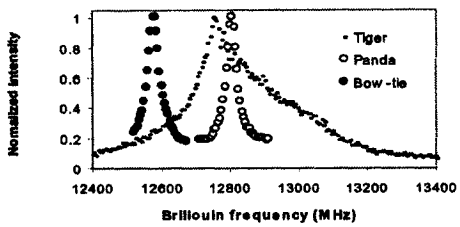

Fig. 2. Spectra of unstrained PANDA, bow-tie, and tiger fibers at 20 °C. The intensity is normalized to 1.

the Brillouin spectrum of the tiger fiber is asymmetric, with a peak intensity that is only one half that of the bow-tie and PANDA fibers and a BW that is 7–9 times broader than those of bow-tie and PANDA fibers. Thus there is high uncertainty in determining the Brillouin frequency, intensity, and BW of tiger fibers. This unique feature of tiger fiber may be attributed to the properties of the core and cladding structures, material, and fabrication.

The Brillouin frequencies of the slow and fast axes in the PANDA fiber are linearly dependent on strain with the same slope (0.077 ± 0.002 and 0.075 ± 0.002 MHz/$\mu\epsilon$, respectively), as shown in Fig. 3. Thus either the slow or the fast axis can be used for strain measurement.

The Brillouin frequency of the fast axis is measured as a function of strain in the temperature range 0 to 50 °C; it shows a linear relationship, with an average slope of 0.077 ± 0.002 MHz/$\mu\epsilon$ (Fig. 4). Like the Brillouin frequency, the BW and the intensity of the Brillouin profile exhibit a linear relationship to the strain over the same temperature range, as shown in Fig. 5. Although the BW and the intensity of the Brillouin spectrum have a linear relationship to the strain for both bow-tie and PANDA fibers, the trend of the bow-tie fiber is quite different from that of PANDA fiber. The intensity increases and the BW decreases with strain over the temperature range 0 to 43 °C, as shown in Fig. 6.

The slopes of intensity–strain linear curves are the same (within experimental error) in the range of temperatures used in the experiment. The strain dependence of the Brillouin intensity for the slow axes of PANDA and bow-tie fibers resembles a similar linear relationship with the same slope (within experimental error) for the fast axis, as demonstrated in Fig. 7. In Fig. 7, to show the linear trend we averaged the intensity–strain results for the slow and the fast axes of PANDA and bow-tie fibers over the temperature range. For both fibers the intensity values that correspond to the slow axis were bigger than those of the fast axis, a result that we attribute to the extra connector and polarizing beam splitter insertion loss of the fast axis. Note that the unstrained BW of the bow-tie fiber in Fig. 6(b) is bigger than that in Fig. 2 because of the residual strain in the poly(vinyl chloride) jacket of the bow-tie fiber after the first elongation. However, this outcome does not affect our measurements because only the slope and the variation with respect to a reference condition are measured in our system. As we can see from Figs. 5(a) and 6(a), the intensity of the bow-tie fiber increased while the PANDA fiber's intensity decreased with strain. One can understand this result by examining the structures of the PANDA and the bow-tie fibers (as depicted in Fig. 8) and the ways in which these structures change under stress. When a PANDA fiber is stretched, the mode confinement factor is affected because the two stress rods (silica doped with B_2O_3) are pressed into the core. The rods degrade the guiding properties and boundary conditions of the core–cladding surface, leading to increased attenuation. In the case of bow-tie fiber, the penetration of the two rods into the core is more nearly uniform because of the circular shape of the internal surface of the two rods (Fig. 8).

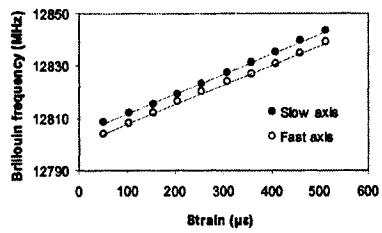

Fig. 3. Strain dependence of Brillouin frequency at slow and fast axes of PANDA fiber at room temperature, 23 °C.

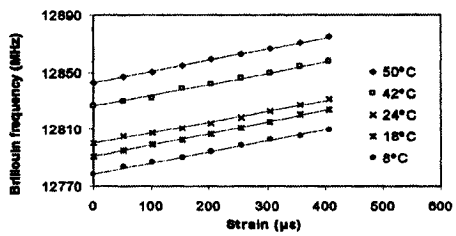

Fig. 4. Strain dependence of Brillouin frequency at various temperatures for PANDA fibers.

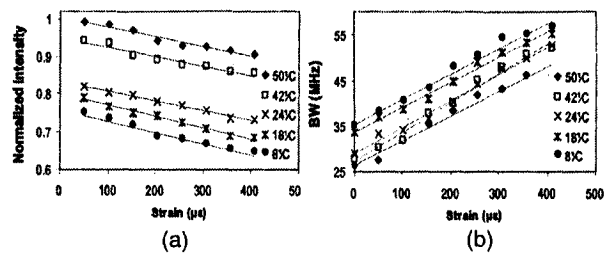

Fig. 5. (a) Strain dependence of intensity normalized to its biggest value at 50 °C and (b) BW of PANDA fiber.

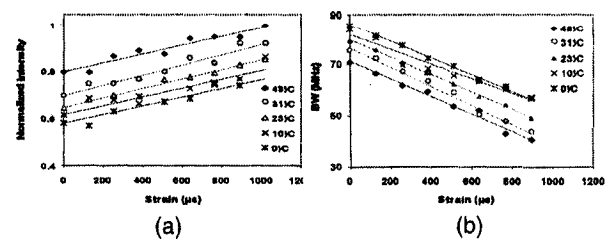

Fig. 6. (a) Strain dependence of intensity normalized to its biggest value at 43 °C and (b) BW of bow-tie fiber.

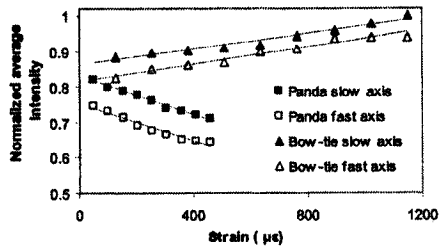

Fig. 7. Strain dependence of Brillouin intensity (normalized to its highest value in a bow-tie fiber's slow axis) averaged over the range of temperature for PANDA and bow-tie PM fibers.

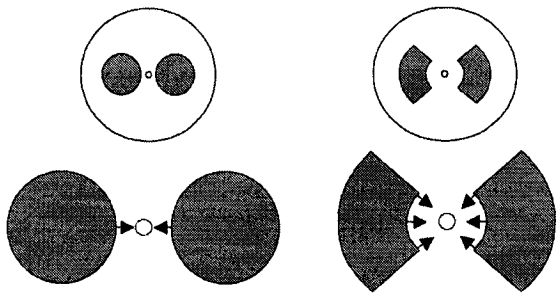

Fig. 8. Structures of (left) PANDA and (right) bow-tie PM fibers and their stress-applying parts. Applied forces at the core for elongated fiber are shown by the arrows.

Table 1. Average Strain Coefficients of Brillouin Frequency, Normalized Intensity, and BW (0–50 °C)

	Fiber Type			
Coefficient	PANDA	Bow-tie	Tiger	SM
C_ν^ϵ (MHz/$\mu\epsilon$)	0.077	0.024	0.091	0.048
	±0.002	±0.002	±0.005	±0.03
C_I^ϵ (%/$\mu\epsilon$)	−0.027	0.020	0.01	−0.0009
	±0.002	±0.003	±0.004	
C_B^ϵ (MHz/$\mu\epsilon$)	0.058	−0.031		
	±0.003	±0.002		

Thus the pressure does not change the core–cladding boundary conditions but simply decreases the core's cross section as the fiber is elongated if the stress is not large, as in our experimental condition. These constant boundary conditions result in higher power density and accordingly in higher Brillouin gain for strained bow-tie fibers. Assuming that for low-power input pump and pulse the integral of the Brillouin spectrum over all frequencies is constant, the decrease (increase) of intensity in the PANDA (bow-tie) fibers as a function of strain results in an increase (decrease) of Brillouin BW, as shown in Figs. 5 and 6. This result indicates that the Brillouin intensity and the BW are not independent parameters and that the linear relationships in Figs. 5 and 6 are valid only for a limited range of strain or temperature.

Table 2. Average Standard Errors of Measured Parameters and Corresponding Strain Uncertainty (0–50 °C)

Fiber Type	PANDA	Bow-tie	Tiger
StdErr frequency (MHz)	0.54	0.85	1.57
Strain uncertainty ($\mu\epsilon$)	7	36	19
StdErr normalized intensity (%)	0.7	2.4	1.2
Strain uncertainty ($\mu\epsilon$)	25	124	110
StdErr BW (MHz)	1.1	1.6	
Strain uncertainty ($\mu\epsilon$)	19	53	

The ratio of strain to Brillouin intensity shows more fluctuations than that of strain to Brillouin frequency. This is so because the laser that we used was frequency stabilized (a drift of a few tens of kilohertz), i.e., the laser intensity is used to compensate for the frequency drift to produce high-frequency stabilization; as a result, the laser's power fluctuation is greater than the laser's frequency fluctuation. The strain coefficients (slopes) of Brillouin frequency, power ratio, and BW for three PM fibers are listed in Table 1. No strain dependence on BW of tiger fiber was observed because of the asymmetry and the broad Brillouin spectrum. The standard errors of measurements and corresponding strain uncertainties are listed in Table 2. For comparison, the results for single-mode fiber[2] are also included. Overall, the PANDA fiber has the highest strain measurement, i.e., 7, 25, and 19 $\mu\epsilon$ for Brillouin frequency, BW, and intensity, respectively.

Support from the Natural Sciences and Engineering Research Council of Canada, Intelligent Sensing for Innovative Structures of Canada, Canada Foundation for Innovation, and the Canada Research Chair programs is greatly appreciated. Q. Yu's e-mail address is qinrong_yu@yahoo.ca.

References

1. X. Bao, D. J. Webb, and D. A. Jackson, Opt. Lett. **19,** 141 (1994).
2. M. Alahbabi, Y. T. Chao, and T. P. Newson, Opt. Lett. **29,** 26 (2004).
3. M. Nikl'es, L. Th'evenaz, and P. A. Robert, J. Lightwave Technol. **15,** 1842 (1997).
4. D. Waddy, L. Chen, and X. Bao, IEEE Photon. Technol. Lett. **15,** 534 (2003).
5. N. Nishizawa, S. Kume, M. Mori, and T. Goto, Opt. Lett. **19,** 1424 (1994).
6. Q. Yu, X. Bao, and L. Chen, Opt. Lett. **29,** 19 (2004).
7. J. Smith, A. Brown, M. DeMerchant, and X. Bao, Appl. Opt. **38,** 5372 (1999).

Simultaneous strain and temperature measurements with polarization-maintaining fibers and their error analysis by use of a distributed Brillouin loss system

Xiaoyi Bao, Qinrong Yu, and Liang Chen

Fiber Optics Group, Department of Physics, University of Ottawa, Ottawa, Ontario K1N6N5, Canada

Received March 3, 2004

Simultaneous temperature and strain measurement with a distributed Brillouin loss system is proposed by use of the parameters Brillouin frequency, power, and bandwidth, for PANDA, bow-tie, and tiger polarization-maintaining fibers for the first time to our knowledge. The expressions for simultaneous temperature and strain sensing and the maximum errors and rms values of temperature and strain measurements are derived with three combinations of the parameters: (1) power and Brillouin frequency, (2) bandwidth and Brillouin frequency, and (3) bandwidth and Brillouin power. Our experiments demonstrate that simultaneous temperature and strain sensing at 20-cm spatial resolution for Brillouin frequency combined with bandwidth the strain/temperature resolutions are 39 $\mu\varepsilon/2\,^{\circ}C$ (PANDA), 126 $\mu\varepsilon/3\,^{\circ}C$ (bow tie), and 598 $\mu\varepsilon/16\,^{\circ}C$ (tiger); for the Brillouin frequency combined with power the strain/temperature resolutions are 153 $\mu\varepsilon/8\,^{\circ}C$ (PANDA) and 237 $\mu\varepsilon/4\,^{\circ}C$ (bow tie); and for the bandwidth combined with power the strain/temperature resolutions are 135 $\mu\varepsilon/38\,^{\circ}C$ (PANDA) and 195 $\mu\varepsilon/38\,^{\circ}C$ (bow tie). © 2004 Optical Society of America

OCIS codes: 060.2310, 060.2370.

Brillouin frequency shift is sensitive to changes in both temperature and strain in single-mode (SM) fibers.[1–4] This leads to a problem common to many sensors: One cannot distinguish a change in the strain or the temperature experienced by the fiber. Neglecting the temperature effect leads to substantial errors in strain measurements. It is important to achieve simultaneous measurement of temperature and strain. It has been reported in SM fibers with Brillouin frequency and power.[2–4] However, because of polarization mode dispersion[5] (PMD) of SM fiber,[6] the polarization state in SM fiber varies randomly along the fiber, as well as with environmental conditions, such as temperature and strain induced by wind. It is impossible to separate the state of polarization changes induced by the temperature and strain from the dynamic features caused by PMD. This sets the power measurement uncertainty in addition to the laser power fluctuation for simultaneous temperature and strain measurement with SM fiber using power and Brillouin frequency. In this Letter we propose to use a polarization-maintaining (PM) fiber that allows the light to travel in one polarization state if the input light is launched into one of the PM fiber axes. As a result, the PMD-induced fluctuation can be eliminated, and the power fluctuation is attributed only to the laser source. Because of the elimination of state of polarization fluctuation in the power of SM fibers, we can achieve a spatial resolution on the scale of centimeters for simultaneous temperature and strain sensing with PM fibers for the first time to our knowledge, whereas SM fiber can have a spatial resolution only on the scale of meters for simultaneous temperature and strain sensing. We used three types of PM fiber—PANDA, bow tie, and tiger—to measure strain coefficients at various temperatures for the Brillouin power, frequency, and bandwidth using our sensor system,[6] and then we calculated the temperature and strain uncertainty. With three measurable parameters for the Brillouin scattering spectrum—power, bandwidth, and frequency—there are three options for simultaneous temperature and strain sensing: (1) power and frequency, (2) power and bandwidth, and (3) bandwidth and frequency. For the second option the Brillouin power integral over the frequency is a constant over the completed frequency range if the input power is not very high (below the stimulated Brillouin scattering threshold), so the power and the bandwidth are two related parameters. However, within a limited temperature and strain range we can ignore the correlation between the power and the bandwidth; hence the power and the bandwidth can be considered two independent parameters for simultaneous temperature and strain sensing.

First, we used power and frequency shift as known parameters, which yielded the following for temperature and strain variation:

$$\Delta T = \frac{\Delta v C_P^{\varepsilon} - C_v^{\varepsilon} \Delta P}{C_P^{\varepsilon} C_v^T - C_v^{\varepsilon} C_P^T}, \tag{1a}$$

$$\Delta \varepsilon = \frac{\Delta v C_P^T - C_v^T \Delta P}{C_v^{\varepsilon} C_P^T - C_P^{\varepsilon} C_v^T}. \tag{1b}$$

Here Δv and ΔP are the frequency and relative power variations, respectively, induced by strain and temperature change, and $C_v^{\varepsilon} = (\partial v/\partial \varepsilon)_T, C_v^T = (\partial v/\partial T)_{\varepsilon}$, $C_P^{\varepsilon} = (\partial P/\partial \varepsilon)_T$, and $C_P^T = (\partial P/\partial T)_{\varepsilon}$ are the temperature and strain coefficients of the frequency and power. If we ignore the uncertainty in the temperature and strain coefficients for Brillouin frequency and power and account for only the uncertainty induced by the Brillouin frequency and power, we can determine the maximum errors for the temperature and strain measurements as follows:

0146-9592/04/121342-03$15.00/0

$$\delta(\Delta T)_{\max} = \frac{|\delta(\Delta v)C_P^{\varepsilon}| + |C_v^{\varepsilon}\delta(\Delta P)|}{|C_v^{\varepsilon}C_P^T - C_P^{\varepsilon}C_v^T|}, \quad (1c)$$

$$\delta(\Delta \varepsilon)_{\max} = \frac{|\delta(\Delta v)C_P^T| + |C_v^T\delta(\Delta P)|}{|C_v^{\varepsilon}C_P^T - C_P^{\varepsilon}C_v^T|}. \quad (1d)$$

If we assume that the probability distributions for ΔT and $\Delta\varepsilon$ are Gaussian functions, we can calculate the rms values for ΔT and $\Delta\varepsilon$ as follows: In all the rms value calculations we ignored the uncertainty of the temperature and strain coefficients for Brillouin frequency, bandwidth, and power.

$$\mathrm{rms}(\Delta T) = \left\{\left[\frac{\mathrm{rms}(\Delta v)C_P^{\varepsilon}}{C_P^{\varepsilon}C_v^T - C_v^{\varepsilon}C_P^T}\right]^2 + \left[\frac{C_v^{\varepsilon}\,\mathrm{rms}(\Delta P)}{C_P^{\varepsilon}C_v^T - C_v^{\varepsilon}C_P^T}\right]^2\right\}^{1/2}, \quad (1e)$$

$$\mathrm{rms}(\Delta \varepsilon) = \left\{\left[\frac{\mathrm{rms}(\Delta v)C_P^T}{C_P^{\varepsilon}C_v^T - C_v^{\varepsilon}C_P^T}\right]^2 + \left[\frac{C_v^T\,\mathrm{rms}(\Delta P)}{C_P^{\varepsilon}C_v^T - C_v^{\varepsilon}C_P^T}\right]^2\right\}^{1/2}. \quad (1f)$$

Similarly, using frequency and bandwidth we have

$$\Delta T = \frac{\Delta v C_B^{\varepsilon} - C_v^{\varepsilon}\Delta B}{C_B^{\varepsilon}C_v^T - C_v^{\varepsilon}C_B^T}, \quad (2a)$$

$$\Delta \varepsilon = \frac{\Delta v C_B^T - C_v^T\Delta B}{C_v^{\varepsilon}C_B^T - C_B^{\varepsilon}C_v^T}, \quad (2b)$$

where ΔB are the variations of the Brillouin bandwidth due to temperature and strain. $C_B^{\varepsilon} = (\partial B/\partial\varepsilon)_T$ and $C_B^T = (\partial B/\partial T)_{\varepsilon}$ are the temperature and strain coefficients of the bandwidth. The maximum errors and rms values for the temperature and strain measurements are given by the following:

$$\delta(\Delta T)_{\max} = \frac{|\delta(\Delta v)C_B^{\varepsilon}| + |C_v^{\varepsilon}\delta(\Delta B)|}{|C_B^{\varepsilon}C_v^T - C_v^{\varepsilon}C_B^T|}, \quad (2c)$$

$$\delta(\Delta \varepsilon)_{\max} = \frac{|\delta(\Delta v)C_B^T| + |C_v^T\delta(\Delta B)|}{|C_v^{\varepsilon}C_B^T - C_v^TC_B^{\varepsilon}|}, \quad (2d)$$

$$\mathrm{rms}(\Delta T) = \left\{\left[\frac{\mathrm{rms}(\Delta v)C_B^{\varepsilon}}{C_v^{\varepsilon}C_B^T - C_B^{\varepsilon}C_v^T}\right]^2 + \left[\frac{C_v^{\varepsilon}\,\mathrm{rms}(\Delta B)}{C_v^{\varepsilon}C_B^T - C_B^{\varepsilon}C_v^T}\right]^2\right\}^{1/2}, \quad (2e)$$

$$\mathrm{rms}(\Delta \varepsilon) = \left\{\left[\frac{\mathrm{rms}(\Delta v)C_B^T}{C_v^{\varepsilon}C_B^T - C_B^{\varepsilon}C_v^T}\right]^2 + \left[\frac{C_v^T\,\mathrm{rms}(\Delta B)}{C_v^{\varepsilon}C_B^T - C_B^{\varepsilon}C_v^T}\right]^2\right\}^{1/2}. \quad (2f)$$

If we use bandwidth and power, we have

$$\Delta T = \frac{\Delta B C_P^{\varepsilon} - C_B^{\varepsilon}\Delta P}{C_P^{\varepsilon}C_B^T - C_B^{\varepsilon}C_P^T}, \quad (3a)$$

$$\Delta \varepsilon = \frac{\Delta B C_P^T - C_B^T\Delta P}{C_B^{\varepsilon}C_P^T - C_P^{\varepsilon}C_B^T}. \quad (3b)$$

The maximum errors and rms values for the temperature and strain measurements are as follows:

$$\delta(\Delta T)_{\max} = \frac{|\delta(\Delta B)C_P^{\varepsilon}| + |C_B^{\varepsilon}\delta(\Delta P)|}{|C_P^{\varepsilon}C_B^T - C_B^{\varepsilon}C_P^T|}, \quad (3c)$$

$$\delta(\Delta \varepsilon)_{\max} = \frac{|\delta(\Delta B)C_P^T| + |C_B^T\delta(\Delta P)|}{|C_B^{\varepsilon}C_P^T - C_v^{\varepsilon}C_B^T|}, \quad (3d)$$

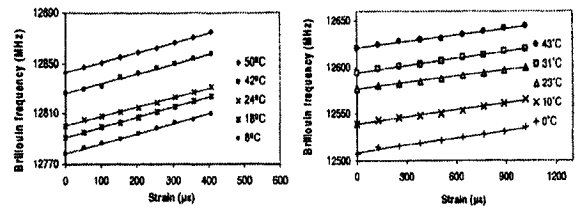

Fig. 1. Strain dependence of Brillouin frequency at different temperatures for (a) PANDA fiber and (b) bow-tie fiber.

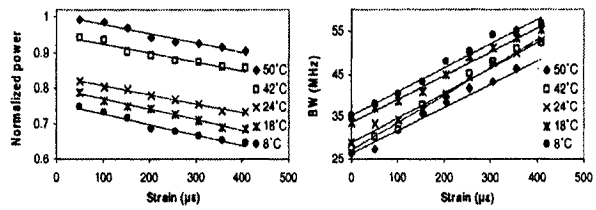

Fig. 2. Strain dependence of (a) power, normalized to the largest value at 50°C, and (b) bandwidth (BW) in PANDA fiber.

Table 1. Temperature and Strain Coefficients of Brillouin Frequency, Power, and Bandwidth

PM Fiber Type	PANDA	Bow Tie	Tiger
C_v^T (MHz/°C)	1.37 ±0.007	2.30 ±0.05	1.66 ±0.07
C_P^T (%/°C)	0.26 ±0.03	0.23 ±0.01	0.04 ±0.09
C_B^T (MHz/°C)	−0.15 ±0.02	−0.20 ±0.02	–
C_v^{ε} (MHz/με)	0.077 ±0.002	0.023 ±0.001	0.091 ±0.005
C_P^{ε} (%/με)	−0.028 ±0.003	0.018 ±0.002	0.011 ±0.004
C_B^{ε} (MHz/με)	0.058 ±0.004	−0.031 ±0.002	–

Table 2. Uncertainty of Temperature and Strain Calculated with Measured Brillouin Frequency (F), Power (P), and Bandwidth (B)

	PANDA			Bow Tie			Tiger
Property	F–P	F–B	P–B	F–P	F–B	P–B	F–P
Uncertainty of temperature (°C)	8	2	38	4	3	38	16
Uncertainty of strain ($\mu\varepsilon$)	153	39	135	237	126	195	598
Maximum error of ΔT (°C)	10	4	58	12	7	137	78
Maximum error of $\Delta\varepsilon$ ($\mu\varepsilon$)	331	82	249	741	490	1096	1308
rms (ΔT) (°C)	2	2	40	8	4	73	38
rms ($\Delta\varepsilon$) ($\mu\varepsilon$)	221	43	149	414	152	567	926

$$\mathrm{rms}(\Delta T) = \left\{\left[\frac{\mathrm{rms}(\Delta B)C_P^{\varepsilon}}{C_P^{\varepsilon}C_B^{T} - C_B^{\varepsilon}C_P^{T}}\right]^2 + \left[\frac{C_B^{\varepsilon}\,\mathrm{rms}(\Delta P)}{C_P^{\varepsilon}C_B^{T} - C_B^{\varepsilon}C_P^{T}}\right]^2\right\}^{1/2}, \tag{3e}$$

$$\mathrm{rms}(\Delta \varepsilon) = \left\{\left[\frac{\mathrm{rms}(\Delta B)C_P^{T}}{C_P^{\varepsilon}C_B^{T} - C_B^{\varepsilon}C_P^{T}}\right]^2 + \left[\frac{C_B^{T}\,\mathrm{rms}(\Delta P)}{C_P^{\varepsilon}C_B^{T} - C_B^{\varepsilon}C_P^{T}}\right]^2\right\}^{1/2}. \tag{3f}$$

The experimental setup is similar to that in Ref. 6, except we designed a new high- and low-temperature strain box that can pull PM fibers. The input power for a cw beam is 5 mW and the pulse power is 6 mW. The pulse width remains 2 ns for all tests. This corresponds to a spatial resolution of 0.2 m.

The Brillouin frequency of the fast axis was measured as a function of strain over the temperature range 8–50°C for PANDA fiber. It shows a linear relationship with an average slope of 0.077 MHz/$\mu\varepsilon$ in Fig. 1(a). The same test was done for a bow-tie fast axis from 0 °C to 43 °C, as shown in Fig. 1(b). The bandwidth and power of the Brillouin spectrum also represent a linear relationship with the strain over the same temperature range, as shown in Figs. 2(a) and 2(b) for PANDA fiber. The same experiment was done for bow-tie fiber that also showed a linear relationship with the strain, except the power increases and the bandwidth decreases with strain.

Clearly the three parameters of the Brillouin spectrum are linear functions of temperature and strain, so that Eqs. (1)–(3) are valid. The temperature[6] and strain coefficients of Brillouin frequency, power ratio, and bandwidth for three PM fibers were measured and calculated as shown in Table 1. The strain coefficients were averaged over the measurements in the temperature range 0–50°C. Substituting the parameters in Table 1 and the directly measured frequency, power, and bandwidth values into Eqs. (1)–(3), we obtain rms and maximum error values for temperature and strain for all three PM fibers. The average strain and temperature uncertainties are listed in Table 2 and are calculated as shown in Figs. 1 and 2 for the measured temperature and strain. The temperature range is 0–50°C, and the strain range is 0–408 $\mu\varepsilon$ for PANDA and 0–1021 $\mu\varepsilon$ for tiger fiber. As expected, the calculated rms values for temperature and strain using the power, bandwidth, and frequency are similar to the strain and temperature uncertainties, which are derived from the strain and temperature measurements in Figs. 1 and 2.

As explained earlier, by using PM fibers we had hoped to achieve better frequency and power measurement accuracy, i.e., better temperature and strain measurement accuracy. However, we found higher uncertainty with a combination of power and frequency. We believe this is due to the nonlinear Brillouin amplification fluctuation induced by the laser power. In SM fiber the polarization state varies randomly along the fiber length, the Brillouin gain takes the average effects between the pump and the probe polarization state variation, which is very low. When the laser power fluctuates, its effect on the Brillouin gain is not obvious because of the average Brillouin gain effects induced by PMD. While in a PM fiber the polarization states of the pump and the probe beams remained parallel when we launched them in the same state, so the Brillouin gain, i.e., nonlinear amplification, grows at an exponential level along the fiber length, because no PMD-induced polarization state variations exist; when the laser power varies, it causes larger fluctuation in the Brillouin gain, and so do the power changes induced by the temperature and strain or the laser power.

This work was supported by a Discovery grant from the National Sciences and Engineering Research Council of Canada, the Intelligent Sensing for Innovation Structures Canada Research Network, the Canada Foundation for Innovation, and the Canada Research Chair. Q. Yu's e-mail address is qinrong_yu@yahoo.ca.

References

1. X. Bao, D. J. Webb, and D. A. Jackson, Opt. Lett. **19,** 141 (1994).
2. H. H. Kee, G. P. Lees, and T. P. Newson, Opt. Lett. **25,** 695 (2000).
3. T. R. Parker, M. Farhadiroushan, R. Feced, and V. A. Handerek, IEEE J. Quantum Electron. **34,** 645 (1998).
4. J. Smith, A. Brown, M. DeMerchant, and X. Bao, Appl. Opt. **38,** 5372 (1999).
5. L. Chen, J. Cameron, and X. Bao, Opt. Commun. **169,** 69 (1999).
6. Q. Yu, X. Bao, and L. Chen, Opt. Lett. **29,** 17 (2004).

Simple method to identify the spatial location better than the pulse length with high strain accuracy

Qinrong Yu, Xiaoyi Bao, Fabien Ravet, and Liang Chen

Department of Physics, University of Ottawa, 150 Louis Pasteur Street, Ottawa, Ontario K1N6N5, Canada

Received March 25, 2005; revised manuscript received May 3, 2005; accepted May 3, 2005

The second-order partial derivative of the Stokes signal with respect to frequency and position shows a maximum or minimum at the boundary between two different strained sections. This idea is used to locate the boundary of different stress regions. Knowing the boundaries, we then fit the Brillouin spectrum at the middle between them to get the strain value. This allows a location accuracy of between 5 and 10 cm, which is shorter than the pulse length of 20 cm used in the experiment. The lowest detectable Brillouin frequency difference between two strain sections is 1.2 MHz. © 2005 Optical Society of America

OCIS codes: 060.2370, 290.5830.

In a Brillouin-loss-based distributed sensor,[1,2] the location information is obtained by measuring the traveling time of the pulse reflected from a specific position in the sensing fiber. The location accuracy is defined as the spatial interval for a signal increased from 10% to 90% or 90% to 10% of the rise or fall time, respectively. Normally, this time is longer than the pulse length because of the noise involved in the signal. The minimum detectable strain or temperature length depends on a short rise or fall time, the pulse length, and the signal-to-noise ratio (SNR). A shorter pulse requires broadband detectors and electronics. This leads to a low SNR and poor strain accuracy. If a broader pulse is used, the strains within the pulse length may not be uniform for a small strain length. Hence the Brillouin spectrum involves multiple peaks (for large Brillouin frequency variation) or a broadened Brillouin profile (small Brillouin frequency variation). Thus finding the boundary of two strained sections is a difficult task, especially for a large strain gradient or a small strain change. With unknown peaks and unknown parameters, it is difficult to get accurate location and strain information. To overcome this difficulty, a frequency modulation method was used to deconvolute the Brillouin spectrum; for instance, Hotate and Tanaka[4] reported 1 cm spatial resolution with a correlation-based Brillouin sensor. A strain of 1000 $\mu\varepsilon$ was applied with a Brillouin frequency uncertainty of 5–6 MHz, equivalent to 100–120 $\mu\varepsilon$, over a limited sensing length (0.3 m). Shi *et al.*[5] used a 10 ns pulse, equivalent to 1 m, to get a spatial resolution of 0.2 m with a frequency bandwidth method. They used the maximum bandwidth (convolution of the Brillouin peaks from two strained sections) as the criterion to determine the boundary of two strained sections. Using this method they obtained an ~100 $\mu\varepsilon$ uncertainty for a 750 $\mu\varepsilon$ measurement.

In this Letter we propose a mixed second-order partial derivative of the Stokes intensity (Brillouin loss signal) with respect to frequency and location to identify the boundary for different Brillouin frequencies. The second-derivative procedure has been used in spectroscopy signal processing to find the peaks of a spectrum (second derivative of amplitude with respect to frequency). Here, the derivative is relative to frequency and location, rather than frequency alone, because the distributed Brillouin sensor needs both location and spectrum information related to strain or temperature.

The reason to use the mixed second derivative instead of the first derivative is to remove the intensity fluctuation. We obtained location accuracy better than the pulse length, yet with the lowest detectable strain. We used a 2 ns pulse for the Brillouin-loss-based sensor and scanned the laser frequency to map the Brillouin spectrum at a step of 5 MHz, and we found that the lowest detectable strain is 16 $\mu\varepsilon$, equivalent to 1.2 MHz at a location accuracy of 5–10 cm.

When the Brillouin frequency changes along the position nonuniformly, the Brillouin intensity experiences nonmonotonic changes within the pulse corresponding to the Brillouin frequency contribution at the strain point to a given time delay. We can find those changes in the Brillouin loss signal versus position as the central Brillouin frequency, thus identifying the boundary between strain sections. In practice, due to the power fluctuation of the lasers and polarization state variation, the Stokes intensity shows no change for a small Brillouin frequency shift. Therefore, strain changing points are not observable in the Brillouin loss versus position. If we use one Lorentzian peak to fit a distorted spectrum (convolution of multiple Brillouin peaks), we will get an offset peak frequency from the real peak frequency. Because one peak Brillouin spectrum fitting represents only uniform strain or temperature, the true spectrum near the boundary is the overlap of multiple peaks, which forms a nonsymmetric and broadened peak for small Brillouin frequency variation.

If the Brillouin frequency change is comparable to the natural linewidth (35 MHz for single-mode fiber[1], SMF), the Brillouin loss signal around the central Brillouin frequency versus position will show an obvious jump because the Stokes intensity change is larger than the power fluctuation.

0146-9592/05/172215-3/$15.00

Using a multiple-peak function to fit the spectrum near a boundary of different strain sections is possible if we know the number of peaks in the Brillouin spectrum in advance. Often this is not the case. Also, with large strain gradients within a small fiber section (less than the pulse length), many fitting parameters would be required and they vary with position. In addition, the experimental data contains noise such as power fluctuation or cross talk from a strain–temperature gradient. It is difficult and time consuming to use a multiple-peak function to fit a distorted spectrum. Our proposed method can be employed to resolve the boundary location of two strain sections with a large strain gradient over a small region (less than the pulse length), resulting in distorted Brillouin profiles for positions close to the boundary region.

Based on Brillouin loss signal changes with strain, we calculated the Brillouin loss versus position at the peak Brillouin frequency and its first-order derivative with respect to location with uniformly strained sections by use of a coupling wave equation,[6] shown in Fig. 1. It can be seen that the first-order derivative of the position reveals the boundaries of the strained sections at positions of 1.0, 2.0, and 3.0 m. In the theoretical calculation, no noise is included; hence the first-order derivative is adequate.

We used polarization-maintaining and absorption-reducing (PANDA) fiber as the strain-sensing fiber. The advantage of using polarization-maintaining fiber (PMF) is the elimination of polarization fluctuation noise. If a SMF is used, the minimum detectable strain will be higher than the PMF result, unless more averaging is introduced, which adds to the signal processing time. For PMF, we can get a 30 dB SNR with 2000 averages for pulses of 1–3 ns. This can result in a minimum Brillouin frequency shift of 1–1.5 MHz. For the SMF at the same power level and averaging number (2000), we can get a SNR of only ~25 dB. This means a minimum Brillouin frequency of ~2 MHz, unless we increase the number of waveform averaging.

The fiber was passed around a pulley with bearings and wrapped and glued to a post. The post was pulled away from the pulley to create a uniform strain on the fiber. The length of the strained sections was physically measured to be 157 cm (=15.7 ns). The strain coefficient was measured as 0.077 MHz/$\mu\varepsilon$. The system includes two tunable diode-pumped

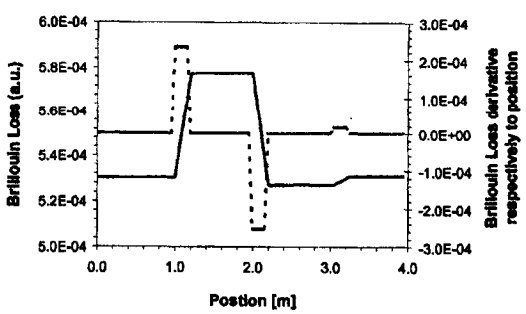

Fig. 1. Brillouin loss (solid curve) and its first-order derivative (dashed curve).

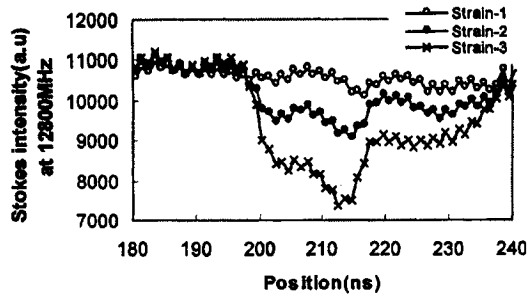

Fig. 2. Stokes intensity versus position for Strain-1, Strain-2, and Strain-3.

Nd:YAG lasers operating at 1319 nm, an electro-optic modulator driven by a pulse generator, a 1 GHz bandwidth photodetector, and a 1 Gbit/s digitizer.

As the spectrum evolves from unstrained to strained fiber, there is a maximum change in Brillouin frequency and Stokes intensity at the strain boundary. At the peak frequency of the unstrained section of 12,800 MHz, the Stokes intensity drops from the unstrained section to the strained section. Figure 2 shows Stokes intensity in three experiments: Strain-1, Strain-2, and Strain-3. The corresponding Brillouin frequency differences between the strained and the unstrained sections are 1.2, 8.4, and 15.4 MHz, respectively. In principle, the first-order derivative of the Stokes intensity with respect to the position at a given frequency is able to reveal the boundary. However, its SNR is low due to the Stokes intensity fluctuation caused by digitizer quantization (rounding) error and input laser power fluctuation.

To minimize the error in finding the boundary, we first calculated the relative change of two consecutive frequencies, the first-order derivative of the Stokes intensity with respect to frequency:

$$\alpha(v,z) = \frac{P(v + \Delta v_{\text{scan}},z) - P(v,z)}{\Delta v_{\text{scan}}}, \tag{1}$$

where $P(v,z)$ is the Stokes intensity near the peak frequency and $P(v+\Delta v_{scan})$ is the intensity at $v + \Delta v_{scan}$. Δv_{scan} is the laser frequency scanning step size. Obviously, $\alpha(v,z)$ has much smaller intensity fluctuation, as shown Fig. 3. Note the Δv_{scan} was 5 MHz in our experiment.

Then we calculated the second-order partial derivative of the Stokes intensity with respect to position:

$$\beta(v,z) = \frac{\Delta\alpha(v,z)}{\Delta z} = \frac{\alpha(v,z + \Delta z) - \alpha(v,z)}{\Delta z}, \tag{2}$$

where Δz is the step size of the digitizer. The plot of $\beta(v,z)$ versus position (z) is shown in Fig. 4 for Brillouin frequency for Strain-1, Strain-2, and Strain-3 corresponding to 1.2, 8.4, and 15.4 MHz, respectively. We see a positive peak [$\alpha(v,z)$ increasing] and a negative peak [$\alpha(v,z)$ decreasing] corresponding to the start and end of the strained section. The SNR of $\beta(v,z)$ is about 6 dB, much higher than that of the

first-order derivative of the Stokes intensity with respect to position. We used a quadratic fitting method to find the peak position at both sides of the maximum, so that it gives a more accurate location. The first boundary location was measured as 200 ns for the three strain cases, and the second boundary location was measured as 216.5 ns for Strain-1 and 216.0 for both Strain-2 and Strain-3. Knowing the two boundaries, the length of the strained section was thus calculated as 16.5 ns (=165 cm) for Strain-1 and 16 ns (160 cm) for both Strain-2 and Strain-3. Comparing the actual length of the strained section, 157 cm, the accuracy is within one to two digitizing steps, which is equivalent to 5–10 cm. Once two boundaries were found we then applied one peak fitting method for the Lorentzian shape of the Brillouin spectrum at the middle point of two boundaries. This will allow us to find the central Brillouin frequency and to get the strain for this section. It is assumed that between two boundaries the strain is uniformly distributed. The accuracy of the boundary measured by this method depends on the SNR, the scanning frequency step, Δv_{scan}, digitizing step Δz, and frequency variation δv between the two sections. For a large scanning frequency increment, $\Delta v_{scan} \gg \delta v$, the accuracy in evaluating $\alpha(v,z)$ decreases. Although it is commonly believed that the spatial resolution is determined by the pulse width, the digitizer step is the ultimate resolving factor in this method, since the recorded spatial information within the pulse width is updated at every digitized step.

Figure 5 shows the strain distribution measured by a sensor with the boundary identification method as Strain-1, Strain-2, and Strain-3 corresponding to strain levels of 16, 108, and 200 $\mu\varepsilon$. The dial-gauge measurements are also plotted as Strain-1′, Strain-2′, and Strain-3′ corresponding to strain levels of 19, 114, and 217 $\mu\varepsilon$. Note that the strain measurement accuracy of the dial gauge is 6 $\mu\varepsilon$. The distributed sensor has a frequency measurement accuracy of 1.2 MHz, equivalent to 13 $\mu\varepsilon$. The difference between the distributed sensor and the dial-gauge reading is within the sum of uncertainties (±21 $\mu\varepsilon$) attributed to both methods. Since this method is not iterative

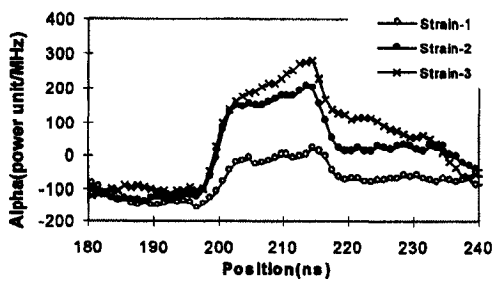

Fig. 3. Alpha (first derivative of Stokes intensity with respect to frequency) versus position for Strain-1, Strain-2, and Strain-3.

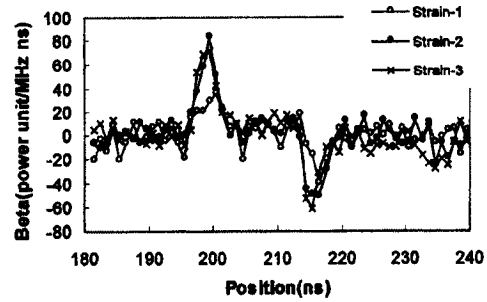

Fig. 4. $\beta(v,z)$ versus position for Strain-1, Strain-2, and Strain-3.

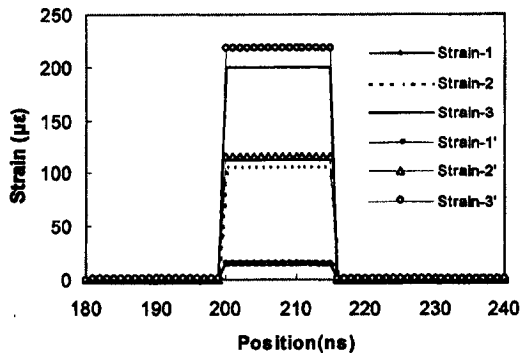

Fig. 5. Strain distribution for Strain-1, Strain-2, and Strain-3 measured by a sensor with a boundary identification method and the dial-gauge measurements Strain-1′, Strain-2′, and Strain-3′.

but a rather simple calculation (all the peak fitting methods use the iteration approach), it is suitable for implementation to real-time measurement.

In summary, using the intensity second-order partial derivative of the frequency and position can improve the location accuracy to 1/2–1/4 of the pulse length with a 1.2 MHz minimum detectable Brillouin frequency between the two sections.

Q. Yu's e-mail address is qinrong_yu@yahoo.ca.

References

1. T. Horigushi, K. Shimizu, T. Kurashima, M. Tateda, and Y. Koyamada, J. Lightwave Technol. **13**, 1296 (1995).
2. M. Niklès, L. Thévenaz, and P. A. Robert, J. Lightwave Technol. **15**, 1842 (1997).
3. S. Afshar V., X. Bao, L. Zou, and L. Chen, Opt. Lett. **30**, 705 (2005).
4. K. Hotate and M. Tanaka, IEICE Trans. Electron. **E84-C**, 12 (2001).
5. B. Shi, H. Z. Xu, D. Zhang, Y. Ding, H. L. Cui, J. Q. Gao, and B. Chen, in *First International Conference on Structural Health Monitoring and Intelligent Infrastructure*, Japan, November 2003, p. 1025.
6. F. Ravet, X. Bao, and L. Chen, IEEE Photon. Technol. Lett. **17**, 1504 (2005).

Influence of transient phonon relaxation on the Brillouin loss spectrum of nanosecond pulses

Xiaoyi Bao, Qinrong Yu, V. P. Kalosha, and Liang Chen

Department of Physics, University of Ottawa, 150 Louis Pasteur Street, Ottawa, Ontario K1N 6N5, Canada

Received October 6, 2005; revised December 15, 2005; accepted December 21, 2005; posted January 4, 2006 (Doc. ID 65222)

For pump–probe stimulated Brillouin scattering with a probe pulse of a few nanoseconds duration and with a finite DC level, the acoustic wave relaxation time varies with the pump power and the DC level. For a pump power of 1–6 mW, the acoustic wave relaxation changes from ~9 to 90 ns for polarization-maintaining fiber at a temperature of −40 °C for a 2 ns pulse width. When the pulse DC ratio of the probe varies from 10 to 20 dB, the acoustic relaxation time changes from 24 to 45 ns for single-mode fiber at 25°C. This induces a power-increment spectral feature in the detected AC pump signal in the Brillouin loss spectrum of two temperature or strain sections, where both spectral components appeared at positions far from those related to the natural phonon relaxation time (~10 ns) equivalent length. The theoretical calculations confirm the prolonged phonon relaxation.

OCIS codes: 060.2370, 290.5830.

Distributed fiber sensors based on Brillouin scattering have drawn increased attention because of their capability of measuring strain and temperature continuously over a long distance.[2] For a pump–probe based distributed Brillouin sensor system, when the probe signal consists of the pulse and DC levels, the Brillouin loss spectral width can be much narrower than the pulse spectrum.[3,4] The advantage of this approach is a high signal-to-noise ratio, which leads to better temperature–strain accuracy.[5] To our knowledge there has been no research conducted on the effects of the phonon relaxation time or the acoustic field decay time by the DC level of the probe signal and pump power in the Brillouin loss spectrum at a pulse width shorter than the natural phonon lifetime (~10 ns).

Here we report experimental and theoretical studies of the effects of the pump and the DC levels of the probe on the acoustic field for a short pulse (<10 ns), by studying the Brillouin loss spectrum at the boundary of two or three temperature and strain sections in the sensing fibers. We demonstrate for what is believed to be the first time that when a 2 ns pulse is used the probe and the pump interact with the acoustic field, resulting in a longer relaxation time. This induces an AC power increment in the Brillouin loss spectrum in the next fiber with a distance much larger than the pulse length. This can cause a problem for a distributed sensor in determining the strain–temperature boundary, and for central Brillouin peak fitting to multiple peak convolution, and it affects temperature and strain accuracy. The measured saturation power of the pump and probe waves of nanosecond pulses is ~4 mW, which is much lower than the stimulated Brillouin scattering threshold.

The prolonged phonon relaxation time, defined as τ_{decay}, depends on the pump and DC levels of the pulsed probe signal. This was detected by an AC-coupled optical receiver. τ_{decay} was measured with two temperature sections of polarization-maintaining (PM) fiber at the end of the first fiber section (the boundary was determined using the second-order derivative[5]) from the maximum Brillouin loss signal ($\nu_1-\nu_2=\nu_{B1}$), decreasing to minimum Brillouin loss in section 2 ($\nu_1-\nu_2\neq\nu_{B2}$), where ν_1 and ν_2 are the frequencies of the pump and probe lasers, respectively, ν_{B1} and ν_{B2} are the Brillouin frequencies for fiber sections 1 and 2, respectively. The Brillouin loss signal shows saturation of ~4 mW for pump power at 2 ns pulse width with a peak power of 2.5 ± 0.5 mW for the probe power.

For the DC level effect on the acoustic field, we have found a minimum phonon relaxation time corresponding to a moderate DC level, if the DC level is higher or lower than this value, then the relaxation time is increased for single-mode (SM) fiber. The same trend is found for increasing pump power; a minimum phonon relaxation time occurs at ~3 mW.

Consider two PM fiber sections with different Brillouin frequencies of ν_{B1} and ν_{B2}. When the pump and probe frequency difference is ν_{B1}, a strong phonon field is created as the pulse is propagated along section 1. Even after the pulse passes section 1 and goes to section 2, the phonon field at ν_{B1} is still sustained by the interaction of the probe DC level and pump signals. When the CW power or the DC level is increased, the acoustic wave does not decay naturally. Rather, it is driven by the CW pump and the DC level of the probe after passage of the pulse. This process can be seen in the Brillouin loss signal when $\nu_1-\nu_2=\nu_{B1}$ (Fig. 1): the ν_{B1} component is seen at time 228 ns (section 2), which is 12 ns from the boundary at 216 ns. This time difference is larger than the 2 ns pulse width and the natural phonon lifetime of ~10 ns.

The experimental setup was similar to that reported in Ref. 5. The DC level was determined by the extinction ratio (ER), the pulse/DC level ratio, an ER of 14 dB, power $P_{probe}\sim 2.5$ mW, and $P_{pump}=3$ mW. 1.6 m Panda PM fiber was stretched by 400 μs, with a small strain gradient between the strained and loose fiber. The equivalent Brillouin frequency shift was ~31 MHz. The acoustic field at section 1 interacts with the CW pump before reaching the mini-

0146-9592/06/070888-3/$15.00

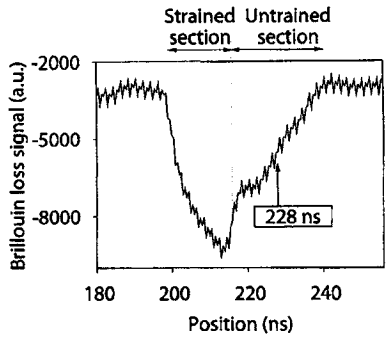

Fig. 1. Brillouin loss signal versus position for a PM Panda fiber when $\nu_1-\nu_2=\nu_{B1}=1280$ MHz. The strained section is between 200 and 216 ns.

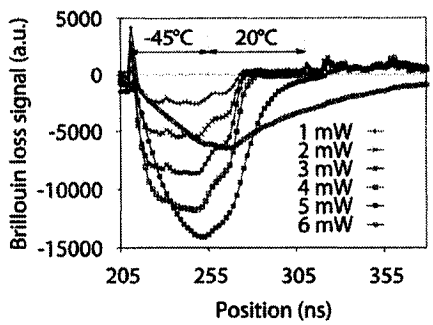

Fig. 2. Brillouin loss signal versus position at ν_{B1} = 12760 MHz with different pump powers for a 2 ns pulse.

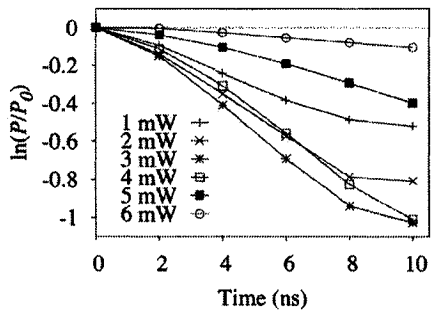

Fig. 3. Brillouin loss signal versus time at $\nu_1-\nu_2=\nu_{B1}$ for different CW pump powers.

mum Brillouin loss at 240 ns, which gives τ_{decay} as 240–216 ns = 24 ns.

We also studied the correlation of the CW pump power with the acoustic field relaxation and the pump saturation power to the Brillouin loss signal. A 10 m Panda PM fiber with a loose 1.2 mm tube was used in two sections: length $L_1=5$ m in an environment chamber of −45 °C ($\nu_{B1}=12\,670$ MHz), and length $L_2=5$ m at room temperature ($\nu_{B2}=12\,790$ MHz). The Brillouin loss signal versus position at different pump powers is plotted in Fig. 2. The small positive peak at the input end is due to the reflection of the connector. At low pump power, the reflection of the probe pulse is added to the pump power as a positive peak. As the pump power increases for a fixed probe power, the reflection of the probe is smaller than the pump power. The Brillouin loss signal shows saturation at a pump power of ~4 mW. Note that this saturation power is much lower than the stimulated Brillouin scattering threshold for a 2 ns pulse, which occurs at a few hundred milliwatts. This means that the optimized pump power for the distributed sensor should be ~4 mW for a pulse width of 1–5 ns.

Figure 3 represents the measured τ_{decay} at different pump powers for a pulse power of 2.3 mW and an ER of 14 dB. As the Brillouin loss signal is proportional to the acoustic wave, we can measure the Brillouin loss signal decay to obtain the relaxation time of the acoustic wave. Acoustic waves decay as Brillouin loss signal $P=P_0\exp(-t/\tau_{decay})$, where P_0 is the maximum Brillouin loss signal at the boundary measured at difference $\nu_1=\nu_2=\nu_{B1}=12\,670$ MHz.

The slopes in Fig. 3 give the acoustic wave relaxation time at the different pump powers shown in Table 1. At a pump power of 3 mW, we observed an ~9 ns relaxation time, which is equivalent to an ~39 MHz Brillouin bandwidth. This bandwidth value matched well with our measured the Brillouin loss spectrum width of ~38 MHz at −45 °C. The bandwidth remains unchanged for pump power of 1–6 mW, as the ER is kept constant. We also find the maximum loss value is at ~3 mW pump power.

The prolonged acoustic field was observed in the Brillouin loss signal by an AC-coupled optical receiver in the form of AC power gain at ν_{B1} in section 2 (ν_{B2}). In the ν_{B2} section, the returned pump signal includes ν_{B2} and was added to the probe DC level signal interaction with a prolonged acoustic field at ν_{B1}. Therefore ν_{B1} appeared in the spectrum corresponding to a time delay at section 2 for a distance much longer than the pulse length and the natural phonon relaxation time. ν_{B2} and ν_{B1} belong to different locations, arrive at the same time, and became evident in the same Brillouin loss spectrum. Hence the probe

Table 1. Phonon Relaxation Time τ_{decay} for PM Fiber

	Pump Power (CW, mW)					
	1	2	3	4	5	6
τ_{decay} (ns)	18.0	11.3	9.0	9.4	24.8	90.1

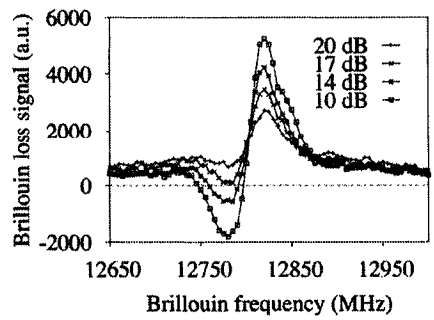

Fig. 4. Brillouin loss spectra at the middle of section 2 (at time 260 ns) for different ERs corresponding to probe powers of 0.1, 0.6, 3.3, and 7 mW; $\nu_{B1}=12780$ MHz, $\nu_{B2}=12820$ MHz, and $\nu_{B3}=12850$ MHz.

Table 2. Phonon Relaxation Time τ_{decay} and Brillouin Loss Spectral Width at Different ERs for SM Fiber

	ER (dB)				
	10	12	14	17	20
τ_{decay} (ns)	23.8	24.0	20.6	34.5	45.2
$\Delta\nu_B$ (MHz)	38	39	42	45	58

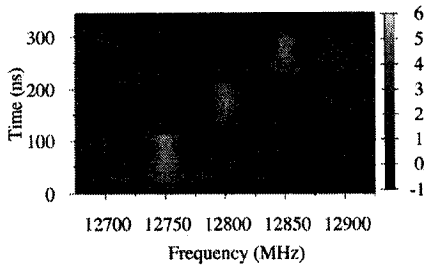

Fig. 5. (Color online) Calculated AC pump power (Brillouin loss signal) in 3-10 m section fibers with ν_{B1} = 12 750 MHz, ν_{B2} = 12 800 MHz, and ν_{B3} = 12 850 MHz. ER = 10 dB, P_{probe} = 10 mW, P_{pump} = 5 mW.

DC level interacts with the prolonged ν_{B1} field, acting as a gain in this Brillouin loss signal at ν_{B2}. We refer to this as an AC power increment to differentiate it from the peak Brillouin loss signal at ν_{B2}. This combined Brillouin loss spectrum continues to exist during τ_{decay} for the acoustic field in section 1. This process was simulated with our theoretical model[6] for AC detection of the Brillouin loss spectrum.

The AC power increment was studied at different DC levels of the probe (the pulse amplitude remains constant) by use of a 30 m SM fiber divided into three 10 m sections, with Brillouin frequencies ν_{B1} = 12 785 MHz, ν_{B2} = 12 820 MHz (25 °C), and ν_{B3} = 12 850 MHz. The maximum peak power for the probe signal is 7 mW. The CW pump power was maintained at 4 mW. Figure 4 shows the Brillouin loss spectrum at section 2 for a DC level corresponding to an ER of 10–20 dB with an AC power increment occurring at 260 ns (the middle of section 2). It is clear that both the ν_{B1} and the ν_{B2} frequency components appeared in the spectrum. If we fit the central peak with a Lorentzian profile, then the Brillouin frequency will be shifted from the true peak position.

This effect may create a drawback to the distributed Brillouin sensing, namely, fitting errors in the central Brillouin peak for the strain and temperature accuracy. Due to the negative peak, the single-peak fit will be shifted from the positive peak, while the multiple-peak fit will give two Brillouin frequencies for the related temperature and strain for this fiber section. To solve this problem, one can use the position correlation in the time domain, combined with the central frequency fitting method, and then find the maximum Brillouin loss and Brillouin frequency for each peak for the location, instead of looking for the highest Brillouin loss signal among Brillouin peaks at a given location. This allows the removal of the different section peaks.

To study the effect of DC level on the prolonged phonon relaxation time τ_{decay} in SM fiber, we measured τ_{decay} for different ERs when $\nu_1 - \nu_2 = \nu_{B2}$ = 12 820 MHz for a pump power of 4 mW. We found a minimum τ_{decay} at a moderate DC level. When the DC level is higher or lower, τ_{decay} tends to be longer. This minimum relaxation time equivalent DC level (~14 dB) is recommended for the sensing operation. The result is shown in Table 2. The Brillouin loss spectral width increases with increasing ER because of the increase of the pulse component.[4] The decay time uncertainty for SM fiber is higher than that for PM fiber because the polarization state changes in the SM fiber, which induces a Brillouin loss signal variation. This translates to decay time uncertainties of ~4 ns for SM fiber and ~1 ns for PM fiber.

Figure 5 shows the calculated Brillouin loss signal at AC detection. It can be seen that the prolonged phonon fields at ν_{B1} and ν_{B2} extend to sections 2 and 3 at lengths >10 and >20 m, respectively. The Brillouin loss also extends more than the natural phonon lifetime. This agrees with the experimental observation shown in Fig. 3. Apparently the interaction between the DC of the probe and pump contributes to this prolonged acoustic field, which is attributed to a long phonon relaxation time. We noticed that the low DC level of the probe corresponds to a shorter phonon relaxation time of ~10 ns.

In summary, we have demonstrated prolonged acoustic field relaxation time and its dependence on the pump power and the DC level of the probe pulse, as well as its effect on the Brillouin loss spectrum. Using two- or three-section sensing fiber and varying DC levels of the probe and pump powers, we observed an AC power increment in the AC-detected signal (Brillouin loss signal) as well as a prolonged acoustic field relaxation process. This effect may create a drawback to the use of a distributed Brillouin sensor in determining the boundary of two different Brillouin frequency sections and the corresponding temperature or strain reading.

The authors thank Evgueni Ponomarev, Lufan Zou, and Shiquan Yang for thoughtful discussions. X. Bao's e-mail address is xbao@uottawa.ca.

References

1. K. Hotate and M. Tanaka, IEEE Photon. Technol. Lett. **14**, 675 (2002).
2. T. Horigushi, K. Shimizu, T. Kurashima, M. Tateda, and Y.Koyamada, J. Lightwave Technol. **13**, 1296 (1995).
3. X. Bao, A Brown, M. DeMerchant, and J. Smith, Opt. Lett. **24**, 510 (1999).
4. V. Lecoueche, D. J. Web, C. N. Pannell, and D. A. Jackson, Opt. Lett. **25**, 156 (2000).
5. Q. Yu, X. Bao, F. Ravet, and L. Chen, Opt. Lett. **30**, 2215 (2005).
6. S. Afshar, V. P. Kalosha, X. Bao, and L. Chen, Opt. Lett. **30**, 2685 (2005).